Development of Optogenetic Approaches to Selectively Modulate G Protein Signalling

Jayde Louise Lockyer

BBiotechMedRes (Hons.)

Tasmanian School of Medicine | College of Health and Medicine

Submitted in fulfilment of the requirements for the Doctor of Philosophy (Medical Studies) University of Tasmania August 2021

Declaration of Originality

This thesis contains no material which has been accepted for a degree or diploma by the University or any other institution, except by way of background information and duly acknowledged in the thesis, and to the best of my knowledge and belief no material previously published or written by another person except where due acknowledgement is made in the text of the thesis, nor does the thesis contain any material that infringes copyright.

_____

Date: 09/07/21

Authority of Access

This thesis may be made available for loan and limited copying and communication in accordance with the Copyright Act 1968.

_____

Date: 09/07/21

Acknowledgements

I would firstly like to extend my greatest thanks to my supervisors, Dr John Lin, Dr Owen Marshall, and Professor Lisa Foa. Thank you for your constant support, advice, and encouragement throughout this project. I would especially like to thank John for providing me with the opportunity to be part of the Lin lab and this project. You have been a fantastic supervisor and I have really enjoyed working with you!

I would also like to thank Dr Zhitao Hu, Dr Lei Li and Dr Haowen Liu from the Queensland Brain Institute for hosting me and teaching me everything there is to know about *C. elegans*.

Many thanks to Professor Bruno van Swinderen from the Queensland Brain Institute and Professor Mark Tanouye from University of California, Berkeley for providing feedback and advice about fly assays. I would also like to thank Dr Harald Janovjak and Dr Elliot Gerrard from Monash University for your assistance with troubleshooting the cAMP assay. All your help was very much appreciated.

A big thank you to Dr Caroline Delandre for helping with all my fly questions and for putting up with my embarrassing lack of fly knowledge. You have been a huge help! I would also like to thank Caroline and John McMullen for providing the fly brain images for this project.

Thank you to my collaborator and friend, Silvia Vicenzi, for testing my tool in your project and for providing much needed confirmation that it worked outside of my own experiments. Thank you also for being such a great friend and for always being so positive and supportive.

To Dr Agnieszka Zbela, thank you for being such a wonderful, supportive friend and for always providing encouragement and creative new career plans in case it all went wrong. It would not have been the same without you!

I would like to thank all the past and present members of the Lin lab for being so friendly and supportive. You have all made the past few years very enjoyable and memorable and I am very grateful for being able to have worked with you all. I would especially like to thank Jenny Smith for providing very unscientific conversation and Dr Dave Gell for all your very scientific advice.

Lastly, I would like to thank my family. Thank you for your unconditional love and support.

Table of contents

List of abbreviations

GPCRs	G protein coupled receptors
GDP	guanosine diphosphate
GTP	guanosine triphosphate
RGS	regulator of G protein signalling
AC	adenylate cyclase
cAMP	cyclic adenosine monophosphate
CNG	cyclic nucleotide-gated
MAPK	mitogen-activated protein kinase
LTCC	L-type calcium channels
CREB	cAMP-response element binding protein
PKA	protein kinase A
LTP	long-term potentiation
ERK	extracellular signal-regulated kinase
NMDAR	*N*-methyl-D-aspartate receptor
M_3R	Muscarinic acetylcholine receptor M_3
$[Ca^{2+}]_i$	cytosolic calcium concentrations
PLC-β	protein lipase C-beta
PIP_2	phosphatidylinositol-4, 5-bisphosphate
IP_3	inositol-1, 4, 5-triphosphate
DAG	diacylglycerol
IP_3R	inositol-1, 4, 5-triphophate receptor
ER	endoplasmic reticulum
TRPC3	transient receptor potential channel 3
LTD	long-term depression
sEPSPs	slow excitatory post-synaptic potentials
GIRK	G protein-coupled inwardly rectifying potassium
PI3 kinase	phosphatidylinositol-4,5-bisphosphate-3-kinase
GAP	GTPase activating protein

RASSL	receptors activated solely by synthetic ligands
DREADD	designer receptors exclusively activated by designer drugs
hM_3Dq	human M_3 muscarinic DREADD Gαq
CNO	clozapine-N-oxide
AlstR/AR	Allatostatin receptor/ Allatostatin system
ChR	channelrhodopsin
PET	positron emission tomography
fMRI	functional magnetic resonance imaging
Ro-4	rhodopsin 4
WT	wild type
PAC	photoactivable adenylate cyclase
BLUF	blue light using FAD
PDE	phosphodiesterase
LAPD	light activated phosphodiesterase
LOV	light-oxygen-voltage domain
ePDZ	engineered PDZ
CRY2	cryptochrome 2
CIB1	cryptochrome-interacting basic-helix-loop-helix 1
TULIPs	tuneable light-controlled interacting protein tags
FMN	flavin mononucleotide
FAD	flavin adenine dinucleotide
CRY2(PHR)	cryptochrome 2 (photolyase homology region)
CIBN	N-terminal domain CIB1
eGFP	enhanced green fluorescence protein
PIGM-Iq	photo-induced G protein modulator – inhibitor Gαq
mAChR	M_1 muscarinic acetylcholine receptor
HEK293A	human embryonic kidney cells
CMV	cytomegalovirus promotor
D_2R	dopamine D2 receptor
O-GECO1	orange fluorescent genetically encoded calcium indicator

ECS	extracellular solution
CCh	carbachol
ISO	isoprenaline
QNP	quinpirole
N2	wild type *C. elegans*
Psnb1	synaptobrevin-1 promotor
MB	mushroom body
KC	Kenyon cell
OA	octopamine
OAMB	octopamine receptor mushroom body
TβH	tyramine β hydroxylase
Shi^{ts}	temperature sensitive *shibire*
cVA	*cis*-Vaccenyl Acetate
GEF	guanine nucleotide exchange factor

List of figures and tables

Figures

Chapter 1

Chapter 2

Chapter 3

Tables

Abstract

G protein coupled receptors, or GPCRs, transduce signals from neuromodulators and permit dynamic regulation of neuronal circuits. Gradually, we have come to understand the processes underlying neural function and the molecular underpinnings of higher cognitive function. However, as we continue to push the limits of our understanding, so too do we push the technical demands required to reach the next breakthrough. Consequently, the need for a more diverse repertoire of tools for neuronal manipulation is continuously increasing.

GPCRs - classified according to G protein association: Gαq, Gαs or Gαi-linked - are fundamentally associated with neuromodulation, as opposed to direct neuronal excitation and inhibition. Due to complexity, an ever-expanding molecular toolbox is needed for the artificial manipulation of these signalling cascades. Despite the large array of chemical and optogenetic-based tools already available; a selective, light-induced inhibitor of endogenous G protein signalling is yet to be described. Thus, this study designs and validates such a tool, with a focus on the selective inhibition of endogenous Gαq-linked GPCR signalling.

The optogenetic tool described in this study utilised the protein domain of RGS2, a member of the regulator of G protein signalling (RGS) family. RGS2 acts as a GTPase-accelerating protein, or GAP, selectively inactivating the Gαq G protein associated with agonist bound GPCRs. It was proposed that optogenetic activation of this protein would allow for a selective, light-dependent tool that would inactivate endogenous Gαq-linked GPCR signalling. This study describes the design and validation of Photo-Induced G protein Modulator – Inhibitor Gαq, or PIGM-Iq.

RGS2 functions at the membrane to inhibit G protein signalling. To control its activity and reduce possible interactions with other signalling pathways, the membrane binding domain, as well as a domain thought in interact with the Gαs signalling pathway, were removed. As expected, the resulting cytosolic variant of RGS2 was unable to inhibit Gαq-linked signalling in mammalian HEK293A cells. To allow for light-induced translocation of this protein to the membrane, the truncated RGS2 (ΔRGS2) was fused to the photoreceptor, cryptochrome 2 (CRY2), with its binding partner, CIBN, localised at the membrane. Blue light illumination was shown to control ΔRGS2 activity via re-localisation of the ΔRGS2 from the cytosol to the membrane. Blue light illumination of cells expressing PIGM-Iq robustly reduced agonist induced Gαq-linked calcium efflux. Inhibition was absent in the three control conditions tested:

1) in cells not illuminated with light, 2) in cells expressing only one component of the system, and 3) in cells expressing a light-insensitive variant of the tool.

The selectivity of the tool towards other GPCR signalling cascades was investigated. Both wild type RGS2 and PIGM-Iq did not possess affinity towards either the Gαi or Gαs-linked signalling pathways in mammalian HEK293A cell culture. It was therefore concluded that the tool selectively interacted with the endogenous Gαq G proteins.

To validate the effectiveness of the tool *in vivo*, the mobility of the nematode, *C. elegans*, and courtship conditioning in the male fruit fly, *D. melanogaster*, were used as assays. In *C. elegans*, a single epoch of blue light delivered to transgenic animals produced a decrease in movement that was rescued after 20 minutes of dark habituation. This is consistent with the known phenotype of the Gαq mutant strains *egl-30(ad803)* and *egl-30(ad806)* in *C. elegans*. This movement deficit could be reinstated upon further illumination, highlighting both the sensitivity and reversibility of the tool. In *D. melanogaster*, the octopamine receptor, OAMB, is necessary for courtship learning and is hypothesised to signal through Gαq. Blue light illumination of expressing flies during courtship training subsequently produced a defect in courtship learning, consistent with the hypothesised function of Gαq-linked signalling in this behaviour.

As this study presents a method to produce RGS-based G protein inhibitors, future studies will focus on the design and validation of a Gαi inhibitor tool. A selective Gαi inhibitor is currently being tested. Together, these tools will provide a valuable addition to the current methods for the modulation of GPCR signalling.

Through the design and validation of an RGS2-based optogenetic tool, this study presents a reversible, light-induced inhibitor of endogenous Gαq-linked GPCR signalling that was previously absent from the molecular toolbox. This tool presents many advantages over current techniques used to manipulate GPCR signalling, including high spatiotemporal resolution, selectivity, and reversibility of inhibition, as well as the ability to be easily packaged for viral delivery. Moreover, its demonstrated ability to effectively function in both mammalian and invertebrate systems drastically increases the scope of its application for the investigation of G protein signalling and neuromodulation in a wide variety of fields.

Chapter 1 | Background and introduction

Neuronal communication has been a subject of intense study for many decades, beginning with the visualisation of the seemingly ubiquitous tissue of the nervous system in the 1870's. This was followed by the seminal works of Santiago Ramón y Cajal beginning in 1888, identifying distinct neuronal cell types. However, it was not until the early 1950's that this theory was validated through the visualisation of the synapse. Together, this confirmed that neurons did not exist as vast continuations, but as discreet structures.

It is well understood that synaptic connections between neurons facilitate the transmission of information throughout the nervous system, and that the processes underlying this communication allow hardwired neural networks to operate in a dynamic manner. The mechanisms behind such dynamic functionality are now beginning to be unravelled using pharmacological manipulation, as well as new technologies that allow for the control of individual cellular pathways with unparalleled precision. However, as we continue to push the limits of our understanding, the technical demands required for further investigation increase. Subsequently, there is a need for a more diverse repertoire of tools for neuronal manipulation.

1.1 Information transfer in the nervous system

Information transfer at synapses can be broadly classified as either electrical or chemical. Electrical synapses involve the direct transmission of signals through cytoplasmic couplings known as gap junctions (Bennett and Zukin 2004, Pereda 2014). Chemical synapses, however, involve the release of neurotransmitters from the pre-synaptic neuron into the synaptic cleft. The reception of these molecules occurs through either ionotropic or metabotropic receptors on the receiving, post-synaptic neuron (Pereda 2014).

Ionotropic receptors are ligand-gated ion channels located close to the neurotransmitter release site and are involved in the rapid transduction of signals from one cell to another (Huang and Thathiah 2015). The resulting signal is designated as either excitatory or inhibitory (Huang and Thathiah 2015). As a result, ionotropic receptors mediate rapid synaptic transmission, occurring in the order of milliseconds. Metabotropic receptors are G protein coupled receptors (GPCRs) and are located distally relative to the neurotransmitter release site (Huang and Thathiah 2015). GPCRs mediate a cascade of intracellular signalling events and are often indirectly coupled to ion channels (Huang and Thathiah 2015). GPCR-mediated synaptic

transmission is generally considered a slow means of signal transduction, with signalling occurring over seconds to minutes. For a more in depth review of GPCRs in neuronal signalling, please see (Huang and Thathiah 2015).

GPCRs transduce signals from neuromodulators, altering the properties of target neuronal circuits to modify their firing, synaptic release and synaptic response properties, as well as transcriptional and translational changes (Huang and Thathiah 2015). This allows neuronal circuits to respond to transmitted information in several ways, increasing the number of functional outputs that can be produced by an anatomically defined circuit. Consequently, neuromodulation through GPCRs permits dynamic regulation of neuronal networks, a property that is believed to underlie many higher processes such as learning and memory.

1.2 GPCRs – a closer look

The GPCR sub-family encompasses the largest class of cell-surface receptors in the human genome. With over 800 GPCRs being expressed in almost every cell in the body, they contribute to an extensive range of bodily functions (Atwood, Lopez et al. 2011, Masseck, Rubelowski et al. 2011, Lane, Abdul-Ridha et al. 2013). Over 90% of GPCRs are expressed within the brain, governing a variety of neural processes ranging from cognition and memory to the regulation of mood and the comprehension of pain (Gainetdinov, Premont et al. 2004, Huang and Thathiah 2015).

The GPCR is comprised of seven transmembrane α-helices, interspersed by three extracellular and three intracellular loops (Kobilka 2007, Zamponi and Currie 2013). The extracellular and membrane spanning components of the receptor are responsible for the binding of ligands resulting in the subsequent activation of the GPCR (Masseck, Rubelowski et al. 2011). The intracellular structures are involved in the subcellular localisation and trafficking of the receptor, as well as the selective binding of G proteins, consisting of the Gα and fused Gβγ subunits (Tuteja 2009, Masseck, Rubelowski et al. 2011, Zamponi and Currie 2013).

1.2.1 G protein-coupled receptor activation

Upon ligand binding, the GPCR undergoes a conformational change resulting in the release of a guanosine diphosphate (GDP) molecule and the ensuing attachment of guanosine triphosphate (GTP) to the G protein (Lane, Abdul-Ridha et al. 2013). This conversion activates

one of three main intracellular cascades depending on the nature of the associated G protein: Gαs, Gαi, or Gαq (Fig. 1.1) (Kobilka 2007, Atwood, Lopez et al. 2011, Masseck, Rubelowski et al. 2011, Zamponi and Currie 2013). However, the exact interactions that occur between the G protein and intracellular signalling elements depend on the time and location of GPCR expression, as well as the signalling dynamics of the ligand (Jaeger, Armstrong et al. 2014). For an extensive review of GPCR structure and function, please see (Rosenbaum, Rasmussen et al. 2009, Gurevich and Gurevich 2017). For an extensive review on GPCRs in CNS health and disease, please see (Leung and Wong 2017, Azam, Haque et al. 2020).

1.2.2 The guanine nucleotide cycle of G proteins

Heterotrimeric GPCRs mediate cellular responses to a wide range of extracellular conditions. As a result of this, the proper coordination of signalling events elicited by GPCRs needs to be attained to ensure an appropriate physiological response. One level of coordination is the cessation of signalling in a manner that prevents over-stimulation of a particular pathway, an event that could lead to disruptions in cellular homeostasis and eventuate in the development of pathophysiological conditions.

G protein coupled receptors transduce signals through interactions with heterodimeric G proteins, enhancing the exchange of the GDP molecule associated with the inactive Gα

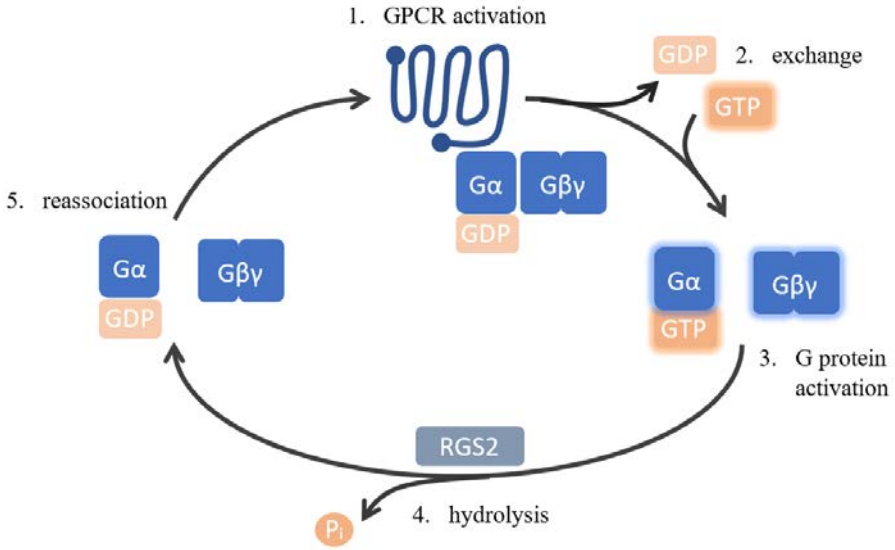

Figure 1.1 | *Canonical RGS protein function as a Gα subunit GAP.* Upon GPCR activation (1), the GDP associated with the inactive Gα subunit of the heterotrimeric G protein is replaced by GTP (2), allowing the Gα subunit to dissociate from the fused Gβγ subunits (3). GTP is hydrolysed to GDP via the intrinsic GTPase activity of the Gα subunit (4). RGS proteins, such as RGS2, bind to and stabilise the transition state of the Gα subunit, thereby increasing the rate of GTP hydrolysis. Once hydrolysed, the GDP-Gα subunit reassociates with the Gβγ subunits (5), and signalling is ceased. Figure based on Kehrl 1998.

subunit to GTP (fig. 1.1) (Kehrl 1998, Sprang 2016) (for an extensive review on G proteins, please see (McCudden, Hains et al. 2005, Syrovatkina, Alegre et al. 2016)). This results in the dissociation of Gα-GTP from the fused Gβγ subunits, allowing for the activation of downstream effectors and resulting signalling cascades. The inactivation of the Gα protein, however, does not occur through GTP-to-GDP exchange, but through an independently regulated hydrolysis reaction (Sprang 2016).

The Gα subunit possess intrinsic GTPase activity, resulting in the hydrolysis of the associated GTP back to GDP, allowing the Gα subunit to reassociate with Gβγ and prevent further signalling (Fig. 1.1) (Sprang 2016). This process is, however, relatively slow and does not account for the transient nature of GPCR-induced intracellular signalling. Therefore, Gα activity requires further cellular control to increase the dynamic capacity of signalling and prevent prolonged activation. This is in part performed by regulator of G protein signalling, or RGS, proteins.

1.2.3 Gαs signalling

Activation of Gαs-linked GPCRs, such as the β_2 adrenergic receptor (β_2AR), allows the GTP-bound G protein to dissociate from the receptor and activate a number of intracellular second messengers such as adenylate cyclase (AC) (Liggett 2002, Masseck, Rubelowski et al. 2011). This enzyme converts ATP to cyclic adenosine monophosphate (cAMP), leading to the ensuing activation of signalling cascades. These result in the activation of cyclic nucleotide-gated (CNG) channels, the mitogen-activated protein kinase (MAPK) pathway, and protein kinase A-associated L-type calcium channels (LTCC) (Fig. 1.2) (Ludwig, Zong et al. 1998, Minobe, Maeda et al. 2014, Peng, Li et al. 2016). The phosphorylation of the cAMP-response element binding protein (CREB) by protein kinase A (PKA) is well established to be involved in long-term memory storage and the late phase of long-term potentiation (LTP) (Ying, Futter et al. 2002, Kandel 2012), as well as mediating increases in spine density of hippocampal neurons associated with plasticity (Murphy and Segal 1997) (Leung and Wong 2017). Gαs signalling has also been associated with cAMP-dependent activation of the mitogen-activated protein kinase/extracellular signal-regulated kinases, or ERKs, crucial for the formation of long-term memories (Hagena, Hansen et al. 2016, Leung and Wong 2017).

1.2.4 Gαi signalling

Conversely, Gαi-linked GPCRs, such as the dopamine receptor D_2 (D_2R), are most often associated with the inhibition of the Gαs pathway (Yin, Chen et al. 2020). This results in a decrease in cAMP concentrations within the cell through negative interactions with AC, resulting in the inactivation of the associated downstream pathways (Fig. 1.2) (Enomoto, Takano et al. 1995, Stryjek-Kaminska, Piiper et al. 1996). Gαi-linked signalling has been associated with reduced hippocampal spine density throughout adolescence via the internalisation of the *N*-methyl-D-aspartate receptor (NMDAR) subunits critical for synaptic plasticity (Jia, Zhao et al. 2013, Leung and Wong 2017). Furthermore, receptors coupled to

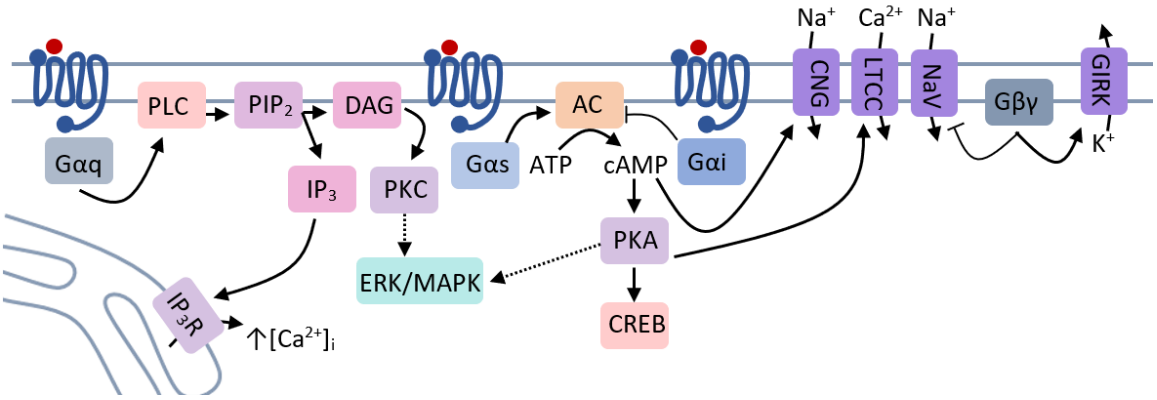

Figure 1.2 | *overview of GPCR signalling.* Upon GPCR activation, the associated Gα protein is activated and triggers an intracellular signalling cascade. Gαq G proteins activate protein lipase C (PLC) (Lane, Abdul-Ridha et al. 2013) which converts the membrane lipid, phosphatidylinositol-4, 5-bisphosphate (PIP_2), into diacylglycerol (DAG) and inositol-1, 4, 5-triphosphate (IP_3) (Gresset, Sondek et al. 2012, Lyon, Dutta et al. 2013). IP_3 causes the release of calcium from the endoplasmic reticulum through the IP_3 receptor (IP_3R) (Neher and Sakaba 2008, Lyon, Dutta et al. 2013). Gαs G proteins activate adenylate cyclase (AC) (Liggett 2002, Masseck, Rubelowski et al. 2011), which converts ATP to cAMP, leading to the activation of protein kinase A and the phosphorylation of cAMP-response element binding protein (CREB). Both PKA and PKC activate the extracellular signal-regulated kinase (ERK) and mitogen-activated protein kinase (MAPK) pathways (Ludwig, Zong et al. 1998, Minobe, Maeda et al. 2014, Peng, Li et al. 2016). cAMP also induces the influx of sodium and calcium ions into the cell through the activation of cyclic nucleotide-gated (CNG) channels and indirectly activates L-type calcium channels (LTCC). The Gαi G protein inhibits AC, causing a decrease in cAMP (Yin, Chen et al. 2020). The fused Gβγ subunits, which dissociate from the Gα subunit upon activation, stimulate the activity of voltage-gated sodium (Nav) channels as well as G protein-coupled inwardly rectifying potassium (GIRK) channels (Berlin, Keren-Raifman et al. 2010). Figure was constructed using information from the cited sources.

Gαi are of interest in cognitive impairment associated with chronic opioid use (Robinson, Gorny et al. 2002, Ersek, Cherrier et al. 2004, Schiltenwolf, Akbar et al. 2014), as well as in analgesia (Vučković, Srebro et al. 2018), addiction (Parolaro, Vigano et al. 2007), and anxiety (Walf and Frye 2007, Niswender and Conn 2010).

1.2.5 Gαq signalling

The Gαq-linked signalling pathway, such as that coupled to the muscarinic acetylcholine receptor M_3 (M_3R), is most often associated with the release of calcium from intracellular stores and the subsequent increase in cytosolic calcium concentrations ($[Ca^{2+}]_i$) (Zhang, Ma et al. 2006, Zamponi and Currie 2013, Maeda, Qu et al. 2019). This occurs through the activation of protein lipase C-beta (PLC-β) by Gαq-GTP (Lane, Abdul-Ridha et al. 2013). Upon activation, PLC-β cleaves the membrane lipid, phosphatidylinositol-4, 5-bisphosphate (PIP_2), into inositol-1, 4, 5-triphosphate (IP_3) and diacylglycerol (DAG) (Gresset, Sondek et al. 2012, Lyon, Dutta et al. 2013). IP_3 binds the IP_3 receptor (IP_3R) located on the endoplasmic reticulum (ER), causing an efflux of stored calcium and the subsequent increase in $[Ca^{2+}]_i$ (Fig. 1.2) (Neher and Sakaba 2008, Lyon, Dutta et al. 2013).

When activated in the neuron, this process results in the modulation of synaptic strength as well as the alteration of neurotransmitter release probability at synaptic sites (Schwartz, Blackmer et al. 2007, Mamidi, Panda et al. 2014, Galvan, Perez-Rosello et al. 2015). ER calcium release triggered by Gαq is also linked to the regulation of transient receptor potential channel 3 (TRPC3) activation (Hartmann, Dragicevic et al. 2008, Huang and Thathiah 2015). These channels are involved in the influx of cations into the cell, resulting in the generation of slow excitatory post-synaptic potentials, or sEPSPs, thought to be important for the induction of long-term depression (LTD) (Konnerth, Dreessen et al. 1992, Huang and Thathiah 2015).
Whilst IP_3 acts at the cytoplasmic level, DAG remains in the membrane where it recruits the enzyme, protein kinase C (PKC) (Huang 1989, Newton 1995). The activation of PKC by DAG leads to several downstream effects. These include alterations in membrane structure, regulation of cell growth, modulation of aspects of learning and memory, transcriptional regulation, and receptor desensitisation (Linden, Murakami et al. 1986, Newton 1995, Namkung and Sibley 2004). An isoform of PKC, PKCγ, is involved in modulating aspects of LTP and LTD, as well as being involved in the processing of sensory inputs such as pain (Linden, Murakami et al. 1986, Malenka, Madison et al. 1986, Linden, Sheu et al. 1987, Linden and Connor 1991).

1.2.6 Gβy signalling

The Gβγ pathway has a prominent role in the activation of downstream signalling pathways. Upon dissociation of the GTP-bound Gα subunit from the GPCR complex, the fused Gβγ

subunits are displaced, allowing them to interact with effectors. These effectors induce the inactivation of voltage-gated sodium channels and the activation of G protein-coupled inwardly rectifying potassium (GIRK) channels (Berlin, Keren-Raifman et al. 2010). The Gβγ subunits also interacts with the MAPK pathway and phosphatidylinositol-4,5-bisphosphate-3-kinase (PI3 kinase) (Mochizuki, Ohba et al. 1999, Mittal, Pavlova et al. 2011).

1.2.7 Termination of signalling

Proceeding GPCR activation and the subsequent interaction between GTP-Gα and its effectors, the GTP molecule is hydrolysed back to GDP (Berman, Wilkie et al. 1996). This reaction results in the conversion of the G protein to an inactive confirmation, thereby terminating further signalling events and increasing its affinity for the GPCR. Additional to the intrinsic GTPase activity of the G protein itself, GTPase activating proteins (GAPs) possess the ability to modulate this process. One such family of proteins, the RGS proteins, act through their RGS domain, decreasing the energy required for the transition state of the G protein, effectively increasing the rate of GTP hydrolysis (Berman, Wilkie et al. 1996). This results in a decrease in the time taken for the activated G protein to return to an inactive confirmation, expanding the GPCR's repertoire of responses to a single ligand. Termination of signalling is also performed through the process of receptor internalisation (Pavlos and Friedman 2017).

1.2.8 Structure and function of regulator of G protein signalling proteins

It was originally proposed that the lifetime of the GTP-bound G protein was governed exclusively by the intrinsic GTP hydrolysis activity of the Gα subunit. However, the rate of GTP hydrolysis observed in purified proteins did not match those seen *in vitro*, suggesting an additional cellular mechanism for the inactivation of GPCR signalling (Breitwieser and Szabo 1988, Yatani, Mattera et al. 1988, Vuong and Chabre 1991). Evidence of such a mechanism was first uncovered in *Saccharomyces cerevisiae* (Chan and Otte 1982, Chan and Otte 1982, Dohlman, Apaniesk et al. 1995), and then further confirmed in *Caenorhabditis elegans* and mammalian cells during the 1990's (De Vries, Elenko et al. 1996, Druey, Blumer et al. 1996, Koelle and Horvitz 1996, Siderovski, Hessel et al. 1996, Watson, Linder et al. 1996, Koelle 1997), followed by the identification of RGS proteins as regulators of G protein signalling.

It is now well established that RGS proteins function as GTPase accelerating proteins, or GAPs, for GTP-bound Gα subunits. This is achieved by binding three flexible Gα switch

domains, resulting in the stabilisation of the transition state of the Gα-GTP complex, a conformation required for GTP hydrolysis (Soundararajan, Willard et al. 2008, Kimple, Bosch et al. 2011). As a result, RGS proteins increase the intrinsic GTPase activity of the Gα subunit (Fig. 1.1). This GTPase accelerating function is performed by a conserved ~120 amino acid RGS domain, or RGS-box, that directly interacts with the GTP-Gα subunit (Soundararajan, Willard et al. 2008). The RGS domain has been shown to be both necessary and sufficient for GAP activity (Soundararajan, Willard et al. 2008).

There are over 35 recorded members of the RGS superfamily known to be encoded by the mammalian genome, with 20 classical and >15 non-classical RGS proteins (Heximer 2013). More than 50% of these display GAP activity towards one or more Gα proteins (Heximer 2013). Based upon sequence and domain homology, the classical RGS proteins can be divided into four main subfamilies (R7, R12, RZ and R4) (Heximer 2013). The largest of these RGS subfamilies is the R4 family, with proteins of this family consisting of an RGS domain with a minimal N- and C-terminus (Xie, Chan et al. 2016). This simplicity of structure is also seen in the three members of the RZ family (Nunn, Mao et al. 2006). RGS proteins of the R12 and R7 families, as well as those of the non-classical RGS subfamilies such as SNX13, show increasingly complex structures (Zheng, Ma et al. 2001, Anderson, Posokhova et al. 2009, Asli, Sadiya et al. 2018). These proteins possess several other domains known to confer Gα-directed GAP specificity, determine subcellular locality, and perform other functions outside of their GAP activity.

For RGS proteins to act as GAPs, the RGS protein itself must be located in proximity to the Gα-subunit. Interestingly, a number of RGS proteins are known to be localised in areas relatively devoid of their target G protein (Chatterjee and Fisher 2000, Heximer, Lim et al. 2001). However, it has been observed that RGS proteins can translocate to the area of GTP-bound G proteins and may present a mechanism by which cells control the level of inhibition evoked by an RGS protein on a given GPCR pathway (Heximer, Lim et al. 2001). Localisation of RGS proteins has also been suggested to play an important role in determining the specificity of a given RGS protein toward Gα subtypes (Heximer, Lim et al. 2001).

RGS proteins possess various degrees of specificity for the different Gα subtypes with the majority of RGS proteins showing affinity for both GTP-bound Gαi and Gαq (Riddle, Schwartzman et al. 2005). However, as the complexity of RGS protein structure increases, a marked specificity for Gαi can be observed, with the exception of SNX13 (Zheng, Ma et al. 2001, Riddle, Schwartzman et al. 2005). Interestingly, one member of the R4 subfamily, RGS2, has been shown to possess markedly high affinity to Gαq, with little to no affinity towards

other G protein subtypes despite its relatively simplistic structure (Heximer, Watson et al. 1997, Bernstein, Ramineni et al. 2004).

1.3 Chemogenetic tools for the study of neuronal networks and neuromodulation

In order to study the complex neural circuitry that governs aspects of cognition such as learning and memory, tools are required that allow for the manipulation of defined neural circuits, connections, and signals. The manipulation of GPCRs through pharmacology has dominated the field for many decades. However, the combination of cell type and receptor heterogeneity poses problems for this technique. To overcome this, recent advances in neuroscience have seen the development of techniques allowing for the stimulation of neurons with high spatiotemporal precision, providing a powerful means of studying the processes of neuromodulation within the brain.

A number of chemicals have been developed that allow for the targeted activation of genetically engineered GPCR variants, a technique known as chemogenetics (Urban and Roth 2015). These include the receptors activated by synthetic ligand, the designer receptors exclusively activated by designer drugs and the Allatostatin receptor/ Allatostatin system (chemogenetic tools summarised in table 1.1). For a more extensive review on chemogenetic tools, please see (Spangler and Bruchas 2017).

1.3.1 Receptors activated solely by synthetic ligands and designer receptors exclusively activated by designer drugs

In 1998, Coward and colleagues developed an engineered GPCR variant that responds solely to synthetic, small molecular drugs (Coward, Wada et al. 1998). To achieve this, the second loop of the kappa opioid receptor was replaced with that of the delta opioid receptor. The resulting chimeric receptor was found to have a decreased sensitivity to endogenous ligands but was able to be activated upon the addition of the exogenous ligand, spiradoline (Coward, Wada et al. 1998). This technique was termed RASSL, or receptors activated solely by synthetic ligands (Coward, Wada et al. 1998, Tschammer, Dorfler et al. 2010) (table 1.1). It was later found that the exogenous ligand used to activate these receptors not only activated the RASSL-based opioid receptor no. 1 (Ro1), but also possessed affinity for endogenous mammalian kappa opioid receptors (Meecham, Boyle et al. 1989). This complicates the use of

this tool as it limits the user's ability to discern the observed response as either background activity or activity due to the activation of the engineered receptor.

Following on from the development of RASSLs, a new technique coined the 'DREADD system', or designer receptors exclusively activated by designer drugs, was developed (Coward, Wada et al. 1998, Armbruster, Li et al. 2007, Tschammer, Dorfler et al. 2010, Urban and Roth 2015) (table 1.1) (for an extensive review on DREADDs, please see (Burnett and Krashes 2016, Roth 2016)). The Gαq-coupled human M_3 muscarinic (hM_3Dq) DREADD employs the use of clozapine-N-oxide (CNO) (Armbruster, Li et al. 2007). This pharmacologically inert clozapine analogue binds to and selectively activates an engineered GPCR. It was reported that the engineered receptor had comparable activation properties to that of an endogenously expressed M_3 muscarinic receptor activated by acetylcholine (Armbruster, Li et al. 2007).

Although widely utilized today with many biological questions and disease mechanisms uncovered through it use, the DREADD system possesses key disadvantages. Firstly, CNO has been found to have a low clearance rate from cells, with levels unable to return to baseline following activation (Bender, Holschbach et al. 1994, Smith, Bucci et al. 2016). Secondly, recent work has uncovered that systemically injected CNO does not enter the brain and has little affinity for the DREADD receptor (Gomez, Bonaventura et al. 2017). This study demonstrated that CNO, when administered *in vivo*, is converted to clozapine, which freely enters the brain and has high affinity for the engineered receptors, inducing potent activation of downstream signalling pathways. This presents several problems, since clozapine can also bind endogenous receptors, which when combined with the late-onset effects of excess systemic CNO, can cause off-target effects and behavioural changes (Armbruster, Li et al. 2007, MacLaren, Browne et al. 2016, Gomez, Bonaventura et al. 2017, Ilg, Enkel et al. 2018, Bærentzen, Casado-Sainz et al. 2019). Furthermore, experiments conducted using the DREADD system must now consider how intrinsic differences in CNO metabolism between animals will affect experimental variability and reproducibility.

To overcome these challenges, a new generation of synthetic ligands have been developed for the activation of DREADDs, including Compound 21, JHU37152 and JHU37160 (Chen, Choo et al. 2015, Bonaventura, Eldridge et al. 2018, Thompson, Khajehali et al. 2018). However, the potential for off-target effects of these compounds are yet to fully investigated (Goutaudier, Coizet et al. 2019). In 2015, the classical DREADD was redesigned by mutating the existing the κ-opioid receptor-DREADD, producing an inhibitory receptor activated by a κ-opioid agonist metabolite, salvinorin B (Vardy, Robinson et al. 2015). This

not only bypasses the need for CNO or CNO-analogues, but allows for the utilisation of multiple, individually activated DREADDs within one system (Vardy, Robinson et al. 2015). However, salvinorin B does possess a level of affinity for endogenous κ-opioid receptors (Roth 2016).

1.3.2 Allatostatin receptor/ Allatostatin system

A more recent chemogenetic mechanism designed to manipulate GPCR signalling is the Allatostatin receptor/ Allatostatin (AlstR/AR) system developed by the Callaway lab in 2002 (Lechner, Lein et al. 2002) (table 1.1). This technique utilises the *D. melanogaster* allatostatin receptor; a GPCR involved in insect hormone synthesis, which was found to be insensitive to the mammalian allatostatin analogue, somatostatin (Birgul, Weise et al. 1999, Lechner, Lein et al. 2002). When activated with insect allatostatin, the exogenous receptor was shown to activate endogenous GIRK channels in mammalian cells. This technique was demonstrated to inhibit mammalian cortical neurons through the Gαi-coupled pathway and presented a reversible mechanism of neuronal silencing (Lechner, Lein et al. 2002). However, due to the nature of the receptor, this system is limited to the inhibition of neuronal signalling, and due to its design, is unable to be used in *D. melanogaster*.

1.3.3 Limitations of chemogenetics

Despite the abundance of chemogenetic techniques used to modulate GPCR signalling, a number of limitations have become apparent through their use (limitations summarised in table 1.1, also see (Spangler and Bruchas 2017)). The first major limitation is temporal resolution. GPCRs regulate aspects of cellular signalling that occur within a minute to second timeframe (Martin, Lopez de Maturana et al. 2005). However, as chemogenetic mechanisms rely on the activity of small molecular drugs to activate engineered GPCR variants, they are inherently limited by the rate of diffusion of these effector molecules into and between cells (Masseck, Rubelowski et al. 2011). Furthermore, the signal duration using these techniques is reliant on the clearance rate of the molecule–a process that can take in the order of hours–from the cytoplasm of the cell, as well as from the body of the animal if used *in vivo*. This is problematic as it presents issues such as continued receptor activation and cytotoxicity, an unappealing feature when designing experiments requiring precise, controlled modulation of intracellular events (Masseck, Rubelowski et al. 2011).

A further limitation that arises from the use of chemogenetic mechanisms for GPCR activation is the potential for off-target effects and the resulting difficulty for their application *in vivo* (Masseck, Rubelowski et al. 2011). Due to the need for synthetic drugs, it is difficult to anticipate whether their application will produce additional effects within the cell other than that intended. This becomes problematic when attempting to determine whether the observed effects are due solely to the interactions occurring between the activated receptor and its downstream targets. Consequently, great interest has been directed towards alternate techniques of cellular activation, such as the development and optimisation of optogenetic tools for receptor stimulation and their application in both *in vitro* and *in vivo* systems (Kennedy, Hughes et al. 2010, Deisseroth 2015).

1.4 Optogenetic tools for the study of neuronal networks and neuromodulation

Optogenetics describes a technique that utilises genetically engineered, light-sensitive proteins that are expressed in cells–typically neurons–to control defined aspects of their physiology when illuminated with a specified wavelength of light (Deng, Goldys et al. 2014, Deisseroth 2015, Hallett, Zimmerman et al. 2016) (optogenetic tools summarised in table 1.1). In comparison to techniques utilising small chemicals, the technique of optogenetics possesses many advantages, particularly in the field of neuroscience research. The use of optogenetic tools offers a higher level of spatiotemporal resolution, making them ideal for the study of physiological and pathophysiological mechanisms of neuronal function, as well as their interactions and circuit properties both *in vitro* and *in vivo* (Koyanagi and Terakita 2014). This technique offers non-intrusive modulation of cellular activity with little to no tissue damage, with genetic targeting for cell-type specificity and no off-target effects due to the nature of the stimulus (Deng, Goldys et al. 2014, Koyanagi and Terakita 2014, Govorunova, Sineshchekov et al. 2015). Furthermore, there is often no requirement for endogenous cofactors and reversion times are frequently superior to those of other techniques (Kennedy, Hughes et al. 2010). For a more extensive review of optogenetic tools, please see (Rost, Schneider-Warme et al. 2017, Spangler and Bruchas 2017)

1.4.1 Microbial rhodopsins

The first generation of optogenetic tools were focused on the use of a light-sensitive cation channel to modulate membrane excitability in mammalian neurons (table 1.1). They were first

implemented upon the discovery of the sensory photoreceptor, channelrhodopsin (ChR), isolated from the unicellular green alga, *Chlamydomonas reinhardtii* (Nagel, Ollig et al. 2002, Nagel, Szellas et al. 2003). When expressed in the membrane of neurons, ChRs evoke action potentials upon exposure to light by transitorily increasing membrane permeability to certain cations, often leading to suprathreshold membrane depolarisation (Nagel, Ollig et al. 2002, Lorenz-Fonfria and Heberle 2014, Govorunova, Sineshchekov et al. 2015). Since their discovery, several variants have been cloned from other algal species or artificially developed to have different kinetics, spectral responses, and light sensitivities (Schobert and Lanyi 1982, Chow, Han et al. 2010). Recent development in this field has focused on engineering variants with altered ion permeability, conductance, and peak excitability; further increasing their potential in neuroscience research (Lin 2011, Lin, Knutsen et al. 2013, Schneider, Grimm et al. 2015). (For a more extensive review on channelrhodopsins, please see the following articles: (Lin 2011, Deisseroth 2015, Rost, Schneider-Warme et al. 2017))

The use of microbial rhodopsins in the field of neuroscience research has led to many notable findings that have drastically furthered the scope of research in the area (Deisseroth 2015). For example, a number of *in vivo* studies exploring the neuronal control of behaviour using ChRs coupled to fibre optics have uncovered cellular projections and circuit patterns that regulate the control of social behaviour such as aggression (Lee, Kim et al. 2014, Takahashi, Nagayasu et al. 2014), anxiety (Tye, Prakash et al. 2011), fear (Haubensak, Kunwar et al. 2010, Tovote, Esposito et al. 2016) and reward (Witten, Lin et al. 2010), as well as defence- related behaviours (Wang, Chen et al. 2015), mating and parenting (Wu, Autry et al. 2014, Stagkourakis, Smiley et al. 2020) (Deisseroth 2015).

Furthermore, the pattern of the circuitries through which information travels throughout the brain are beginning to be mapped in detail with high precision using ChRs coupled with other techniques (Hunnicutt, Long et al. 2014). This has led to the improvement of other research technologies allowing positron emission tomography (PET) imaging and functional magnetic resonance imaging (fMRI) to map brain-wide activity patterns with cellular patterns (Lee, Durand et al. 2010, Thanos, Robison et al. 2013). Moreover, ChRs have made it possible to investigate other phenomena such as the regulation of excitation and inhibition in the brain, and the modulation of oscillatory activity in both sleeping and waking states (Cardin, Carlen et al. 2009, Sohal, Zhang et al. 2009, Yizhar, Fenno et al. 2011, Pfeffer, Xue et al. 2013, Siegle and Wilson 2014). For a more extensive review of the implication of channelrhodopsins within the field of neuroscience, please see the review article by Karl Deisseroth (Deisseroth 2015).

Nonetheless, although the use of ChRs and other light-sensitive channels have thus far presented the field with an invaluable understanding of brain circuitry and function, neurons are not exclusively activated by ion influx. It is well known that neurons possess many other membrane receptors that govern aspects of their activation and overall function, a number of which are GPCRs (Dong, Han et al. 2001, Maurel, Le Digarcher et al. 2011). Thus, great interest in the fields of optogenetics and neuroscience research has been directed towards the development of light-controllable mechanisms to modulate GPCR function and their downstream effectors. To date, a small number of light-activatable GPCR variants, as well as light-controllable effectors, have been developed and trialled.

1.4.2 Vertebrate and invertebrate rhodopsins

The first attempt to modulate GPCRs with light utilised invertebrate rhodopsin, a photosensitive receptor linked to Gαq that is known to activate non-selective cation channels resulting in membrane depolarisation in the insect eye (Palczewski 2006). It was believed that this response could be activated within mammalian cells in response to light. Through the expression of three components of the *D. melanogaster* visual transduction cascade in the *Xenopus* oocyte and hippocampal neurons (chARGe), it was demonstrated that action potentials could be consistently induced upon light illumination (Zemelman, Lee et al. 2002) (table 1.1). However, due to the requirement of three separate protein components, the chARGe system has been considered too complicated for *in vivo* use and has subsequently been underutilised in the field (Rost, Schneider-Warme et al. 2017). Moreover, its use of components involved in *D. melanogaster* signal transduction limits its use in this model organism.

Vertebrate rhodopsins such as rhodopsin 4 (Ro-4) have also been applied to control neuronal excitability (table 1.1). Upon illumination of heterologously expressed Ro-4, the associated Gαi G protein causes the activation of post-synaptic potassium currents paired with the inactivation of pre-synaptic calcium influx, resulting in an overall reduction in neuronal excitability (Rost, Schneider-Warme et al. 2017). In 2005, Li et al. utilised this system in combination with ChR2 to modulate the frequency of spontaneous bursting activity within the spinal cord of embryonic chickens (Li, Gutierrez et al. 2005). This is the first reported use of optogenetics within an *in vivo* system. However, despite this promising start, it was found that continuous or repeated light stimulation of Ro-4 resulted in a decline in the ability of the receptor to evoke a response (Rost, Schneider-Warme et al. 2017).

Building on the idea of using opsins as a method of optically inducing GPCR activation, the Deisseroth lab utilised vertebrate rhodopsins to activate both the Gαq and Gαs pathways in a system termed OptoXR (Airan, Thompson et al. 2009) (table 1.1). This was achieved by engineering adrenergic receptor-like opsin GPCRs. The chimeric receptors were designed through alignment of either the Gαq-coupled human α1a-adrenergic receptor or Gαs-coupled hamster β2-adrenergic receptor with the Gt-coupled bovine rhodopsin as demonstrated previously by Kim et al. (2005) (Kim, Hwa et al. 2005). The conserved receptor residues were subsequently identified, allowing for the replacement of the intracellular rhodopsin loops with the corresponding adrenergic loops. This resulted in a light responsive rhodopsin tool linked to the corresponding adrenergic intracellular pathways. However, as with Ro-4, issues pertaining to signalling termination and repetitive stimulation were also present for this technique (Bailes, Zhuang et al. 2012, Spangler and Bruchas 2017).

The biochemical basis of this limitation is the reliance of such rhodopsin-based tools on 11-*cis*-retinal to function and recover from bleaching post-activation (Bailes, Zhuang et al. 2012). When exposed to light, 11-*cis*-retinal is converted to all-*trans*-retinal and needs to be replaced to ensure the subsequent activation of the receptor (Fung, Hurley et al. 1981). Within the retina, enzymatic pathways exist to convert vitamin A into the *cis*-isoform of retinal needed by rhodopsin; a pathway not present elsewhere in the mammalian body (Fung, Hurley et al. 1981). Thus, unless continuously supplied by an exogenous source of 11-*cis*-retinal, opsin-based optogenetic systems will diminish in activity (Bailes, Zhuang et al. 2012). Although previous analysis of this system has shown robust responses upon illumination, these experiments have purely focused on end-point measurements of second messengers or single stimulation protocols (Airan, Thompson et al. 2009, Oh, Maejima et al. 2010). Nevertheless, it has now been demonstrated experimentally using live cAMP imaging in cells expressing the published optoXR constructs that, without 11-*cis*-retinal supplementation, the response generated upon illumination halved upon second stimulation, and diminished rapidly thereafter (Bailes, Zhuang et al. 2012).

Despite these limitations, rhodopsin-based tools have been widely used in the literature. An example is the use of OptoXRs in awake, behaving mice in a two-choice preference apparatus (Airan, Thompson et al. 2009). It was demonstrated in this research that illumination of the nucleus accumbens expressing the Opto-α1AR variant to evoke Gαq signalling was able to induce positive associations with one compartment of the apparatus, an association not observed in wild type mice. This technique has also allowed for the light-induced control of a

variety of other GPCRs, with the basis of their design utilised as a method for uncovering the G protein associations of orphan GPCRs (Morri, Sanchez-Romero et al. 2018).

To overcome the limitation of signal termination and issues relating to repetitive stimulation seen with rhodopsin-based tools, two alternative approaches have been developed. The invertebrate melanopsin engineered from the light activated Gαs-linked jellyfish opsin, JellyOp, can be repetitively stimulated, with cAMP levels able to be stably maintained for 15 minutes with repeated light exposure and terminated within 5 seconds (Bailes, Zhuang et al. 2012) (table 1.1). Alternatively, bistable opsins that can be dynamically controlled through exposure to different wavelengths of light allow for either transient or sustained activation of Gαi and Gαq-linked intracellular pathways (Spoida, Eickelbeck et al. 2016). As a result of the versatility of these melanopsin-based tools, *in vivo* applications have been innovative, ranging from vision restoration and the control of the sleep/wake cycle in behaving mice (Lin, Koizumi et al. 2008, Tsunematsu, Tanaka et al. 2013) (Rost, Schneider-Warme et al. 2017).

1.4.3 Photoactivated enzymes for the modulation of cyclic nucleotides

In addition to the modulation of GPCRs themselves, photoactivable enzymes involved in the production and degradation of cyclic nucleotides, the downstream molecules often associated with the activation of Gαs and Gαi/o pathways, have also been developed (Rost, Schneider-Warme et al. 2017). Photoactivable adenylate cyclase (PAC) enzymes found in bacteria (bPAC) and algae (euPAC and OaPAC) consist of a BLUF domain, involved in light sensing, coupled to a cAMP-producing catalytic domain (Iseki, Matsunaga et al. 2002, Ntefidou, Iseki et al. 2003, Stierl, Stumpf et al. 2011, Hirano, Takebe et al. 2019). These modular proteins have been utilised in the increase of cAMP levels in many model systems ranging from the modulation of grooming behaviour in *D. melanogaster* (Stierl, Stumpf et al. 2011) and pituitary-driven augmentation of the stress response in zebrafish larvae (De Marco, Groneberg et al. 2013), to the light-induced restoration of motility in AC-deficient rodent sperm cells (Jansen, Alvarez et al. 2015) (Rost, Schneider-Warme et al. 2017).

To compliment the light-induced production of cAMP, a light activated phosphodiesterase (PDE), LAPD, for the degradation of cAMP and cGMP was designed by Gasser et al. in 2014 (Gasser, Taiber et al. 2014) (table 1.1). This was achieved through the generation of a chimeric protein comprising the catalytic domain of human PDE2A and the red light-sensing phytochrome domain from *Pseudomonas aeruginosa*. This tool has been used to reduce cyclic nucleotide levels in a light-dependent manner in both Chinese hamster ovary

cells and zebrafish embryos (Gasser, Taiber et al. 2014, Rost, Schneider-Warme et al. 2017). Its use in neuroscientific research may be limited, however, due to the relatively low neuronal concentration of the heme-metabolite, biliverdin, needed to act as a chromophore for these phytochrome-based tools.

Table 1.1 Summary of current chemogenetic and optogenetic tools for neuroscience research

Technique		**Strengths**	**Weaknesses**
Chemogenetics	RASSLs, DREADDs, and AlstR/AR	• Non-invasive stimulation • Moderate spatial resolution • No specialised equipment needed • Potential for multiplexing (Vardy, Robinson et al. 2015).	• Cross-reactivity with endogenous receptors (Vonvoigtlander and Lewis 1988, Meecham, Boyle et al. 1989, Armbruster, Li et al. 2007, MacLaren, Browne et al. 2016, Gomez, Bonaventura et al. 2017, Ilg, Enkel et al. 2018, Bærentzen, Casado-Sainz et al. 2019). • Low clearance rate of some synthetic ligands (Bender, Holschbach et al. 1994, Smith, Bucci et al. 2016) • Low diversity of available receptors
Optogenetics	All optogenetic tools	• High spatiotemporal resolution	• Invasive stimulation • Specialised equipment required • Potential for thermal and phototoxicity
	Channelrhodopsins	• Potential for multiplexing (Schobert and Lanyi 1982, Chow, Han et al. 2010) • Many variants – altered ion permeability, conductance, and peak excitability (Lin 2011, Lin, Knutsen et al. 2013, Schneider, Grimm et al. 2015) • Repeated stimulation	• Limited to control of membrane excitability.
	chARGe and Ro-4	• Gαq and Gαi-linked signalling pathways	• Complicated as required many components • Reduction in response with repeated stimulation (Rost, Schneider-Warme et al. 2017)
	OptoXRs	• GPCR-specific signalling (Gαq, Gαs and Gαi pathways) • Potential for multiplexing • May have reduced background activation due to need for exogenous cofactor	• Long-sustained activation • Cannot be activated repetitively • Each receptor requires a chimeric protein to be produced
	JellyOP	• No exogenous cofactor needed • Transient and sustained activation, as well as repeated	• Limited to the Gαs signalling pathway

		stimulation (Bailes, Zhuang et al. 2012)	
	LAPD	• Possibility to multiplex with other tools • High tissue penetration of red light	• Low specificity - degrades both cAMP and cGMP (Gasser, Taiber et al. 2014) • Cofactor present at low concentration in many tissues. Biliverdin co-factor has limited membrane permeability in cells.

1.5 Future perspectives - light-induced protein dimerising systems for the modulation of protein-protein interactions

Recently, a new method to optically control proteins has been employed in the literature: a technique that utilises reversible, light-induced dimerisation. This system involves the use of naturally occurring protein dimers that can be fused to an engineered or 'split' variant of a protein of interest (Ballister, Aonbangkhen et al. 2014, Guntas, Hallett et al. 2015). Thus, upon illumination of the photosensitive portion of the dimer pair, light-induced conformational changes increase the affinity for the binding partner, resulting in dimerisation (Ballister, Aonbangkhen et al. 2014). Consequently, the fused protein of interest can be localised in a specific location or reconstituted, restoring its native activity. Examples of such systems include the light-sensing light-oxygen-voltage (LOV) domain and its engineered PDZ (ePDZ) binding partner, and the cryptochrome 2 (CRY2) and cryptochrome-interacting basic-helix-loop-helix 1 (CIB1) system (Liu, Yu et al. 2008, Kennedy, Hughes et al. 2010, Strickland, Lin et al. 2012, Rost, Schneider-Warme et al. 2017).

1.5.1 TULIP system

The TULIP system–a version of the LOV/ePDZ system–is structured so that the ePDZ-binding motif is engineered into the LOV-Jα caging domain (Strickland, Lin et al. 2012). The LOV domain incorporates the endogenous ubiquitous flavin mononucleotide (FMN) as a cofactor (Rost, Schneider-Warme et al. 2017). Illumination with blue-light induces a conformational change in the LOV-Jα domain, relieving the occlusion of the ePDZ-binding motif, leading to dimerisation (Strickland, Lin et al. 2012). This allows for the fused split protein of interest to be reconstituted, regaining its native function. The TULIP system has been demonstrated to function in both yeast and mammalian cells but has higher background activity in comparison to similarly functioning systems (Pathak, Strickland et al. 2014). This system has a binding

stoichiometry of 1:1 and a defined structural model of binding (Salomon, Christie et al. 2000, Salomon, Eisenreich et al. 2001, Crosson and Moffat 2002, Swartz, Wenzel et al. 2002, Freddolino, Gardner et al. 2013, Glantz, Carpenter et al. 2016). A similar system, iLID, has also been developed and utilised to control G protein localisation and activity (Guntas, Hallett et al. 2015, Guntas, Hallett et al. 2015).

1.5.2 Cryptochrome 2/ cryptochrome-interacting basic-helix-loop-helix 1 system

Another light-induced dimerisation system recently described in the literature is the CRY2/CIB1 system, a naturally occurring dimer isolated from the plant, *Arabidopsis thaliana* (Liu, Yu et al. 2008, Liu, Wang et al. 2013). In response to blue light, a conformational change in CRY2 exposes a binding site and allows it to form a complex with CIB1. This system has been confirmed to function in mammalian cells using the endogenous ubiquitous flavin adenine dinucleotide (FAD) as a cofactor, with rapid dimerisation and tuneable reversion kinetics following blue light illumination (Deisseroth 2015). A study published by Kennedy et al. in 2010 investigated the reaction kinetics between the fluorescently labelled, mammalian-optimised CRY2 N-terminal photolyase homology region (PHR) and CIBN (N-terminal domain of CIB1) expressed in HEK293 cells (Kennedy, Hughes et al. 2010). In this study, it was found that, in the 95% of cells that successfully expressed the system, mCherry-tagged CRY2(PHR) was able to interact with membrane-localised CIBN-eGFP within 300ms following illumination with 488 nm light. Translocation was said to be 90% complete within 10 seconds proceeding light stimulation, with complete dissociation occurring over the course of 12 minutes.

Furthermore, it was also demonstrated in this study that CRY2(PHR) translocation to the membrane could be activated to near identical magnitude upon repeated stimulation. Moreover, little to no loss in efficacy was recorded for up to six inductions. The CRY2(PHR)/CIBN system was also shown to have less background activity in the dark than comparable light-induced dimer systems. Furthermore, stimulation via two-photon microscopy was reported; this permits its use in both *in vitro* and in *vivo* models. In 2016, an optimised second-generation CRY2/CIB1 dimer was released, offering tuneable reversion kinetics in the form of fast and slow-cycling CRY2 mutants, as well as variants with further reduced background activity (Taslimi, Zoltowski et al. 2016). It was also later reported that CRY2 undergoes an oligomerisation process before binding to CIB1, which could increase the local

concentration of CRY2-fusion protein domains at the site of light-induced recruitment (Duan, Hope et al. 2017, Park, Kim et al. 2017).

Due to the promising nature of this tool, it is believed that the CRY2(PHR)/CIBN dimer pair presents a valuable opportunity for the development of a reversible, light activated mechanism of GPCR pathway modulation.

1.5.3 Selective optogenetic inhibitors of G protein signalling

In neuroscientific research, the disruption of signal processing pathways or circuitry tends to have more physiological relevance than artificially controlled activation. The disruption of specific cellular signalling and events in genetically defined cells during the performance of behavioural tasks can inform researchers as to the involvement of specific cellular events in that behaviour. In addition to their involvement in central nervous system, G protein signalling is a fundamental aspect of many physiological and pathophysiological processes such as the textbook examples of cardiovascular control, direct control of non-neuronal tissues for the fight or flight response, and the peripheral sensing of sight, smell, and taste. Despite intense investigation, there are still numerous GPCRs in the mammalian genome with physiological roles yet to be fully understood. In addition, despite the large array of chemical and optogenetic-based tools already available to manipulate these processes, tools that can achieve selective, light-activated inhibition of G protein signalling are still lacking. These tools, if available, would be greatly beneficial at uncovering the physiological roles of many GPCRs.

We hypothesise that an optogenetic tool design that can disrupt G protein signalling can be developed by combining a photodimeriser system and protein domains that selectively disrupt G protein signalling via a mislocation and light-induced relocalisation approach. The proceeding study establishes a mechanism to produce RGS-based tools to selectively inhibit Gα-linked GPCR signalling both *in vitro* and *in vivo*, utilising the CRY2/CIBN system and the selective Gαq modulator, RGS2. Future studies will focus on the inhibition of the Gαi and Gαs signalling pathways using a similar design.

1.6 Aims

1. Develop an optogenetic system to selectively inhibit Gαq signalling based on the light-induced relocalisation of a selective RGS domain.

2. Validate the ability of the system to selectively inhibit the Gαq-linked signalling pathways in response to light in behaving animals.

Chapter 2 | Design and validation of Photo-Induced G protein Modulator – Inhibitor Gαq (PIGM-Iq) in mammalian cells

2.1 Introduction

One possible approach to produce an optogenetic Gαq inhibitor is to identify either a strong inhibitor of the active site of activated Gαq or an enzyme that accelerates the termination of Gαq signalling and use light to control its function. The control of enzyme activity with light was previously described in a review by Liu and Tucker and can include the relocation of target proteins as well as the reconstitution of split enzymes (Liu and Tucker 2017).

2.1.1 Regulator of G protein signalling 2 – A GAP for Gαq.

The ideal optogenetic tool for the inhibition of Gαq would have highly selective, potent inhibitory activity towards Gαq under light exposed conditions, whilst possessing no activity under dark conditions. The RGS domain of RGS2 appears to be a good candidate as a selective Gαq inhibitor as it has been previously demonstrated to possess a higher affinity for Gαq over Gαi (Heximer, Srinivasa et al. 1999, Gu, He et al. 2007). For a review on RGS proteins and RGS2 selectivity, please see (Heximer 2013).

Unlike most other RGS proteins which are either Gαi selective or possess affinity for multiple Gα proteins, RGS2 is known to possess a high level of GAP specificity towards GTP-bound Gαq. While it has been proposed that RGS selectivity towards different G proteins is likely due to cell-type restricted gene expression and compartmentalisation within different cell populations, it is believed that RGS2 itself possesses three additional unique attributes that increase its affinity towards Gαq over the structurally similar Gαi (Heximer 2013):

I. RGS2 is recruited to Gαq-linked GPCRs

When the different domains and segments of the RGS2 protein were purified and expressed in various mammalian cell lines, the N-terminus of RGS2 was found to bind to the intracellular loop of several Gαq-linked receptors such as the M_1 muscarinic acetylcholine receptor

(mAChR), the α1A-adrenergic receptor and the androgen receptor (Bernstein, Ramineni et al. 2004, Hague, Bernstein et al. 2005, Wang, Zeng et al. 2005). However, no coupling has been observed towards the highly homologous Gai-linked receptors of the same subfamilies (Bernstein, Ramineni et al. 2004).

It was demonstrated by Gu et al. that the disruption of the N-terminal amphipathic helix of RGS2 and the subsequent removal of its ability to associate with the plasma membrane did not prevent binding to the Gαq-linked M_1 muscarinic receptor (Gu, He et al. 2007). This indicated that the association exists outside of the ability of RGS2 to associate with the plasma membrane but does depend on the presence of the N-terminus of the protein.

II. RGS2 has a uniquely selective RGS domain

RGS2 possesses three unique residues (C106, N184 and E191) within its RGS domain not seen in other members of the R4 subfamily. These residues are thought to confer binding specificity towards Gαq over Gαi (Heximer, Srinivasa et al. 1999). By replacing these three residues with the corresponding residues of RGS4, it was found that RGS2 no longer possessed high affinity towards Gαq, allowing it to act as an efficient GAP for Gαi (Heximer, Srinivasa et al. 1999). By comparing the three analogues residues of RGS4 in the RGS4/Gαi structure, it was found that C106 and N184 made important contacts within the RGS-Gα interface, whilst the third residue lay outside of this region (Nance, Kreutz et al. 2013).

The aforementioned residues are believed to result in an orientation distinct from that observed in the 3D structural models of the nine other RGS-Gαi complexes, and this difference in binding prevents RGS2 from serving as an efficient GAP for Gαi whilst retaining potent activity towards Gαq (Nance, Kreutz et al. 2013). The SwI switch region and T187 of Gαq uniquely interact with the C106 and N184 residues of RGS2 (Nance, Kreutz et al. 2013). It is further hypothesised that the E191 residue of RGS2 may help in selecting against Gαi binding as it does not appear to directly interact with Gαq (Nance, Kreutz et al. 2013). However, despite the apparent importance of these residues in governing RGS2 GAP specificity toward Gαq, introducing the reverse substitutions into RGS4 (S85C, D163N, K170E) does not increase its GAP potency towards Gαq (Nance, Kreutz et al. 2013). This suggests that other structural differences contribute to the selectivity of RGS2.

Nance et al. (2013) demonstrated that in addition to these residues, the α6 and α7 regions of RGS2 are imperative in allowing a conformation that promotes increased association

with Gαq-GTP (Nance, Kreutz et al. 2013). Mutating this region caused dramatic effects on the ability of RGS2 to bind and regulate the function of Gαq. The residues of α7 helix were found to be particularly important, making extensive contacts with the Gαq α-helical domain, hypothesised to directly govern the selectivity of the RGS domain of RGS2 for Gαq.

Gu et al (2007) found that the RGS domain of RGS2 is necessary to promote Gαq-binding, an association not dependent on amphipathic helix at the N-terminus. RGS2 mutants possessing disrupted N-terminal helices were still found to associate with GTP-bound Gαq, whilst an RGS2 mutant containing a defective RGS domain was not able to bind activated Gαq (Gu, He et al. 2007). Despite this, expression of the RGS domain of RGS2 was not found to impart measurable inhibitory activity towards activated Gαq when compared to full-length RGS2 (Gu, He et al. 2007). This loss of inhibitory function was rescued by plasma membrane-targeting of the RGS-box domain (Gu, He et al. 2007). This suggests that, although the RGS domain of RGS2 may impart selectivity of its GAP function, it is not sufficient to account for the potency of Gαq inhibition.

III. RGS2 has higher membrane affinity than other R4 family members

The amphipathic helix at the amino terminal of RGS2 is sufficient for pronounced membrane targeting and is necessary for recruitment of nuclear RGS2 to the plasma membrane upon expression of a constitutively active variant of Gαq (Heximer, Lim et al. 2001). This helix is predicted to extend from amino acids 33-53 of the protein (Heximer, Lim et al. 2001, Chidiac, Sobiesiak et al. 2014). This pattern of membrane association and translocation has not been observed for any other R4 family RGS protein, with the exception of RGS3, with most RGS proteins localised throughout the cell (Dulin, Sorokin et al. 1999). It is believed that the increase in membrane localisation of RGS2 is due to a slightly expanded N-terminal region which is predicted to extend the amphipathic helix by one extra turn, thus allowing for a more efficient association with the plasma membrane (Gu, He et al. 2007). Furthermore, membrane targeting of RGS2 has been found to be a critical functional determinant of the potency of RGS2 inhibition of Gαq, as the expression of only the RGS-box domain of RGS2 markedly impairs Gαq inhibition when compared to the full-length protein (Gu, He et al. 2007).

RGS2 as an inhibitor of adenylate cyclase

In addition to its function as a GAP for Gαq, RGS2 has been found to inhibit the function of AC type III, V and VI (Sinnarajah, Dessauer et al. 2001, Salim, Sinnarajah et al. 2003). It has been shown in experiments utilising AC-expressing insect cell membranes that a decrease in cAMP production stimulated by Gαs or direct AC activation is decreased in the presence of recombinant RGS2 (Sinnarajah, Dessauer et al. 2001).

In a study by Salim et al. (2003), the mechanism of RGS2 inhibition of AC was found to be independent of its GAP activity and dependent on the presence of the first 19 amino acids of the N-terminus (Salim, Sinnarajah et al. 2003). The potential for mis-localisation of RGS2 as an explanation for the loss of AC inhibition due to the removal of the 19 N-terminal amino acids was also ruled out as the truncated variant of RGS2 was still able to associate with the plasma membrane.

2.1.2 Optogenetic control of RGS2 and RGS4

The optogenetic control of RGS2 and RGS4 have been described previously, however, their design was not intended as G protein inhibitors, but rather as a means of investigating the

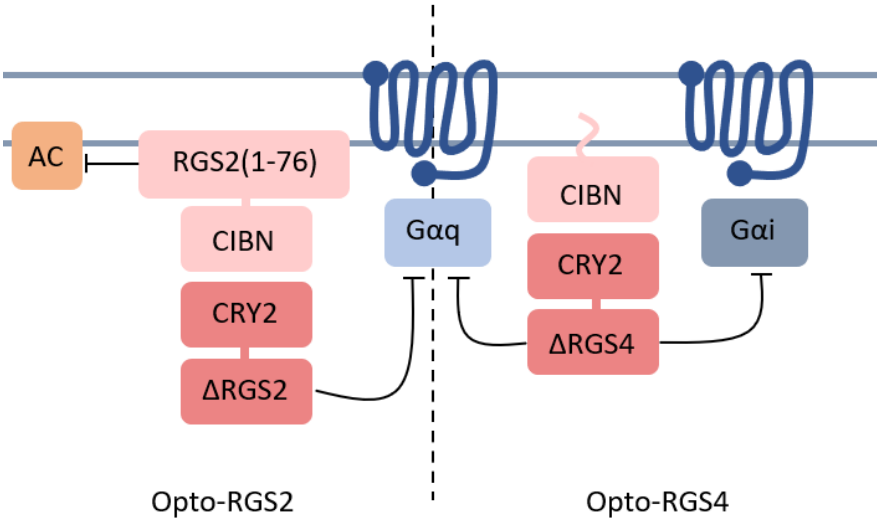

Figure 2.1 | Proposed mechanism of opto-RGS2 and opto-RGS4. Opto-RGS2 (Hannanta-anan and Chow, 2018) consists of the N-terminal amphipathic helix of RGS2 (amino acids 1-76) fused to CIBN, whilst amino acids 77-211 containing the RGS domain (ΔRGS2) are fused to CRY2(PHR). Blue light illumination induces the binding of CRY2(PHR) to CIBN, localising it in subcellular compartments designated by the RGS2 N-terminus. The N-terminus of RGS2 is a known inhibitor of adenylate cyclase (AC), whilst the RGS domain of RGS2 inhibits activated Gαq-GTP through GTP hydrolysis. Opto-RGS4 (O'Neill and Gautam 2014) consists of membrane-localised CIBN and an N-terminally truncated RGS4 missing amino acids 1-33 (ΔRGS4) fused to CRY2(PHR). Illumination localises ΔRGS4 at the membrane where it inhibits both Gαi-GTP and possibly Gαq-GTP through GTP hydrolysis. Figure based on works by Hannanta-anan and Chow, 2018 and O'Neill and Gautam 2014.

function of RGS2 and RGS4 themselves (O'Neill and Gautam 2014, Hannanta-Anan and Chow 2018). The first of these studies was the development of an optogenetically controlled RGS4 by O'Neill and Gautam in 2014 (O'Neill and Gautam 2014). In this study, a truncated variant of RGS4 missing the first 33 amino acids of the amino terminal membrane binding domain, was fused to C-terminus of the fluorescently tagged photosensory domain, CRY2(PHR), with its binding partner, CIBN, localised to the membrane via a targeting domain from KRas (CRY2(PHR)-mCh-ΔRGS4 and CIBN-CaaX) (opto-RGS4) (Fig. 2.1). Blue light illumination of cells expressing this system saw a reversal of the translocation of a fluorescently tagged Gβγ dimer, suggesting acceleration of GTP-hydrolysis of the Gα subunit and the resulting re-association of the G protein heterotrimer at the membrane. Light-induced G protein inhibition was further confirmed through the inhibition of Gαi-mediated migratory responses of RAW264.7 macrophage cells upon activation of the chemokine receptor, CXCR4. However, as RGS4 is a known inhibitor of both Gαi and Gαq signalling, this tool may inhibit multiple Gα-linked signalling cascades (Yan, Chi et al. 1997).

The second study by Hannanta-anan and Chow (2018) described the generation and validation of a light-induced activator of RGS2, opto-RGS2 (Hannanta-Anan and Chow 2018). This system was designed by fusing the N-terminal amphipathic helix of RGS2 (amino acids 1-76) to the N-terminus of CIBN and the remainder of the protein (amino acids 77-211), including the RGS domain, to the C-terminus of CRY2(PHR) (CRY2(PHR)-RGS2(77-211) and RGS2(1-76)-CIBN) (Fig. 2.1). The light-induced inhibition of Gαq-linked calcium signals was then achieved. However, this tool cannot be effectively used to investigate Gαq-linked signalling due to the presence of the over-expressed N-terminus of the protein - a known inhibitor of adenylate cyclase - which could lead to both constitutive inhibition of Gαs signalling and light induced inhibition of Gαq signalling.

Consequently, discrete conclusions about GPCR function cannot be drawn through the use of these tools alone due to the potential for the modulation of signalling events related to more than one G protein subunit. In this study, emphasis was placed on the development of a selective optogenetic inhibitor of Gαq signalling with the RGS domain from RGS2, ensuring minimal disruption of other G protein related signalling associated with wild type RGS2.

2.1.3 Design of Photo-Induced G protein Modulator – Inhibitor Gαq (PIGM-Iq)

It is thought that the ability of RGS2 to act as a GAP for Gαq with such high specificity is due to a combination of the properties described above. RGS2 has a structural preference for Gαq-

GTP over Gαi-GTP, but its binding affinity to Gαq is insufficient for it to act as a GAP on Gαq unless it is localised to the membrane (Gu, He et al. 2007). These properties of RGS2 could be used to design an optogenetic tool for the selective inhibition of Gαq signalling.

The following points were considered when designing the proposed optogenetic tool:

1. The RGS domain is required for the ability of RGS2 to act as a GAP for Gαq. This domain is also a key determinant in Gαq selectivity as it contains both the α6 and α7 helices as well as the two key residues (C106 and N184) needed for selective Gαq binding. Therefore, the proposed optogenetic tool must contain this domain to selectively inhibit Gαq.
2. Membrane association is also imperative to the potent inhibitory activity of RGS2, as is the pre-coupling of RGS2 to Gαq-linked GPCRs, both of which are attributed to the presence of the N-terminus of the protein.
3. The inhibition of AC has been localised to the first 19 amino acids of the N-terminus.

Considering the above points, it is proposed that the truncation of the N-terminus from amino acids 1-53 would effectively remove the ability of RGS2 to associate with the membrane and inhibit AC, whilst leaving the rest of the protein - including the RGS domain - intact. It is proposed that by artificially localising the truncated variant of the protein, RGS2(Δ1-53), using light-induced membrane targeting, the ability of RGS2(Δ1-53) to inhibit Gαq will be restored. This would allow for limited inhibition of Gαq in the dark due to the hypothesised cytosolic locality of RGS2(Δ1-53), whilst allowing for inhibition upon light illumination and the resulting translocation of RGS2(Δ1-53) to the membrane.

2.2 Methods

2.2.1 Plasmid construction

Construction of cDNA library from rat brain RNA

RNA to produce cDNA was obtained from adult female Sprague-Dawley rat brains using the TRIZOL method of extraction and was performed by Dr Agnieszka Zbela. The synthesis of cDNA from isolated RNA was then performed using the Maxima H Minus First Strand cDNA Synthesis Kit (Thermo Scientific, Cat# K1651) as per the manufacturer's instructions. Briefly, 1µg of RNA was used for first strand cDNA synthesis. The reaction was incubated at

50°C for 30 minutes, followed by termination at 85°C for 5 minutes. The resulting cDNA library was then used as a template for further polymerase chain reaction (PCR) using specific primers described below for the amplification of mammalian RGS2, RGS4 and the dopamine D2 receptor.

All plasmids used in this study were constructed using standard molecular biology techniques consisting of PCR using Phusion Flash High-Fidelity PCR MasterMix (Thermo Fisher Scientific, Cat# F-548), two-step overlapping PCR, restriction enzyme digest of completed DNA inserts, ligation of completed inserts into expression vectors, transformation into KCM-competent DH5α *E. coli* bacterial cells (Invitrogen, Cat# 18265-017), plasmid purification via minipreperation kit (GenElute™ HP plasmid MiniPrep kit, Sigma-Aldrich, Cat# NA0160) and Sanger sequencing (BigDye Terminator v3.1 Cycle Sequencing Kit (Applied Biosystem, Cat# 4337455.))

For the generation of RGS2 variants, primers were designed using the plasmid editing software, A Plasmid Editor (ApE©) (v2.0.51) against *Rattus norvegicus* mRNA RGS2 sequence sourced from the National Centre for Biotechnology Information (NCBI) search engine, GenBank® (NCBI Reference Sequence NM_053453.2). Inserts were cloned from a *Rattus norvegicus* cDNA library generated as described previously using specific oligonucleotide primers for

PCR, with products separated by size using agarose gel electrophoresis purified using standard gel extraction techniques. All constructs used in this chapter are listed in table 1.

Table 2.1 Generated DNA constructs for mammalian cell studies

	Name of construct
Constructs encoding sensor proteins	
1	pLenti-CMV-O-GECO1
2	pcDNA3.1H-CMV-GloSensor
Template constructs	
3	pcDNA3.1H-CMV-CRY2(PHR)
4	pcDNA3.1H-CMV-CRY2(PHR)-mCh
5	pcDNA3.1H-CMV-CIBN-eGFP-CaaX
6	pcDNA3-CMV-CRY2(PHR)-T2A-CIBN-eGFP-CaaX
7	pcDNA3-CMV-CRY2(PHR)-mCH-T2A-CIBN-eGFP-CaaX
Constructs encoding RGS-related proteins	
8	pcDNA3.1H-CMV-RGS2
9	pcDNA3.1H-CMV-RGS2-eGFP
10	pcDNA3.1H-CMV-RGS2(Δ1-53)-eGFP
11	pcDNA3.1H-CMV-RGS2(Δ1-53)-eGFP-CaaX
12	pcDNA3.1H-CMV-RGS2(Δ1-53)-CRY2(PHR)
13	pcDNA3.1H-CMV-RGS2(Δ1-53)-CRY2(PHR)-eGFP
14	pcDNA3.1H-CMV-CRY2(PHR)-RGS2(Δ1-53)
15	pcDNA3.1H-CMV-RGS4-eGFP
Bicistronic constructs encoding RGS-related proteins	
16	pcDNA3-CMV-RGS2(Δ1-53)-CRY2(PHR)-mCH-T2A-CIBN-eGFP-CaaX
17	pcDNA3-CMV-RGS2(Δ1-53)-CRY2(PHR)-T2A-CIBN-eGFP-CaaX
18	pcDNA3-CMV-RGS2(Δ1-53)-CRY2(PHR)(D387A)-mCH-T2A-CIBN-eGFP-CaaX
19	pcDNA3-CMV-RGS2(Δ1-53)-CRY2(PHR)(D387A)-T2A-CIBN-eGFP-CaaX
Constructs encoding GPCRs	
20	pcDNA3.1H-D2R

Rat brain cDNA was used as a template to amplify full length RGS2 DNA sequence using the following oligonucleotides: BamHI-RGS2-5F: 5'-attggatccatgcaaagtgccat-3' and RGS2-AgeI-TAA-XbaI-3RC: 5'-agccccatgctacaaccggttaatctagaatt-3'. The resulting RGS2 DNA (~660bp) was fused to eGFP with a linker (GGGGAG) between their coding sequences. This was cloned into a pcDNA3.1H vector to create: pcDNA3.1H-RGS2-eGFP. The truncated variant of RGS2 (RGS2(Δ1-53)) was cloned using BamHI-ATG-RGS2(Δ1-53)-5F': 5'-attggatccatgactcctgggaag-3' and RGS2-AgeI-TAA-XbaI-3RC: 5'-agccccatgctacaaccggttaatctagaatt-3'. The truncated RGS2 fragment (~550bp) was fused to the 5'-end of the mammalian codon-optimized photolyase homology region (PHR) of cryptochrome 2 (Cry2(PHR)) through a linker (TGGGSGGGS) and cloned into a pcDNA3.1H vector to create the following construct: pcDNA3.1H-CMV-RGS2(Δ1-53)-CRY2(PHR). The

pcDNA3.1H-CMV-RGS2(Δ1-53)-CRY2(PHR) construct was moved to a pcDNA3 vector containing a T2A-containing transgene, followed by CIBN-eGFP-CaaX to create pcDNA3-CMV-RGS2(Δ1-53)-CRY2(PHR)-T2A-CIBN-eGFP-CaaX (see appendix for full protein sequence).

For experiments looking at cross-reactivity between RGS2 and Gαi, RGS4 was used as a positive control. Rat brain cDNA was used as the template to amplify full length RGS4 (NCBI Reference Sequence NM_017214.1) using BamHI-RGS4-5F: 5'-attggatccatgtgcaaaggactcgctggtc-3' and RGS4-AgeI-3RC: 5'-c cctagtccctcagtgtgccaccggtatt-3'. The resulting fragment (~610bp) was fused to the 5'-end of eGFP and cloned onto a pcDNA3.1H vector to create pcDNA3.1H-CMV-RGS4-eGFP.

For all other constructs listed in table 1, fluorescent proteins were linked to target construct via a C- terminal linker (GGGGAG). A CaaX polybasic sequence (GKKKKKKSKTKCVIM) was used to target fusion constructs to the membrane where necessary.

All template vectors used, unless otherwise specified, were synthesized by the Lin Lab. Template vectors used were pcDNA3.1H for single component transgene expression in HEK293A cells; pcDNA3 for multiple component, T2A-containing transgene expression in HEK293A cells; and pLenti for stable cell line production; with all transgenes under the cytomegalovirus (CMV) promotor.

The orange fluorescent genetically encoded calcium indicator (O-GECO1) was used as a calcium sensor (Addgene (Wu, Liu et al. 2013)). The pLenti-CMV-O-GECO1 construct was created by Dr John Lin. GloSensor™ cAMP sensor was used for cAMP assays (Promega, Cat # E2301). The pcDNA3.1H-D_2R construct was prepared by Dr John Lin.

2.2.2 Cell culture, transduction, and transfection

Cell culture

HEK293A (Life Technologies,) and O-GECO1-HEK293A (Lin Lab) cells were maintained in 5.5cm^2 culture dishes (Corning) under standard conditions (37°C, 95% humidity, 5% CO_2). Cells were cultured in Dulbecco's Modified Eagles Medium (DMEM; Gibco, Cat# 11885-084) (1000mg/L D- glucose, L-glutamine, 110mg/L sodium pyruvate) containing 1% penicillin/ streptomycin antibiotic solution (Sigma-Aldrich, Cat# P4333-100ML) and supplemented with 8% foetal bovine serum (FBS; Gibco, Cat# 10099141). Cells were passaged when their confluency exceeded 85- 90% using standard techniques. Briefly, cells were washed using

Dulbecco's Phosphate Buffered Saline (DPBS; Sigma-Aldrich, Cat# D1408-500G) containing 20 mM HEPES (Sigma-Aldrich, Cat# H3375-250G) and 1 mM EDTA (pH 7.4, Sigma-Aldrich, Cat# E5134-500G) followed by trypsinisation with TrypLE Express (Gibco, Cat# 12604-013) and subcultured into new dishes at a ratio of 1:10.

Transduction

HEK293A cells stably expressing O-GECO1 were created by performing lentivirus transduction. Recombinant lentivirus was generated using HEK293A cells at a confluency of 80- 85% in a 10cm culture dish (Corning). Standard DMEM culture media with serum was removed and replaced with serum-free DMEM. Transfection solution containing 2.5µl polyethylenimine (PEI, Sigma-Aldrich, Cat# 408727-100ML), 2.25µg PMDG.2, 3.5µg psPAX2, and 2.2µg pLenti-transfer vector containing the construct of interest (CMV promotor driving expression of O-GECO1), was added to serum-free media and added to the cells (PMDG.2 and psPAX2 plasmids were a gift from Professor Didier Trono, Federal Institute of Technology, Lausanne). After 8-18 hours, the transfection serum-free media was removed, and cells were returned to normal culture media. 48-72 hours after, the culture media containing the lentivirus from the transfected cells was aspirated and used to transduce a new plate of HEK293A cells (80% confluency). Fresh DMEM was replaced on the transfected cells. The transduction was repeated the following day. Successful transduction was confirmed upon the visualisation of cellular fluorescence. Transduction efficiency of the O-GECO1-HEK293A line used was approximately 90%.

Transfection

Transient expression of constructs was performed by transfecting either HEK293A or O-GECO1-HEK293A cell lines using PEI or X-tremeGENE™ 9 (Roche, Cat# 06365787001). Briefly, HEK293A or O-GECO1-HEK293A cells were seeded onto glass coverslips (ø 13 mm, Thermo Fisher Scientific) in a 24-well culture plate 24 hrs prior to transfection. HEK293A were transfected at ~50% confluency and O-GECO1-HEK293A cells were transfected at a confluency of ~30-40%. A lower confluency was used for O-GECO1-HEK293A cells to ensure limited cell-to-cell contacts at the point of imaging to limit Ca^{2+} transfer through gap junctions. To perform transfection, media containing serum was removed and replaced with serum-free

DMEM for the PEI transfection method (no media change for X-tremeGENE 9 transfection). 0.1μg of each construct used was then combined with 0.1 M PEI (pH 7.0) in 2:1 ratio (e.g., 0.2 μg DNA + 0.1 μl PEI) or X-tremeGENE 9 (Roche) 1:3 ratio (e.g., 0.1 μg DNA + 0.3 μl X-tremeGENE 9) and incubated at room temperature for 20 minutes. The solution was then directly added to wells containing cells and incubated at 37°C in a humidified 5% CO2 environment for 3-5 hours. Serum-free media was removed and replaced with serum-containing DMEM for the PEI transfection method. Cells were imaged 48 hours post-transfection to ensure adequate expression of the transgenes.

Transfection conditions were kept constant for all constructs tested. This resulted in a transfection efficiency ranging from 30-60%. In experiments using O-GECO1-HEK293A, this resulted in a number of untransfected cells within the field of view during image acquisition which were used as controls. This also allowed for the confirmation of sensor function and drug activity upon commencing each experiment.

2.2.3 Light stimulation and microscopy

All imaging was performed at room temperature. Cells were imaged in either calcium-containing extracellular solution or calcium-free extracellular solution 48-hours post transfection. Cells were imaged using a fixed stage upright fluorescent microscope (Olympus BX51WI) equipped with a Scientific CMOS camera ((Hamamatsu, ORCA- Flash4.0) and water immersion objectives (all expression and translocation experiments performed using 40×/NA0.8 (Olympus) and calcium imaging experiments obtained using 20×/NA0.5 (Zeiss)) and a white light LED excitation source (X-Cite 110LED, Excelitas Technologies). Light intensity of the X-cite 110LED was maintained at 20% of maximum intensity for all experiments. Cells were imaged at 2x2 binning with a 300.028ms exposure time. Calcium imaging using O-GECO1 and mCherry-tagged constructs were imaged with a TRITC filter set (FF01-543-22, 562-Di03, FF01-593/40). GFP-tagged constructs (excitation at 470 nm) were imaged using a GFP filter set (472/30, FF495-Di03, FF01-520/35). Image acquisition was performed using Micro-Manager© 1.4.22. In experiments requiring blue-light stimulation, cells were pulsed with a 480nm LED (Luxeon rebel LED) for 4 seconds through the condenser located under the recording chamber and was controlled using a digitally controlled constant current LED power supply with LED Driver Control Panel V3.2.2 software (Mightex) (Fig 2.2). The majority of experiments were performed using a stimulation intensity of 0.22 mW/mm^2. All experiments were performed in extracellular solution (ECS) (140 mM NaCl, 2.8

mM KCl, 10 mM HEPES, 1 mM $MgCl_2$, 2 mM $CaCl_2$, 10 mM D-glucose, pH 7.4, 290-310 mOsm/l). In calcium-free extracellular solution, the 2mM $CaCl_2$ was omitted from the solution. All drugs were diluted in ECS to the desired concentration and administered to the cells via manual perfusion. Drugs were perfused directly into the extracellular solution during the imaging session at the desired time point.

Expression tests and translocation experiments

To confirm transgene expression and visualise sub-cellular expression pattern, constructs were

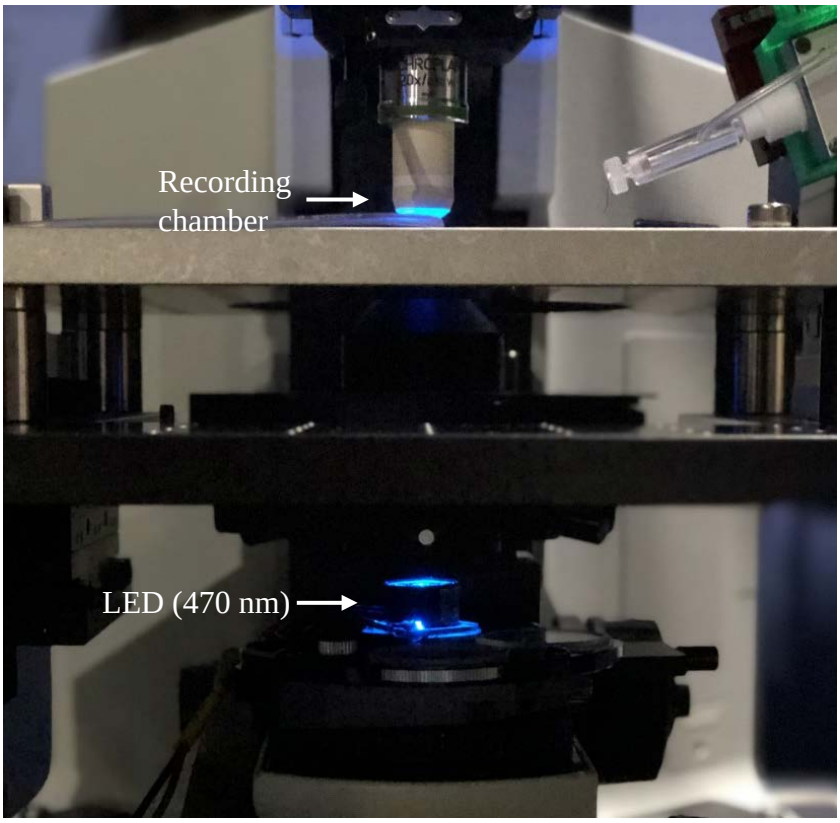

Figure 2.2 | *customised LED device for the stimulation of cells during live cell imaging.* Blue light was delivered through the condenser to cells in the recording chamber during live cell imaging sessions. Light intensity and duration were controlled through a LED Driver Control Panel V3.1.0 (Mightex).

tagged with either mCherry or eGFP. These were visualised using the TRITC and GFP filter sets, respectively. Translocation of CRY2(PHR) fused constructs was captured at 1 Hz for all experiments (2x2 binning, 300.028ms exposure time). mCherry fluorescence (tagged to CRY2(PHR)) was monitored through the TRITC channel so as not to activate the CRY2(PHR)/CIBN dimer pair. Blue light (470nm, 4 seconds, 0.22 mW/mm^2) was delivered at 30 seconds from the initiation of image acquisition. For experiments analysing reversion time,

cells were imaged for 20 minutes at 0.5 Hz with blue light illumination at 30 seconds. In the case of experiments determining the intensity of blue light needed for maximal translocation, various light intensities were used (0.002 mW/mm^2, 0.02 mW/mm^2, 0.11 mW/mm^2, 0.22 mW/mm^2 and 0.82 mW/mm^2). For prolonged activation, cells were imaged for 60 minutes at a frame rate of 0.001 Hz with blue light stimulation occurring at 30 seconds, and then every 5 minutes for the duration of the experiment. At the end of image acquisition for all experiments, an image was taken through the GFP channel to confirm the expression of CIBN.

Calcium imaging experiments

The O-GECO1 genetically encoded calcium sensor was utilised to observe changes in intracellular calcium concentrations upon the addition of carbachol (final concentration of 20μM in ECS, CCh (Sigma-Aldrich)) (Haraguchi and Rodbell 1991). O-GECO1 possess a peak absorption of 543nm and emission of 564nm and possesses a K_d for calcium of 1500nM, with a large increase in fluorescence generated upon binding calcium (Wu, Liu et al. 2013). This sensor was used to avoid spectral overlap with that of the wavelength employed for CRY2(PHR)/CIBN activation (470 nm), enabling the visualisation of intracellular calcium concentrations before and after blue light stimulation of the CRY2(PHR)/CIBN pair.
Calcium imaging experiments were conducted as described above. Briefly, O-GECO1 fluorescence was visualised using the TRITC filter set. Image acquisition was performed at 1 Hz for all experiments (2x2 binning, 300.028ms exposure time). For the majority of experiments (excluding those in which blue light was not delivered), blue light (470nm, 4 seconds, 0.22 mW/mm2) was delivered at 10 seconds from the initiation of image acquisition, followed by carbachol addition at 40 seconds. Calcium levels were monitored for 3 minutes. Following image acquisition, an image was taken through the GFP filter set to identify expressing cells.

For experiments performed in the presence of nominally calcium free media, calcium omitting ECS was used. The absence of 2 mM $CaCl_2$ was made up by the addition of 2 mM NaCl to maintain osmolarity. For experiments using the PLC inhibitor, U73122 (Sigma-Aldrich, Cat# U6756), was pre-incubated with cells at a concentration of 2.5 μM in ECS for 10 minutes. Cells were then transferred to the imaging chamber also containing 2.5 μM U-73122 and imaged as described above. For experiments using the SERCA pump inhibitor, thapsigargin (Alomone Labs, Cat # T-650) (Sehgal, Szalai et al. 2017), cells were pre-incubated

with 7.5 μM thapsigargin in ECS for 10 minutes before being transferred to the imaging chamber also containing 7.5 μM thapsigargin in ECS and imaged as described above.

Image processing and analysis

Image processing was performed using ImageJ 1.50i (http://imagej.nih.gov/ij/). Fluorescence was analysed by outlining the cytoplasm of the cell using the 'free-hand' selection tool. The mean grey value was then recorded for each cell of interest for every frame in the image stack. Three background measurements were also taken for each frame. These background values were then averaged and subtracted from the experimental values to acquire a true representation of cell pixel intensity (Microsoft Excel, 2010). The change in fluorescence over initial fluorescence (ΔF/F0) was calculated for each cell using the following method: initial fluorescence (F0) was determined by averaging the ten values immediately preceding the frame of blue light stimulation. The following equation was then used:

$$\Delta F/F0 = (Ft-F0)/F0$$

with Ft being the fluorescence value at a given time.

For the analysis of calcium spike parameters, raw calcium imaging traces were analysed using Clampfit 11.1. To report percentage of responding cells versus non-responding cells, cells with a ΔF/F0 value below 1.0 were considered "non-responders" whilst those exhibiting a ΔF/F0 value above 1.0 were considered "responders". Statistical analysis was performed, and graphs were produced using GraphPad Prism 8.3 (GraphPad Software, San Diego, California USA, www.graphpad.com).

2.2.4 GloSensor cAMP assay

HEK293A cells were seeded at a density of $1.5x10^5$ cells per ml as specified by the manufacturer's instructions into a black, clear-bottomed 96-well plate (Falcon) pre-treated with poly-L-lysine (PLL; final concentration of 50 μg/ml, Sigma-Aldrich, Cat# P4832-50ML). Cells were transfected using PEI as described previously (0.1ug GloSensor™ plasmid (Promega), 0.1μg test construct, 0.1μg D_2R (for Gαi assay)) 24 hours following plating. 24 hours post-transfection, media was removed from cells and replaced with 50μl luciferin (Cayman Chemicals, Cat# 14681) (2 mM final concentration diluted in ECS) and incubated at room

temperature for 2 hours. Luminescence was then measured using Spark® multimode microplate reader (Tecan) (integration time: 1000ms).

For experiments looking at the inhibition of Gαi, background luminescence was measured every 1 minute for 5 minutes. Cells were then exposed to blue light by placing them upon the Midi LED transilluminator (IORodeo) for 30 seconds (blue light intensity of 0.04 mW/mm^2 at 470nm). Quinpirole (QNP (Sigma-Aldrich, Cat# Q102-10MG); final concentration of 5 μM in ECS) was added to each well and luminescence recorded every 1 minute for 5 minutes. Proceeding this, acquisition was paused, and the plate removed from the instrument. Cells were once again illuminated for 30 seconds, followed by the addition of isoprenaline (ISO (Cayman Chemicals, Cat #: 15592); final concentration of 10 μM in ECS). Luminescence was once again recorded for a further 5 minutes, the cells illuminated once more, and luminescence recorded for 5 minutes. Total acquisition time for luminescence was 20 minutes with recordings performed every 1 minute. For experiments looking at Gαs inhibition, luminescence was measured as described above. However, no QNP was added at time zero for these experiments.

All data was initially processed using Microsoft Excel, 2010. Statistical analysis was performed, and graphs were produced using GraphPad Prism 8.3 (GraphPad Software, San Diego, California USA, www.graphpad.com).

2.3 Results

2.3.1 Design and mechanism of Photo-Induced G protein Modulator – Inhibitor Gαq (PIGM-Iq)

The truncation of the first 53 amino acids of the N-terminus may disrupt the ability of the proposed tool to couple to Gαq-linked GPCRs, a hypothesised requirement for increased Gαq selectivity. Although required in some capacity for selectivity, this pre-coupling feature may prove to be a disadvantage in the design of the proposed tool. This is because the pre-coupling function may localise the tool in such a manner that allows for background inhibition in the absence of light due to the proximity of the RGS domain to Gαq-GTP. It is not yet known where this domain resides within the amphipathic helix of the full-length RGS2 that enables coupling to target GPCRs, but as previously mentioned, the ability of the helix to associate with the membrane is not required. As a result, the proposed tool features a truncation of the

first 53 amino acids of the N-terminus rather than a series of point mutation within the amphipathic helix that would result in the removal of membrane binding.

Due to the translocation and dimerisation kinetics mentioned previously, it is believed that the CRY2(PHR)/CIBN photo-induced dimerization system presents a justifiable means of light-induced control over RGS2(Δ1-53). This is due to its ability to act on a millisecond timescale, an attribute that is considered important when attempting to inactive processes that occur during a similar timeframe. This is opposed to other light responsive modules that can require several minutes to activate. Furthermore, the system's reversal speed is a further advantage to Gαq modulation. In view of this, it is proposed that the CRY2(PHR)/CIBN system presents a viable means of optogenetically inhibiting Gαq through its fusion with RGS2(Δ1-53) in a physiologically relevant manner.

The N-terminus of CRY2(PHR) will be fused to the C-terminus of RGS2(Δ1-53) (Fig. 2.4). This is due to the oligmerisation mechanisms of CRY2(PHR) and CIBN. Firstly, is has been previously reported by Tucker et al. (2010) that localising CRY2(PHR) at the membrane via its C-terminus decreased its ability to bind cytosolically localised CIBN, suggesting that steric hinderance of CRY2(PHR) may inhibit this interaction (Kennedy, Hughes et al. 2010). Therefore, it is possible that the fusion of RGS2(Δ1-53) to the C-terminus may decrease, to some extent, the ability of CRY2(PHR) to interact with CIBN.

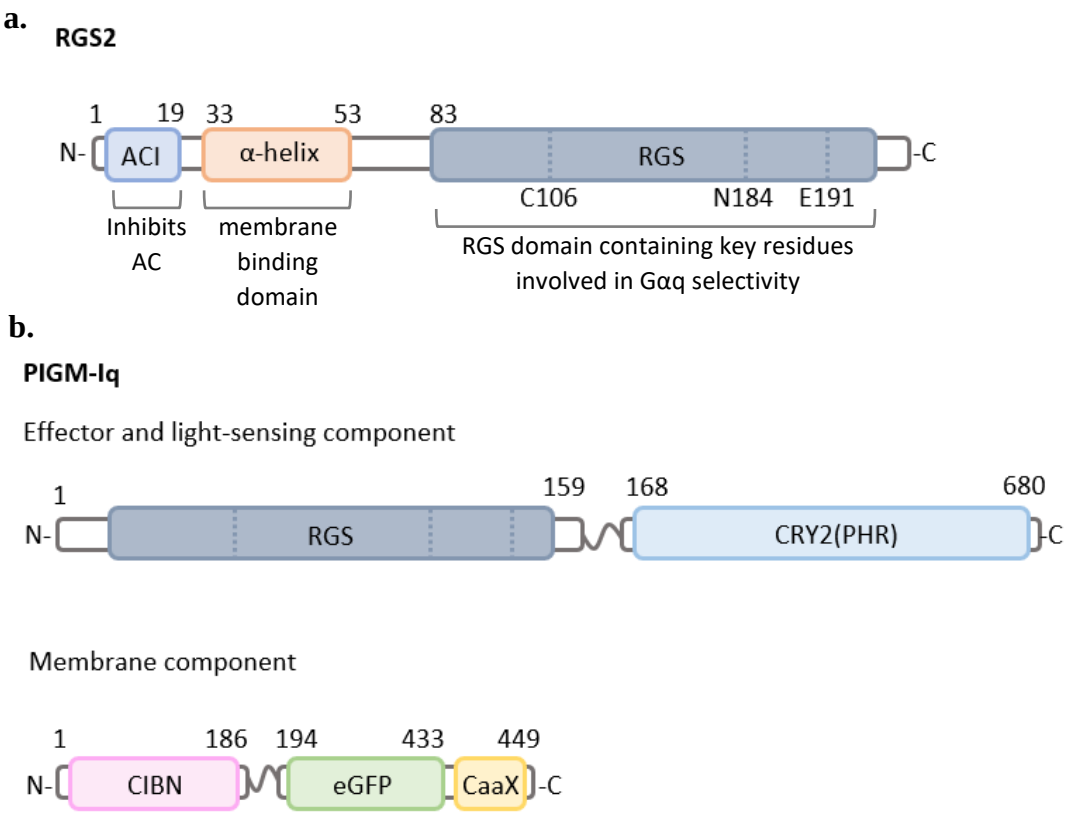

Figure 2.3 | *Design of PIGM-Iq.* **a,** A basic schematic of full-length RGS2 showing the layout of key domains known to affect GPCR signalling (AC inhibitory domain (ACI) in blue, α amphipathic helix involved in membrane binding in orange and the RGS domain in grey highlighting key unique residues involved in Gαq selectivity). **b,** Schematic of the proposed PIGM-Iq tool. The effector and light-sensing component of the tool consist of a truncated RGS2(Δ1-53) consisting of a short N- and C-terminus flanking the RGS domain, joined to the light-responsive CRY2(PHR) domain (blue) by a short linker to the C-terminus of RGS2. The membrane localised component of the tool consists of CRY2(PHR) dimerising partner, CIBN (pink), tagged with eGFP (green). This component of the tool will be localised at the membrane via a CaaX-box prenylation motif (yellow).

Moreover, it is well documented that CRY2 possesses the ability to concurrently undertake light-dependent CRY2-CRY2 homo-oligmerisation and CRY2-CIB1 heterodimerisation, with different variants of CRY2 showing varied homo-oligmerisation tendencies. It has been noted in previous literature that the C-terminus of CRY2 is important in allowing for CRY2-CRY2 homo-oligmerisation (Duan, Hope et al. 2017, Park, Kim et al. 2017). Although it has been reported that the C-terminal fusion of dimeric and tetrameric fluorescent proteins to CRY2(PHR) can greatly increase its ability to homo-oligomerise, it is unlikely that the fusion of RGS2(Δ1-53) would cause such an increase due to its monomeric nature (Park, Kim et al. 2017). It is also possible that the fusion of CRY2(PHR) to the N-terminus of RGS2(Δ1-53) may reduce CRY2(PHR) oligomerization by means of steric hinderance, whilst the opposite orientation leaves the C-terminus of CRY2(PHR) unperturbed.

Therefore, it is believed that a C-terminal fusion of CRY2(PHR) to RGS2(Δ1-53) will result in maximum translocation and oligmerisation, increasing the inhibitory capabilities of the tool.

The optogenetic RGS2 system for the selective inactivation of the endogenous Gαq subunit will be generated through a C-terminus fusion of RGS2(Δ1-53) to the CRY2 photolyase homology region, or CRY2(PHR), with the N-terminus of CIB (consisting of the first 170 amino acids (CIBN)) localised at the membrane via a CaaX-box prenylation motif (Fig. 2.3). Upon illumination with blue light, it is hypothesised that CRY2(PHR) will translocate to the membrane, localising RGS2(Δ1-53) in proximity to the endogenous GPCR-fused Gαq subunit. Upon stimulation of the Gαq-linked pathway, it is proposed that the RGS domain of RGS2(Δ1-53) will facilitate the hydrolysis of GTP to GDP, thus converting the Gαq subunit to an inactive form and preventing further activation of the downstream pathways (Fig. 2.4).

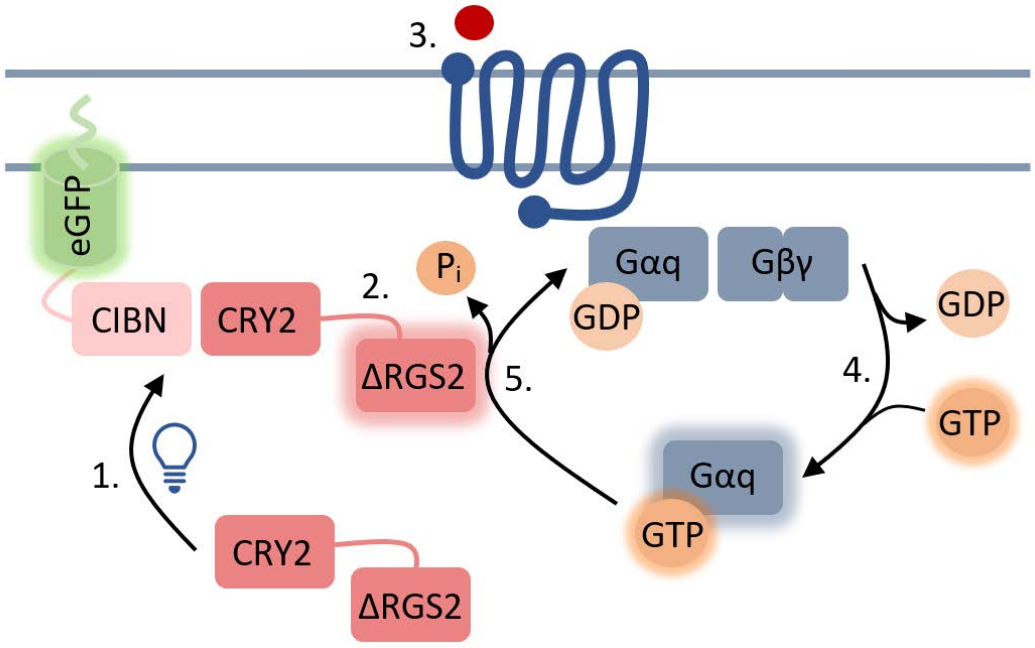

Figure 2.4 | *Proposed mechanism of action of the Photo-Induced G protein Modulator – Inhibitor Gαq (PIGM-Iq).* (1) Upon blue light illumination, the cytosolically localised RGS2(Δ1-53)-CRY2 (2) translocates to the membrane and binds CIBN-eGFP-MP. (3) Ligand binding to the GPCR causes the activation of the associated Gq protein by displacement of (4) GDP by GTP. (5) The RGS domain of PIGM-Iq is then able to act as GTPase accelerating protein, hydrolysing the GTP associated with the active G protein to GDP, thereby terminating signalling.

2.3.2 Validation of carbachol-induced calcium efflux as a measure of Gαq-linked GPCR activation.

In HEK293A cells, CCh activates Gαq-coupled M_3 muscarinic receptors, leading to a calcium increase reflected as a change in O-GECO1 fluorescence (Fig. 2.5, a). 20 µM carbachol in 2

mM Ca^{2+}-containing medium induced a rapid, transient increase in $[Ca^{2+}]_i$ ($\Delta F/F_o$) in HEK293A cells followed by a more gradual decline, with basal $[Ca^{2+}]_i$ remaining slightly elevated compared to pre-stimulation levels (Fig. 2.5, b). An increase in calcium was observed in 99.1% of cells measured. When cells were stimulated with carbachol in the presence of nominally Ca^{2+}-free medium, an increase in $[Ca^{2+}]_i$ was again observed in all cells tested, indicating release of Ca^{2+} from intracellular stores (Fig. 2.5, c).

Pre-treatment of cells for 10 minutes with the 2.5 μM PLC-inhibitor, U-73122 (Fig. 2.5, d) (Macmillan and McCarron 2010), or 7.5 μM of the SERCA pump-inhibitor, thapsigargin (Fig. 2.5, e), decreased carbachol-evoked increases in $[Ca^{2+}]_i$ by 99.5% (96.4% of cells) and 98.0% (96.0% of cells) in comparison to untreated cells, respectively. This indicates a necessary involvement of PLC in this pathway and the downstream release of calcium from the endoplasmic reticulum (Fig. 2.5, a). A comparison of the averages of each condition demonstrates the reliance of carbachol-mediated Ca^{2+} signalling on intracellular calcium stores (Fig. 2.5, f).

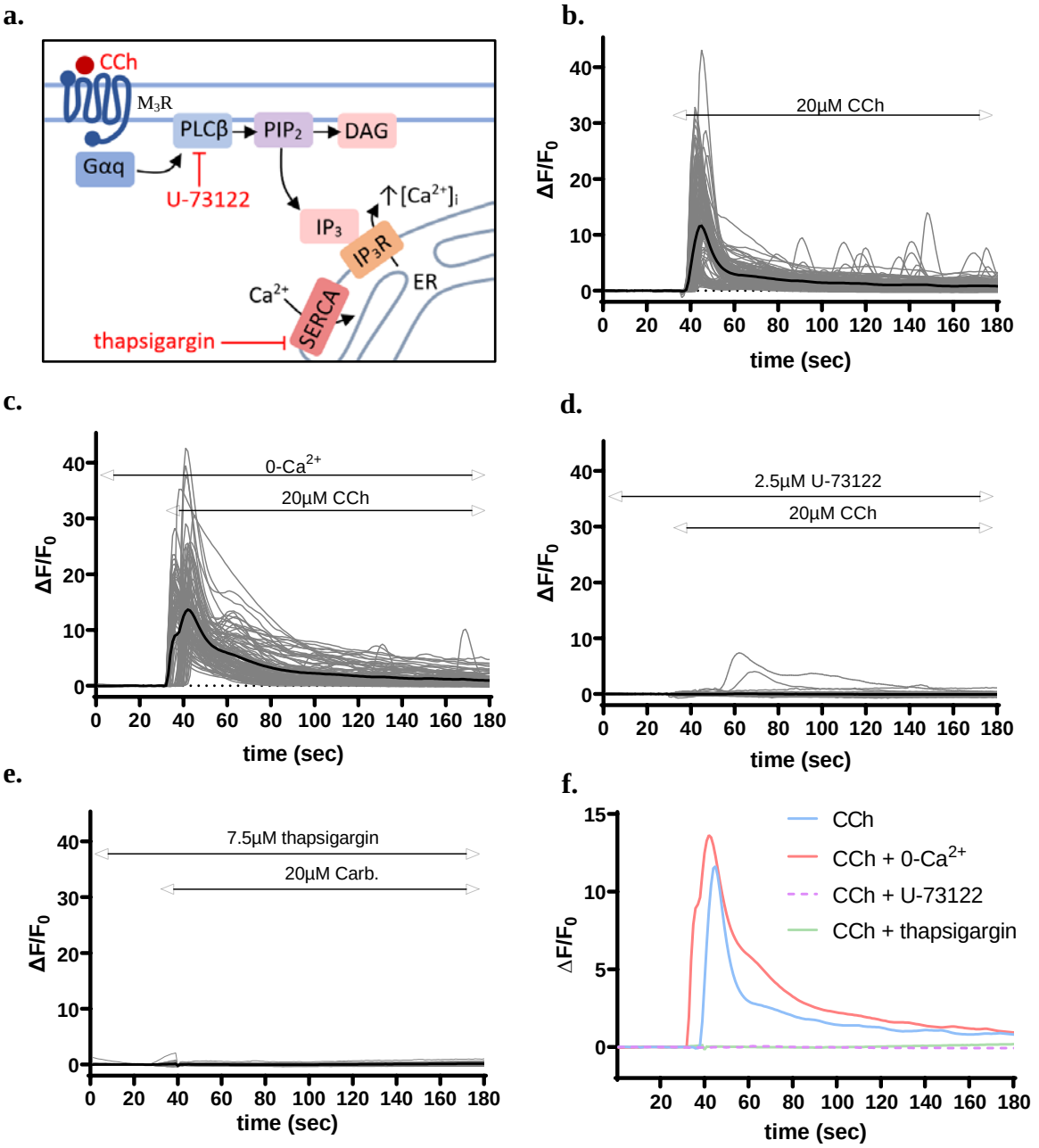

Figure 2.5 | *Validation of carbachol-induced calcium efflux as a readout of Gαq-linked GPCR activation in HEK293A cells.* **a,** Gαq-linked GPCR activation by carbachol (CCh) (Haraguchi and Rodbell 1991) causes the activation of PLCβ (inhibited by U-73122 (Macmillan and McCarron 2010)), resulting in the cleavage of PIP_2 into IP_3 and DAG. IP_3 then triggers the release of Ca^{2+} from ER stores via IP_3R. ER stores are replenished by active transport of Ca^{2+} from the cytosol into the ER lumen by SERCA pumps (inhibited by thapsigargin (Sehgal, Szalai et al. 2017)). This is thought to occur through the M_3 muscarinic receptor (M_3R) (Haraguchi and Rodbell 1991). Figure made using information from cited sources **b-f,** Individual calcium traces in HEK293A cells expressing the calcium sensor O-GECO1 stimulated as indicated with 20 μM CCh (black line indicates average). **b,** Calcium response upon addition of CCh, **c,** in the absence of extracellular Ca^{2+} **d,** in cells pre-treated (10min) with 2.5 μM U-73122, and **e,** in cells pre-treated (10min) with 7.5 μM thapsigargin. **f,** comparison of the averages of each condition. N = 105-115 cells/condition from ≥ 3 experiments.

2.3.3 Validation of the individual PIGM-Iq components in HEK293A cells.

To confirm the expression pattern of N-terminal truncation of RGS2, eGFP-tagged full-length RGS2 (RGS2(WT)-eGFP) and an N-terminally truncated RGS2 (RGS2(Δ1-53)-eGFP) were transiently expressed in HEK293A cells. RGS2(WT)-eGFP displayed robust nuclear, nucleolus and membrane localisation, as expected (Fig. 2.6, a, I) (Heximer, Lim et al. 2001). The truncated variant of RGS2, RGS2(Δ1-53)-eGFP, did not show any clear membrane localisation, but displayed a uniform distribution throughout the cytosol and nucleus (Fig. 2.6, a, II). Nuclear levels of RGS2(Δ1-53)-eGFP appeared markedly decreased compared to that of RGS2(WT)-eGFP, with no expression observed in the nucleolus of these cells. Adding a membrane tether to the C-terminus of RGS2(Δ1-53) (RGS2(Δ1-53)-eGFP-MP) resulted in clear membrane expression (Fig. 2.6, a, III).

To validate the suitability of the intended light-induced Gαq inhibitor, PIGM-I_q, each component of the proposed tool was transiently expressed in O-GECO1-HEK293A cells. The effect of carbachol-induced increases in $[Ca^{2+}]_i$ was then observed. All experiments were conducted in 2 mM Ca^{2+}-containing medium.

Expression of full-length wild-type RGS2 (RGS2(WT)-eGFP) inhibits Gαq-linked increase in $[Ca^{2+}]_i$, (94.6% reduction in mean peak calcium response) (Fig. 2.9, c) compared to untransfected cells (Fig. 2.6, b, c, g). 81.6% of expressing cells showed complete inhibition. Cells expressing the truncated version of the protein, RGS2(Δ1-53)-eGFP, had slightly reduced calcium spikes compared to those seen in untransfected cells stimulated with CCh (Fig. 2.6, d, g). 90.1% of cells expressing RGS2(Δ1-53)-eGFP still responded to CCh. When the truncated variant of RGS2, RGS2(Δ1-53)-eGFP, was again localised to the membrane, but through its C-terminus (RGS2(Δ1-53)-eGFP-MP), inhibitory activity was restored (Fig. 2.6, e, g).
The light-induced dimer system, CRY2(PHR)-mCh and CIBN-eGFP-MP, were also assessed for possible interactions with the Gαq pathway. Blue-light illumination was delivered to cells 30 seconds preceding carbachol addition. Expressing cells showed a level of calcium spike amplitude reduction compared to untransfected cells (34.8% reduction in mean peak calcium response compared to untransfected cells) with 94.4% of the total cells measured responding to CCh. (Fig. 2.6, f, g).

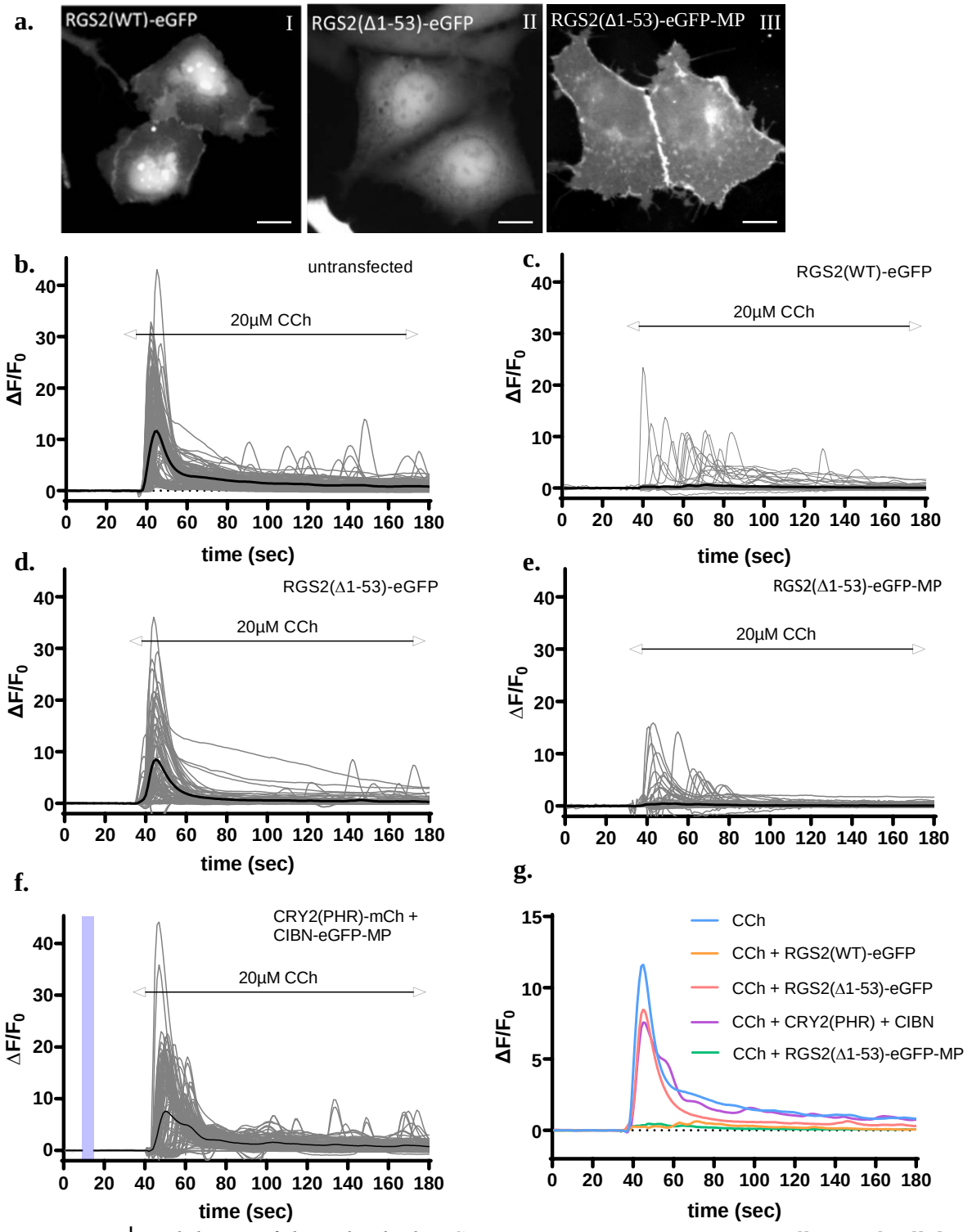

Figure 2.6 | *Validation of the individual PIGM-Iq components in HEK293A cells.* **a,** subcellular localisation of eGFP-tagged (I) RGS2(WT), (II) RGS2(Δ1-53) and (III) RGS2(Δ1-53)-MP in HEK293A cells, scale bar = 10 μm. **b-g,** Individual calcium traces in HEK293A cells expressing the calcium sensor O-GECO stimulated as indicated with 20 μM carbachol (CCh) (black line indicates average). **b,** Calcium response upon addition of CCh in untransfected cells, **c,** in cells transiently expressing RGS2(WT)-eGFP, **d,** cytosolic RGS2(Δ1-53)-eGFP or **e,** membrane bound RGS2(Δ1-53)-eGFP-MP. **f,** CCh-induced calcium response in cells expressing the optogenetic heterodimerising system, CRY2(PHR)-mCh and CIBN-eGFP-MP, stimulated with blue light as indicated by the blue bar (470 nm, 4 sec, 0.11 mW/mm^2) **g,** comparison of the averages of each condition. N = 80-140 cells/condition over ≥2 experiments.

2.3.4 Light-triggered translocation of PIGM-Iq in HEK293A cells

To confirm the ability of cytosolic PIGM-Iq component to translocate upon blue-light illumination, a variant containing C-terminal fluorescent tags on both the cytosolic (RGS2(Δ1-53)-CRY2(PHR)-mCh and membrane bound (CIBN-eGFP-MP) portions of the tool were transiently transfected into HEK293A cells. RGS2(Δ1-53)-CRY2(PHR)-mCh was localised in the cytoplasm and nucleus preceding illumination (Fig. 2.7, a, I). Upon blue light illumination, the cytosolically-localised RGS2(Δ1-53)-CRY2(PHR)-mCh rapidly (within 1 second) translocated to the membrane (Fig. 2.7, a, II) in the approximate location to that seen of CIBN-eGFP-MP (Fig. 2.7, a, IV). RGS2(Δ1-53)-CRY2(PHR)-mCh was then observed to slowly diffuse back into the cytosol over the course of 20 minutes (Fig. 2.7, a, IV). Measurement of cytosolic mCh fluorescence ($\Delta F/F_0$) in individual cells demonstrated the time course of PIGM-Iq translocation and reversion upon blue-light illumination (Fig. 2.7, b), with reversion occurring after approximately 15 minutes post-illumination and remaining steady up to 20 minutes post-illumination.

To establish the intensity of blue light needed to elicit the largest decrease in cytosolic RGS2(Δ1-53)-CRY2(PHR)-mCh, a measurement of cytosolic mCh fluorescence ($\Delta F/F_0$) in individual cells was again measured (Fig. 2.7, c). All light intensities tested resulted in a significant decrease in cytosolic fluorescence when compared to control cells. The decrease in cytosolic fluorescence appeared to increase with increasing light intensity, with 0.22 mW/mm^2 causing the largest movement of RGS2(Δ1-53)-CRY2(PHR)-mCh from the cytoplasm. Increasing the light intensity above 0.22 mW/mm^2, however, resulted in a counterintuitive diminution of movement comparable to that of lower light intensities.

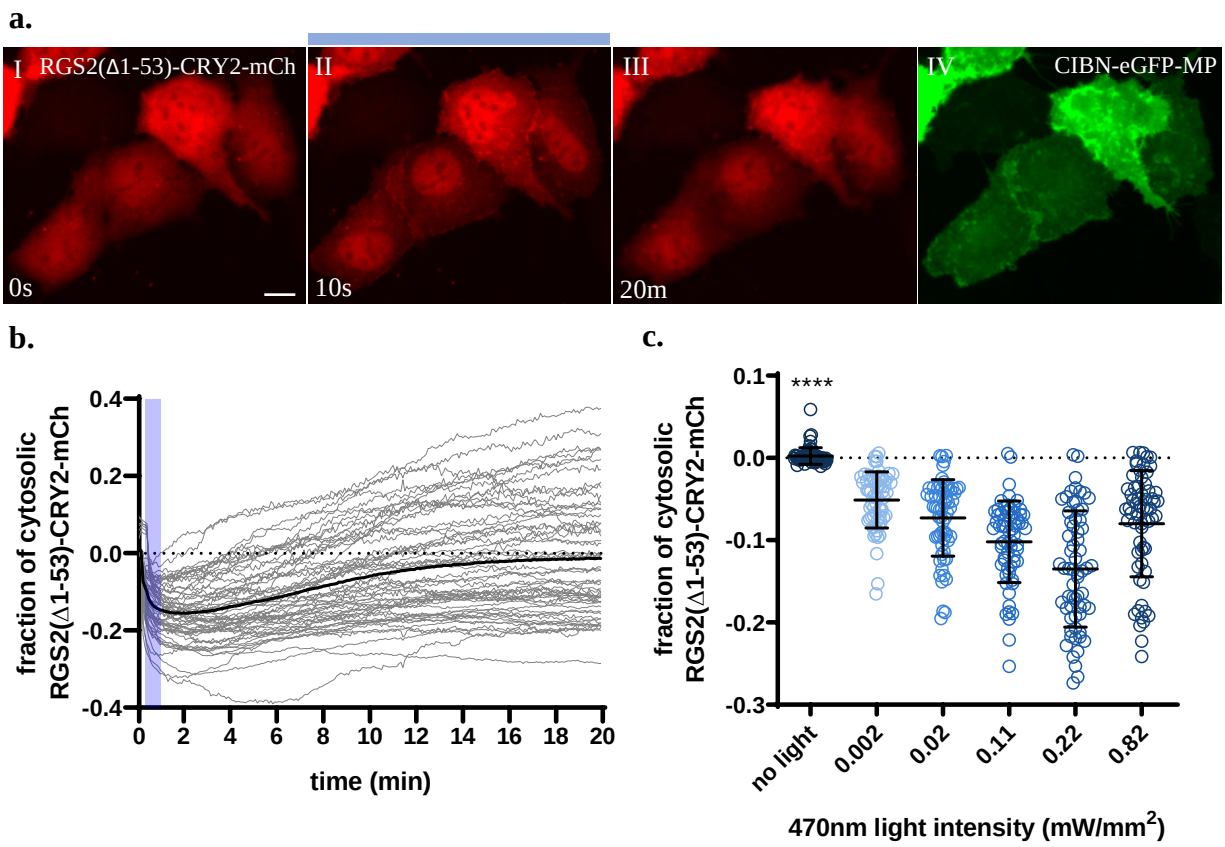

Figure 2.7 | *Light triggered translocation of PIGM-Iq in HEK293A cells.* **a,** Subcellular localisation and reversion of PIGM-I_q before (I), 10 seconds (II) and 20 minutes (III) proceeding blue light exposure (blue bar) (470 nm, 4 sec, 0.11 mW/mm2), with eGFP expression showing the localisation of CIBN-MP (IV), scale bar = 10 µm. **b,** Activation and reversal time course of PIGM-Iq upon illumination with blue light (blue bar) (470 nm, 4 sec, 0.11 mW/mm2) (grey lines indicate individual cell responses, black line indicates average response). Dotted line indicates baseline preceding illumination, N = 57 cells recorded over 3 experiments. **c,** Fraction of cytosolic mCh-tagged RGS2(Δ1-53)-CRY2 directly proceeding illumination with altering intensities of blue light (470 nm, 4 sec), Kruskal-Wallis test with Dunn's multiple comparisons test, P = <0.0001, N = 64 cells/condition recorded over 4 experiments, error bars are SD.

2.3.5 Repeated stimulation of PIGM-Iq

The ability of PIGM-Iq to undergo prolonged membrane association upon exposure to repeated blue light pulses was also tested. Blue light was delivered for 4 seconds every 5 minutes over a 60-minute time course. Robust membrane translocation was observed in cells for the full 60-minute period with no noticeable loss of binding or toxicity (Fig. 2.8, a). This was confirmed by measuring the cytosolic fraction of RGS2(Δ1-53)-CRY2(PHR)-mCh, which demonstrated a rapid decrease upon delivery of the first blue light pulse, followed by a steady decrease in fluorescence over 60 minutes (Fig. 2.8, b). An oscillating pattern was observed every 5 minutes in RGS2(Δ1-53)-CRY2(PHR)-mCh localisation as cytoplasmic levels began to rise following blue light but decreased again upon re-exposure.

a.

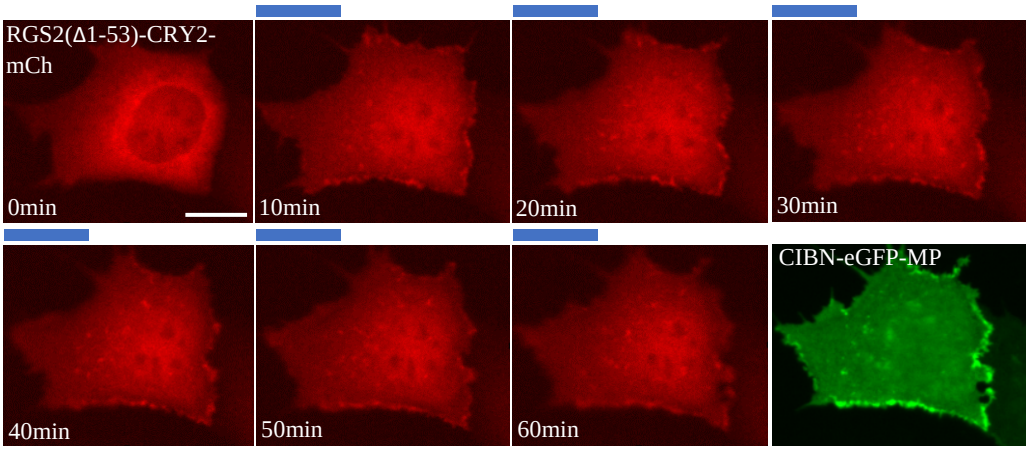

b.

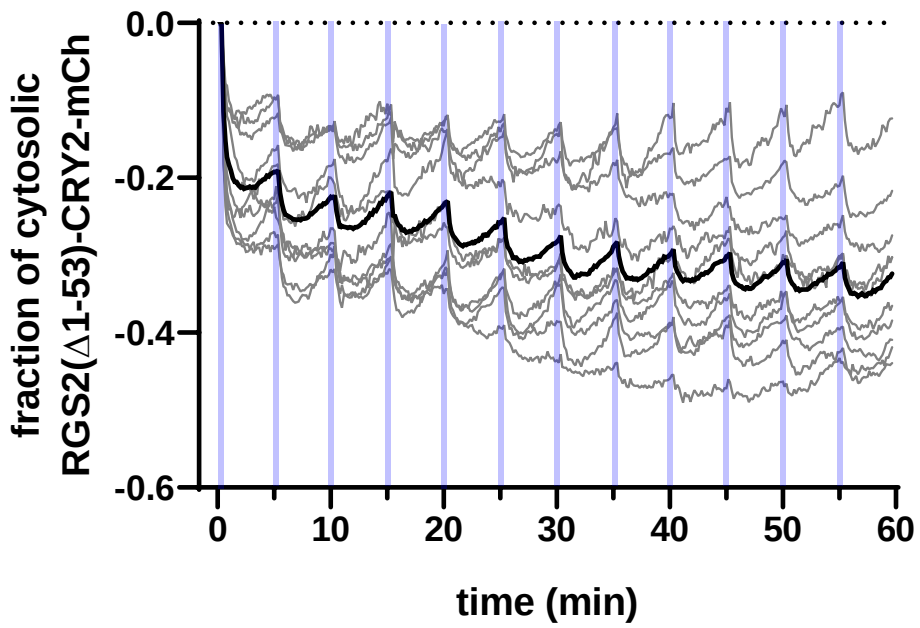

Figure 2.8 | Light triggered reactivation of PIGM-Iq in HEK293A cells. **a,** sustained membrane translocation and prolonged association of cytosolic component of PIGM-Iq upon repeated blue light exposure over 60 minutes (blue bars) (470 nm, 4 sec/5min, 0.11 mW/mm^2), scale bar = 10 µm. **b,** Repeated activation time course of PIGM-Iq upon illumination with blue light every 5 minutes for 60 minutes (blue bars) (470 nm, 4 sec/5min, 0.11 mW/mm2). Black trace indicates averaged response. Dotted line indicates baseline preceding illumination, N = 10 cells over two experiments.

2.3.6 Validation of PIGM-Iq in HEK293A cells

To test the ability of PIGM-Iq to inhibit Gαq-linked increase in $[Ca^{2+}]_i$ upon M_3R activation by carbachol, OGECO-1-HEK293A cells were transiently transfected with the PIGM-Iq construct and fluorescence measured. Cells not expressing the tool demonstrated an increase in fluorescence indicative of an increase in $[Ca^{2+}]_i$ upon carbachol addition in 96.08% of the cells

measured. eGFP-positive cells, denoted by the asterisks, expressing PIGM-Iq did not show an increase in $[Ca^{2+}]_i$ when exposed to blue light (Fig. 2.9, a).

Analysis of changes in $[Ca^{2+}]_i$ of individual cells demonstrated that activation of PIGM-Iq by 4 seconds of blue light resulted in an average decrease of 80.57% in carbachol-induced calcium spikes in expressing cells (Fig. 2.9, c) compared to untransfected cells also exposed to light (Fig. 2.9, b) at the collective peak. This inhibition of responsiveness to CCh was observed in 57.61% of expressing cells. The remaining 42.39% of cells were observed to have calcium spikes that often occurred later and with lower amplitudes than those seen in untransfected cells (Fig. 2.9, c).

Cells expressing the PIGM-Iq system but not exposed to light showed calcium spikes similar to those seen in untransfected cells (Fig. 2.9, d). Calcium amplitudes in these cells were, on average, 27.92% smaller than those seen in untransfected cells, with a total of 79.22% of expressing cells responding to CCh. Likewise, 81.96% of cells expressing the light-insensitive variant (RGS2(Δ1-53)-CRY2(PHR)^{D387A}) of the tool responded to CCh and had similar calcium spike profiles to that of untransfected cells (Fig. 2.9, e), with the average spike amplitude 18.68% lower than that of untransfected cells. Cells expressing the cytosolic variant (RGS2(Δ1-53)-CRY2-eGFP (no CIBN)) of PIGM-Iq had an average spike amplitude 21.72% larger than untransfected cells, with 93.78% of cells responding upon CCh addition (Fig. 2.9, f). A comparison of the averages of each condition demonstrates the differences in calcium spikes between conditions (Fig. 2.9, g).

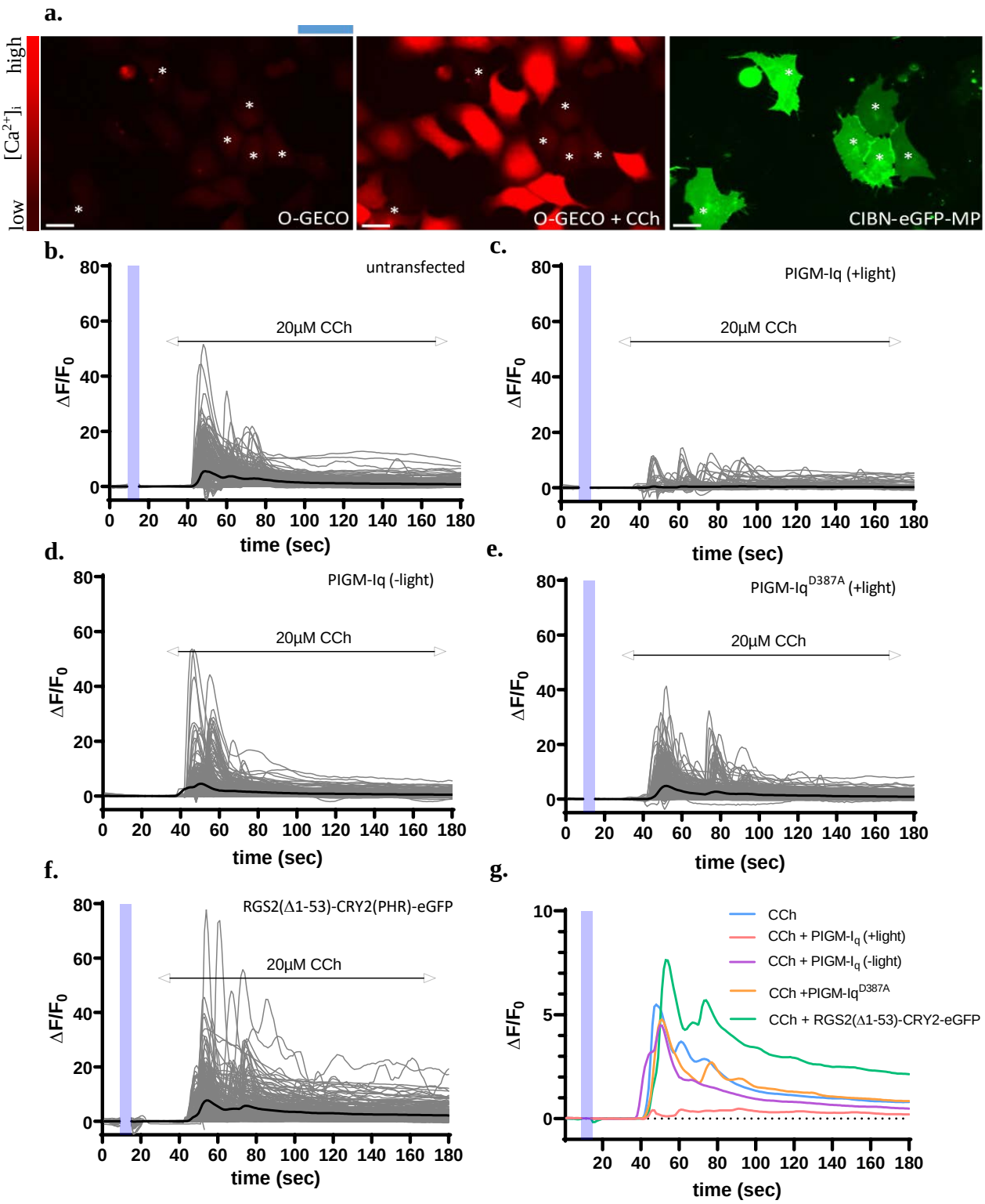

Figure 2.9 | Validation of PIGM-Iq in HEK293A cells. **a,** O-GECO cells expressing PIGM-Iq (CIBN-eGFP-MP-positive cells denoted by asterisks) exposed to blue light (blue bar) and stimulated with 20 µM CCh, scale bar = 20 µm. **b-g,** Individual calcium traces in HEK293A cells expressing the calcium sensor O-GECO stimulated as indicated with 20 µM carbachol (CCh) (black line indicates average) and blue light (blue bar) (470 nm, 4 sec, 0.11 mW/mm2). **b,** Calcium responses upon addition of CCh in untransfected cells, **c,d,** in cells transiently expressing PIGM-Iq or **e,** the light-insensitive PIGMI-q variant, or **f,** the cytosolic PIGM-Iq variant. **g,** comparison of the averages of each condition. N = 225-255 cells/condition from ≥3 experiments.

2.3.7 Light intensity alters the level of calcium efflux inhibition by PIGM-Iq

To test whether different intensities of blue light could alter the level of calcium inhibition by PIGM-Iq, peak calcium amplitudes were recorded in expressing cells after exposure to increasing intensities of 470 nm light (Fig 2.11). All intensities trialled resulted in a significant decrease in peak calcium amplitude when compared to untransfected cells. As expected,

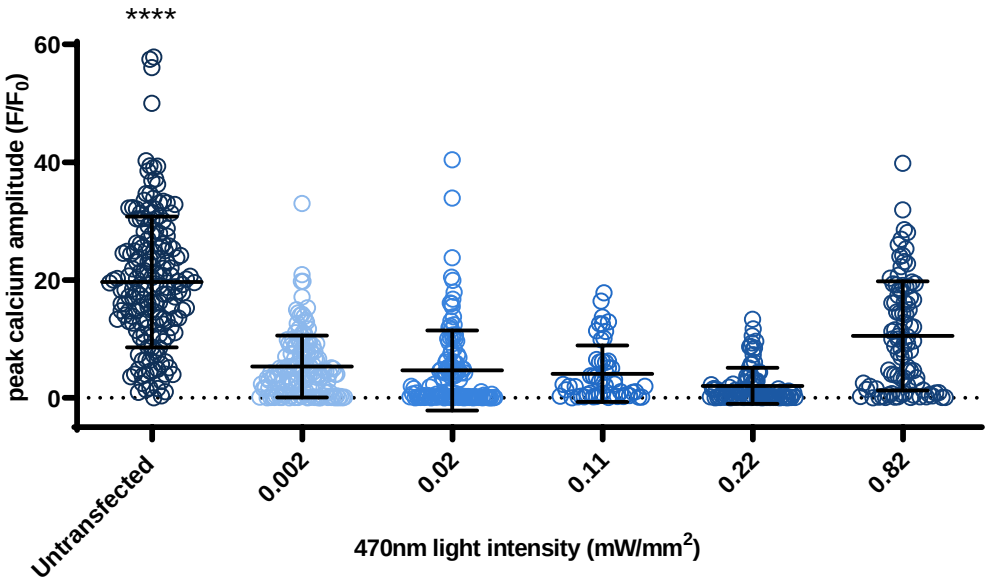

Figure 2.10 | Inhibition of calcium efflux by PIGM-Iq is response to varying intensities of blue light. Peak calcium efflux in PIGM-Iq-expressing cells proceeding illumination with altering intensities of blue light (470 nm, 4 sec). All intensities caused a significant decrease in comparison to untransfected cells, Kruskal-Wallis test with Dunn's multiple comparisons test, P = <0.0001, N = 53-180 cells/condition recorded over at least 3 experiments.

increasing the intensity of blue light delivered to cells resulted in an increase in calcium efflux suppression, with maximum suppression achieved at 0.22 mW/mm^2. However, increasing the light intensity to 0.82 mW/mm^2 resulted in a slight decrease in calcium efflux suppression compared to that observed for 0.22 mW/mm^2, but was still significantly reduced compared to untransfected cells.

2.3.8 Effect of PIGM-Iq on calcium spike dynamics in HEK293A cells

To determine if PIGM-Iq altered calcium spike dynamics when not activated, CCh-induced increases in $[Ca^{2+}]_i$ of individual OGECO-1-HEK293A cells transfected with PIGM-Iq variants were recorded. The peak amplitude, half-width and time of peak was then measured for each fluorescence-based calcium spike and compared to that of untransfected cells (Fig. 2.11, a).

In terms of peak amplitude, PIGM-Iq could effectively inhibit $[Ca^{2+}]_i$ after light stimulation (80.57% reduction) (Fig. 2.11, b). However, cells expressing either PIGM-Iq not exposed to light or light-insensitive variant of the tool were also found to differ significantly from untransfected cells, demonstrating a 27.92% decrease and 16.68% decrease in spike amplitude compared to control, respectively (Fig. 2.11, b). Cells expressing the cytosolic variant of PIGM-Iq without CIBN demonstrated an average peak amplitude 21.72% higher than that observed in control cells (Fig. 2.11, b).

Cells expressing PIGM-Iq exposed to light also showed a significant 10.96% decrease in calcium spike half-width compared to untransfected cells (Fig. 2.11, c). A number of cells in this group demonstrated fast transients unlike those seen in other groups, with an average spike half-width of 11.0 seconds, compared to 12.3 seconds for untransfected cells (Fig. 2.11, c). Cells expressing PIGM-Iq^{D387A} (RGS2(Δ1-53)-CRY2(PHR)^{D387A} + CIBN-eGFP-MP) had a half-width of 15.8 seconds, a 18.30% increase compared to untransfected cells (Fig. 2.11, c). All other conditions had a similar half-width induced by CCh application as untransfected cells (PIGM-Iq (-light): 12.5 seconds, 1.7% increase; RGS2(Δ1-53)-CRY2-eGFP: 17.86 seconds, 30.7% increase.

Furthermore, analysis of the time of peak calcium amplitude in PIGM-Iq expressing cells was significantly delayed by an average of 16.8% compared to untransfected cells (Fig. 2.11, d). Peak spike amplitude for these cells was recorded 31.3 seconds

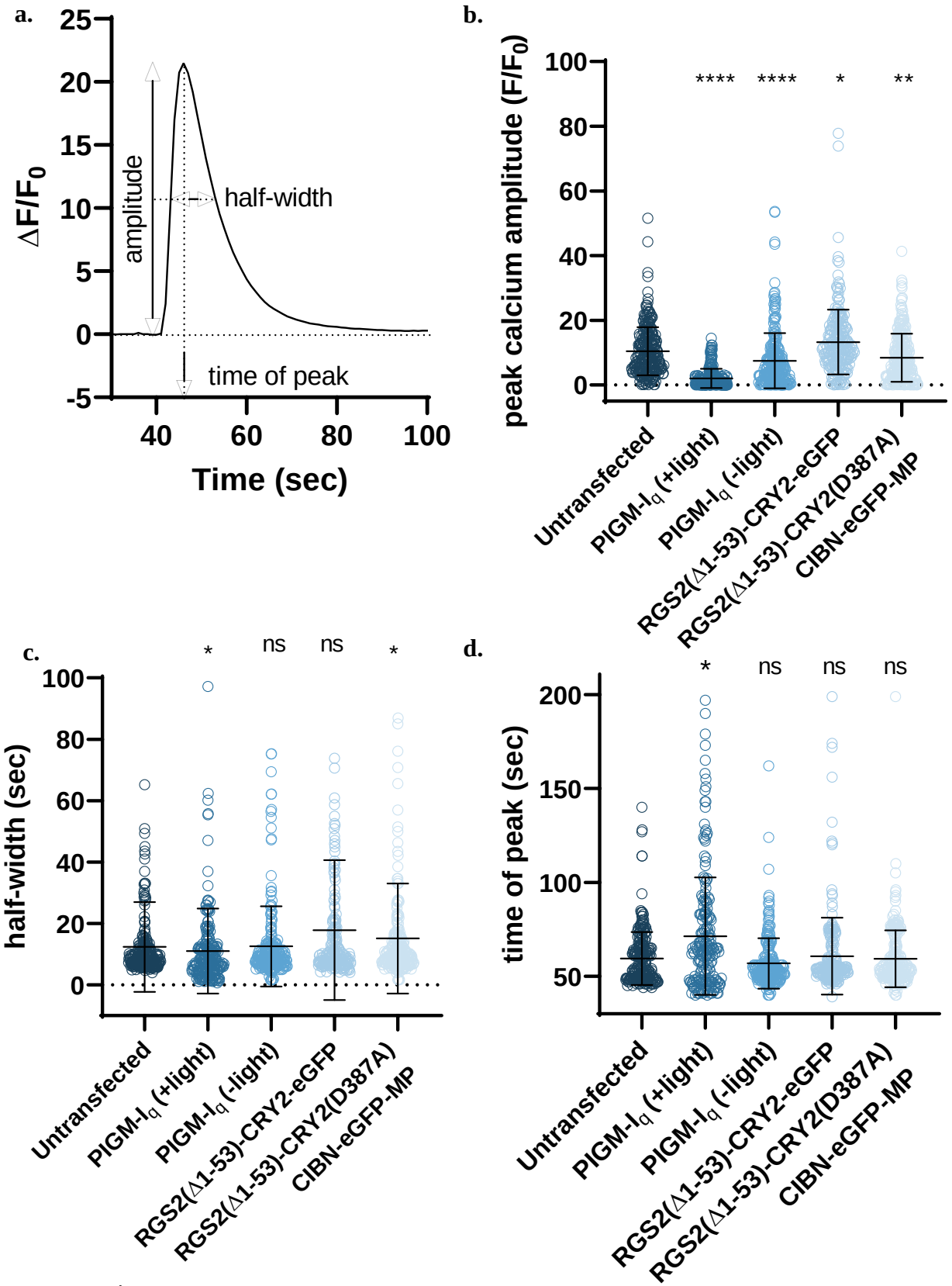

Figure 2.11 | *Effect of PIGM-Iq on calcium spike dynamics in HEK293A cells.* **a,** Typical example of calcium trace in OGECO-1-HEK293A cells stimulated with 20 µM CCh showing spike dynamics analysed - spike amplitude, half-width, and time of calcium peak. **b,** Peak calcium spike amplitudes, **c,** half-width of calcium spike and **d,** time of maximum calcium spike peak of individual cells expressing variants of PIGM-Iq system compared to untransfected cells. Kruskal-Wallis test with Dunn's multiple comparisons test, ns P >0.05, **P < 0.005, ****P < 0.0001. N = 124-190 cells/condition from ≥ 3 experiments. Error bars indicate SD.

proceeding CCh addition (administered at 40 seconds from the initiation of image acquisition), whereas untransfected cells were seen to respond maximally by 19.3 seconds following CCh (Fig. 2.11, d). No significant difference in peak time was seen for cells expressing either PIMG-Iq but not exposed to light, the light insensitive variant of the tool, or the cytosolic variant of the tool, with an average delay of 16.8 seconds, 19.3, and 20.7 seconds following CCh stimulation compared to that of untransfected cells, respectively (Fig. 2.11, d).

2.3.9 Correlation between calcium spike suppression and PIGM-Iq expression level

To assess the correlation between PIGM-Iq expression level and calcium spike amplitude, OGECO-1-HEK293A cells expressing variants of the PIGM-q system were stimulated with carbachol (20uM) and the maximum spike amplitude and eGFP intensity recorded for individual cells (Fig. 2.12). eGFP intensity was used as a proxy for PIGM-Iq expression as a bicistronic vector was used. Cells expressing the PIGM-Iq system exposed to light showed a moderate, negative correlation between expression level and spike amplitude, with the majority of cells showing little to no response upon carbachol addition (ρ -0.33) (Fig. 2.12, a).

Cells expressing either PIGM-Iq not exposed to light (Fig. 2.12, b) or the light-insensitive variant of the tool (Fig. 2.12, d) both demonstrated a moderate, negative correlation between expression levels and calcium spike amplitude (ρ -0.39; ρ -0.43, respectively). Cells with lower eGFP expression showed calcium amplitudes of increased magnitude compared to those with eGFP expression. Expression of the cytosolic variant of PIGM-Iq without CIBN resulted in no correlation between expression level and calcium response, with the majority of cells possessing calcium spikes of similar amplitude upon carbachol addition (Fig. 2.12, c). However, a trend towards larger calcium spike amplitudes in lower expressing cells was observed, although this was found to be insignificant (ρ 0.092).

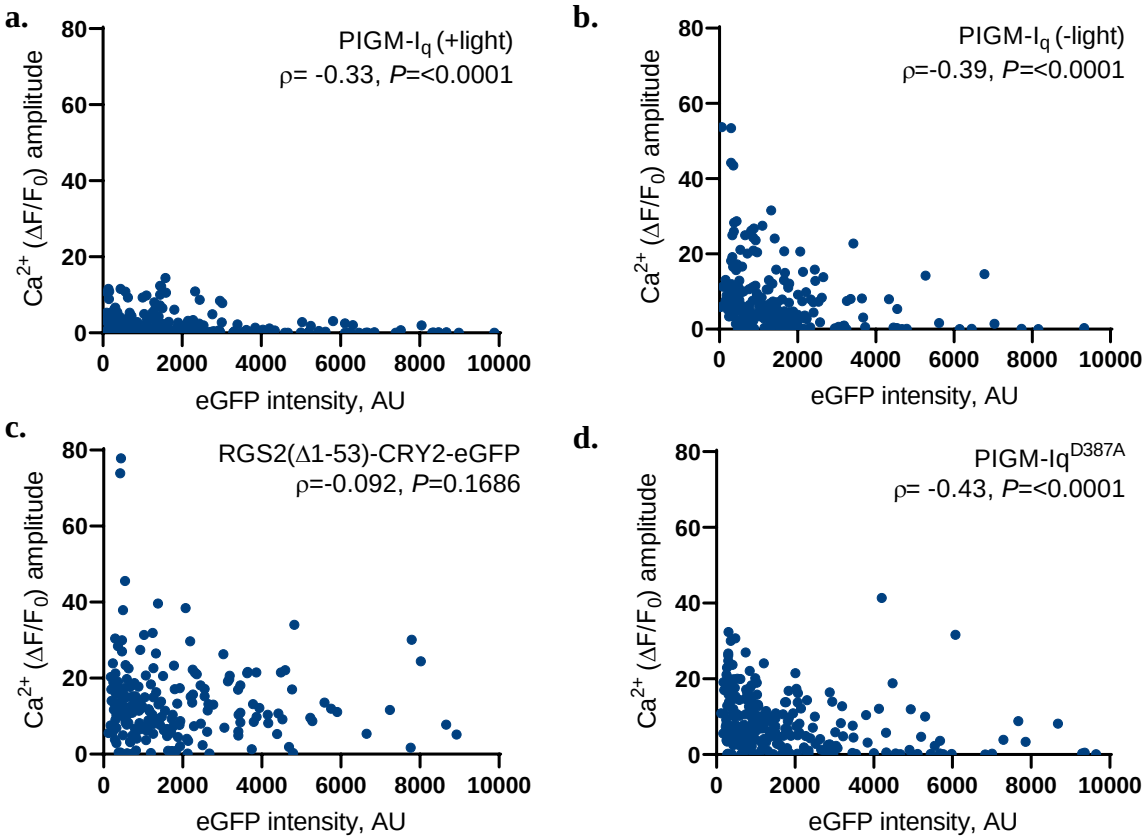

Figure 2.12 | *Correlation analysis between maximum calcium spike amplitude suppression and PIGM-Iq variant expression level in HEK293A cells* stably expressing the calcium sensor O-GECO stimulated with 20 µM carbachol and blue light (470 nm, 4 sec, 0.11 mW/mm^2) expressing **a,** PIGM-Iq exposed to light **b,** PIGM-I_q not exposed to light **c,** the cytosolic PIGM-Iq variant or **d,** the light-insensitive PIGM-Iq variant, N =225-255 cells/condition from ≥ 3 experiments. ρ = non-parametric Spearman's correlation with two-tailed P value.

2.3.10 Effective reversion of PIGM-Iq is expression-level dependent

To test whether PIGM-Iq possessed the ability to revert to an inactive state following illumination, OGECO-1-HEK293A cells were first stimulated by blue light followed by 20µl carbachol. As expected, 96.6% of untransfected cells demonstrated a large increase in $[Ca^{2+}]_i$, with 96.6% of recorded cells responding to CCh, whilst 69.0% of those expressing PIGM-Iq showed little to no increase upon carbachol addition (Fig. 2.13, a). An average suppression of 94.6% of the total amplitude of untransfected cells was observed in expressing cells upon illumination.

To test whether the effects of PIGM-Iq is reversible, cells were first imaged and treated with CCh and light, then the media was replaced to remove CCh and incubated in the dark for

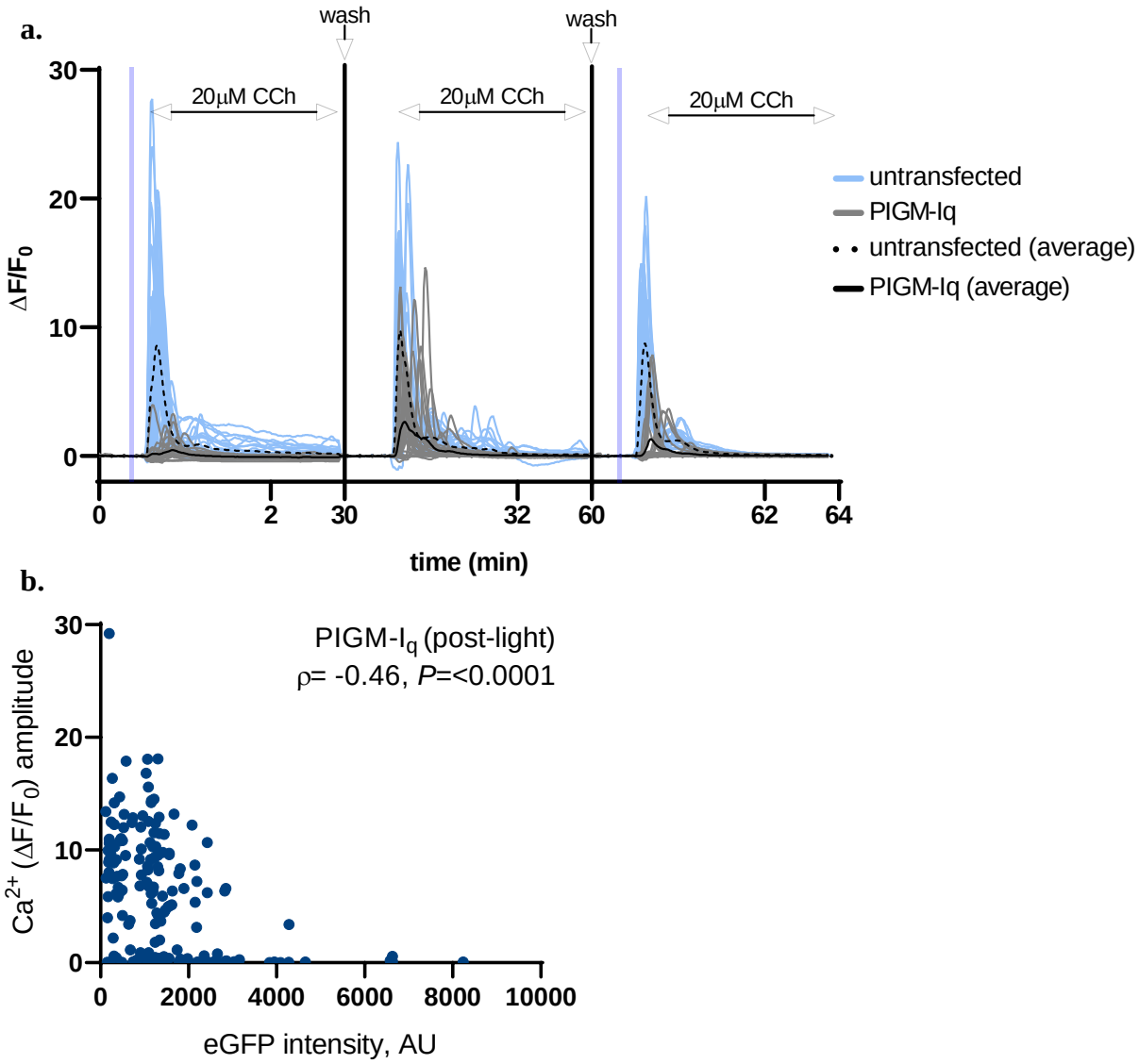

Figure 2.13 | *Activation, reversion, and reactivation of PIGM-Iq.* **a,** Individual calcium traces in HEK293A cells expressing the calcium sensor O-GECO and PIGM-Iq stimulated as indicated with 20 μM carbachol (CCh) (black line indicates average) and blue light (blue bar) (470 nm, 4 sec, 0.11 mW/mm2). Calcium signals were measured for 200 seconds, followed by a media change and 30 minutes incubation in the dark. Light blue traces represent individual calcium traces in untransfected cells (average, dotted line), and grey traces represent those in cells expressing PIGM-Iq (average, bold line). N = 29 cells/condition over 3 independent experiments **b,** Correlation analysis between maximum calcium spike amplitude and PIGM-Iq variant expression level in HEK293A cells following blue light stimulation and 30 minutes incubation in the dark. N =164 cells. ρ = non-parametric Spearman's correlation with two-tailed P value.

30 minutes to allow reversion. Cells were then stimulated with carbachol, but without blue light stimulation. A population of PIGM-Iq-expressing cells (89.7%) demonstrated near comparable increases in $[Ca^{2+}]_i$ to that seen in untransfected cells (96.6% responded). However, 10.3% of cells failed to respond despite the lack of light stimulation. However, this value is similar to the expected value of non-responding cells expressing PIGM-Iq without light stimulation

(20.78% in previous experiment (Fig. 2.9, d)). As a result, the average increase in $[Ca^{2+}]_i$ upon carbachol stimulation was only 27.0% of that seen for untransfected cells. Following further washing and 30-minute incubation period, blue light illumination was again seen to drastically reduce the ability of 52.8% of PIGM-Iq cells to respond to carbachol, whilst untransfected cells appeared unaffected, with 96.9% of cells measured displaying a response. This resulted in an average suppression of CCh-induced calcium spikes by 85.0% of that seen for untransfected cells.

To assess if the expression level of PIGM-Iq was contributing to the lack of reversion seen in some cells, the expression level of PIGM-Iq (as measured with CIBN-eGFP-CaaX) was correlated to the $[Ca^{2+}]_i$ level in response to the second CCh application 30 minutes later (Fig. 2.13, b). A significant negative association (ρ -0.46) was found to exist between expression level and calcium amplitude, with increased expression level likely to result in a reduction of reversion despite an absence of light stimulation.

2.3.11 PIGM-Iq does not inhibit Gαi-linked GPCR signalling

To assess whether PIGM-Iq is selective for Gαq, we tested the possible suppression of Gαi activity in cells. Gαi activation suppresses cAMP production when the Gαs pathway is co-activated, hence a reduction of cAMP production can be used as a measure Gαi activity. We established an assay involving HEK293A cells transiently transfected with two constructs: i) Gαi-linked D_2R and, ii) GloSensor™, a live-cell luciferase-based reported of cAMP. Additional constructs (PIGM-Iq, PIGM-Iq^{D387A}, RGS2 and RGS4) were co-expressed in some experiments.

In the positive control cells, GloSensor-HEK293A cells were first illuminated with blue light for 30 seconds, and after 5 minutes of incubation, isoprenaline (ISO) was then added (for activation of endogenous β2 adrenergic receptor/Gαs). ISO application results in an increase in luminescence indicative of cAMP increase. (Fig. 2.14, a). Quinpirole (QNP/activates D_2R/Gαi (Sullivan, Talangbayan et al. 1998)) application after blue light illumination but 5 minutes prior to ISO application, resulted in a decrease of cAMP within the first 5 minutes, followed by a plateau upon ISO addition that did not increase over the following 10-minute period (Fig. 2.14, b). In cells over-expressing RGS4, which is expected to inhibit Gαi activity, the effect of QNP was absent. The over-expression of full-length RGS2 did not cause any obvious change in cAMP levels, suggesting RGS2 has negligible effects on Gαi. This was also seen in cells expressing PIGM-Iq (+light) and the light-insensitive variant, PIGM-Iq^{D387A}.

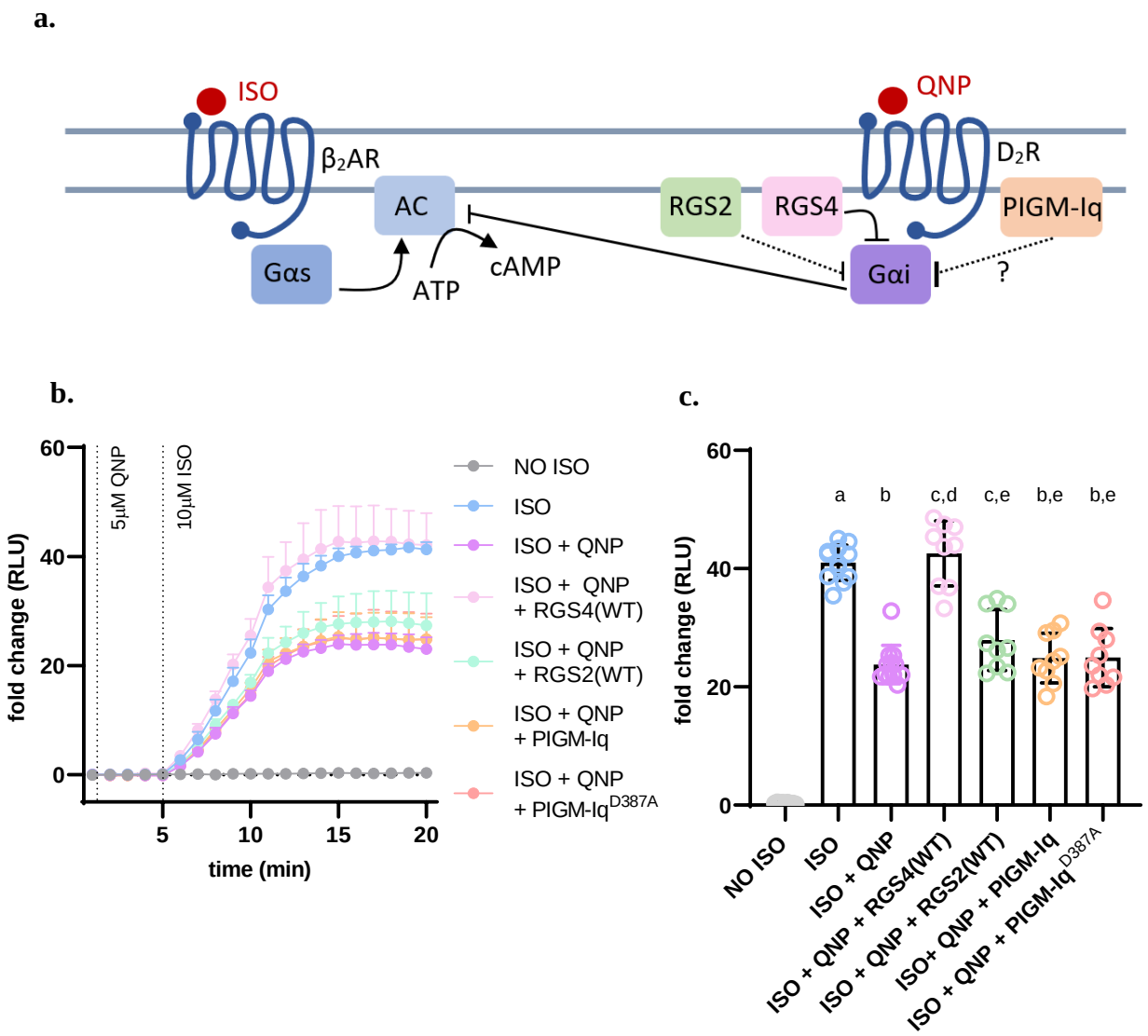

Figure 2.14 | *Gαi cross-reactivity assessment of PIGM-Iq in HEK293A cells.* **a,** Isoprenaline (ISO) activation of Gαs-linked β2 adrenergic receptor (β_2AR) and adenylate cyclase (AC) results in the conversion of ATP to cAMP. Quinpirole (QNP) activation of the Gαi-linked dopamine D2 receptor (D_2R) (Sullivan, Talangbayan et al. 1998) results in the inactivation of AC and the subsequent inhibition of cAMP production. RGS4 is a known inhibitor of Gαi, whilst full-length RGS2 may inhibit Gαi. It is unknown whether PIGM-Iq inhibits Gαi **b,** time course of cAMP in GloSensor-HEK293A cells expressing the PIGM-Iq system in comparison to RGS4 and cells only expressing GloSensor™ exposed to blue light (30 s/5 min, 470 nm, 0.11 mW/mm^2) upon the addition of 5 μM QNP and 10 μM ISO. Error bars are SD **c,** Comparison of end-point cAMP measurements in cells expressing the PIGM-Iq system in comparison to RGS4 and cells only expressing GloSensor™ exposed to blue light (30s/5min, 470 nm, 0.11 mW/mm^2) pre-incubated with 5 μM QNP and 10 μM ISO. Bars indicate mean and SD, Kruskal-Wallis test with Dunn's multiple comparisons test: [a] denotes significance difference from No ISO ($P < 0.0001$), [b] denotes significance difference from ISO ($P < 0.01$), [c] denotes no significance difference from ISO ($P \geq 0.05$), [d] denotes significance difference from ISO + QNP ($P < 0.01$)) and [e] denotes no significant difference form ISO + QNP ($P \geq 0.05$). All results are from at least three independent experiments repeated in triplicate.

This was further confirmed through the assessment of end-point luminescence values of the different treatment groups (Fig. 2.14, c). A significant increase was observed from baseline luminescence upon the addition of ISO. A significant decrease was observed upon the addition

of QNP compared to ISO alone; however, this decrease was eliminated in the presence of over-expressed RGS4, with cAMP levels not differing from that observed for ISO alone but differing from cAMP levels following the addition of both ISO and QNP. QNP addition to cells expressing full length RGS2 caused a decrease in luminescence that was similar to that seen for ISO and QNP; however, levels did not differ significantly from that seen for ISO alon. Contrary to this, QNP addition to cells expressing either PIGM-Iq or PIGM-Iq^{D387A} caused a significant decrease in cAMP compared to ISO alone, with levels not differing from those seen for the addition of both QNP and ISO.

2.3.12 PIGM-Iq does not inhibit Gαs-linked GPCR signalling

ISO is known to activate Gαs-linked endogenous β_2AR, resulting in an increase in cAMP upon activation of AC, with full-length RGS2 acting as a modulator of AC activity (Fig. 2.15, a). To further assess the selectivity of PIGM-Iq for Gαq, the ability of PIGM-Iq to inhibit cAMP production of AC upon Gαs stimulation was tested. To do this, ISO was added to HEK293A cells expressing GloSensor with blue light pulsed every 5 minutes for 30 seconds. As the GloSensor assay is based on the 'collective' luciferase activity of all cells in the culture surface, a transilluminator with light output of 0.04 mW/mm^2 was utilised to achieve the uniform illumination of multiple wells simultaneously for comparison. Although this light intensity was lower than the calcium imaging assay, this light intensity was previously shown to be sufficient to achieve the membrane recruitment of CRY2 and inhibition of calcium elevation by PIGM-Iq (Fig 2.7 and 2.10). Upon stimulation with ISO, an increase in cAMP was observed in untransfected cells compared to unstimulated cells (Fig. 2.15, b). A slight decrease in luminescence upon ISO addition was seen in cells expressing full-length RGS2 in comparison to cells expressing only GloSensor™; however, this change was not found to be significantly different. Cells expressing either PIGM-Iq or PIGM-Iq^{D387A} caused no change in Gαs-mediated cAMP increases within the timeframe measured. This was further confirmed through the assessment of end-point luminescence following blue light illumination and ISO addition (Fig. 2.15, c). ISO addition caused a significant increase in luminescence compared to unstimulated cells. No statistical difference was found between ISO and cells expressing either full-length RGS2, PIGM-Iq or PIGM-Iq^{D387A}.

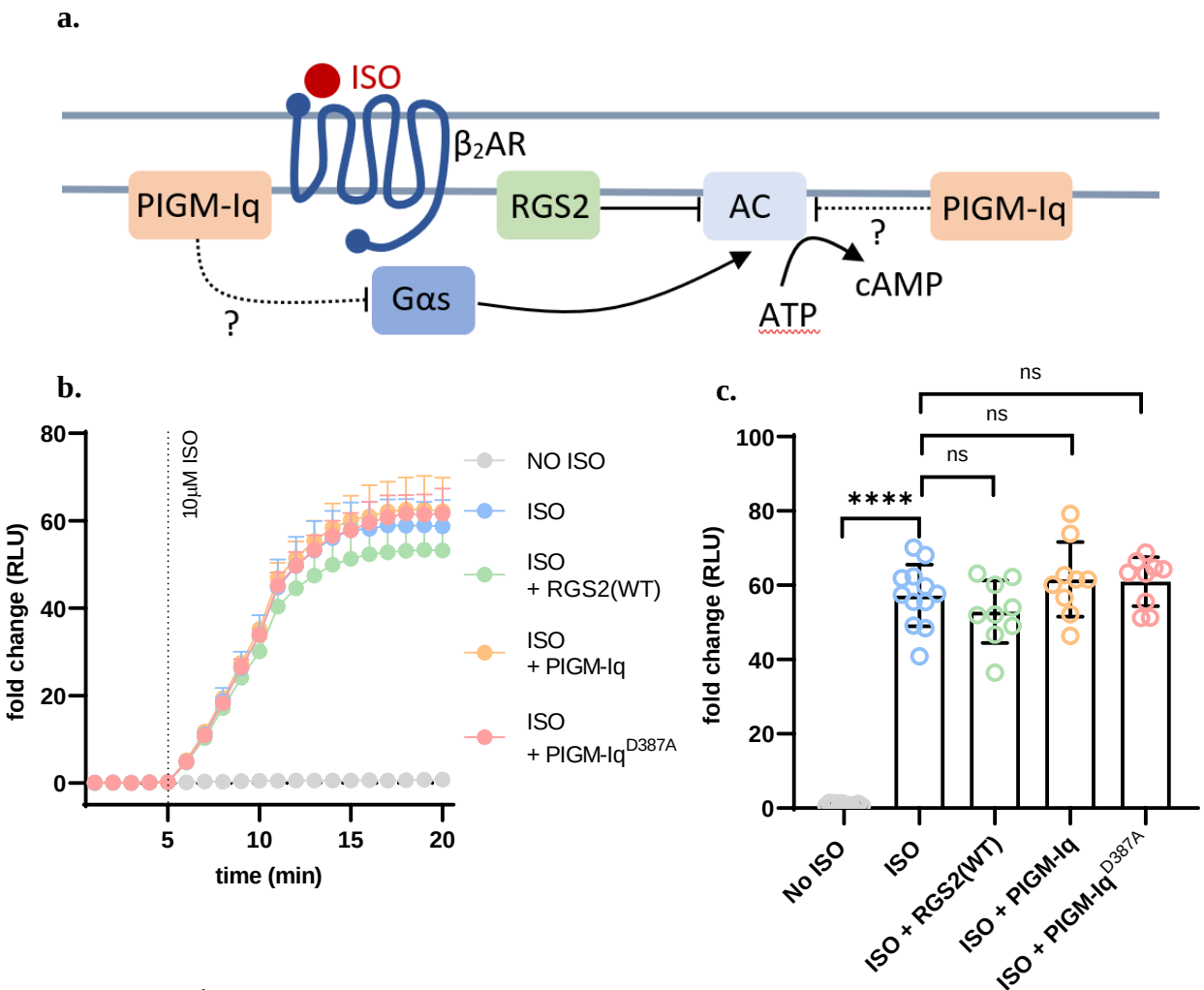

Figure 2.15 | *Gαs cross-reactivity assessment of PIGM-Iq in HEK293A cells.* **a,** Isoprenaline (ISO) activation of Gαs-linked β2 adrenergic receptor (β_2AR) and adenylate cyclase (AC) results in the conversion of ATP to cAMP. Full-length RGS2 has no activity towards Gαs, but the N-terminus of RGS2 is a known inhibitor of AC activity. It is unknown whether PIGM-Iq inhibits Gαs or AC. **b,** time course of cAMP in cells GloSensor-HEK293A cells expressing the PIGM-Iq system compared to untransfected cells exposed to blue light (30 s/5 min, 470 nm, 0.11 mW/mm^2) exposed to 10 μM ISO. Error bars are SD **c,** Comparison of end-point cAMP measurements in cells expressing the PIGM-Iq system in comparison to untransfected cells exposed to blue light (30 s/5 min, 470 nm, 0.11 mW/mm^2) pre-incubated with 10 μM ISO. Bars are mean and SD, one-way ANOVA with Tukey's multiple comparisons test: ****P = <0.0001, ns P >0.05. All error bars are SD. All results are from at least three independent experiments repeated in triplicate.

2.4 Discussion

G protein signalling is a fundamental aspect of neural function, and its physiological role in neuromodulation has yet to be fully understood. Despite the large array of chemical and optogenetic-based tools already available to manipulate neuromodulation, tools that can achieve selective, light-activated inhibition of G protein signalling are still lacking. Thus, we

aimed to design and validate an optogenetic system to inhibit endogenous Gαq signalling through selective inactivation of the Gαq subunit.

The optogenetic system for the selective inactivation of the endogenous Gαq subunit, PIGM-Iq, described in this chapter was generated through a C-terminal fusion of RGS2(Δ1-53) to CRY2(PHR), with CIBN localised at the membrane via a CaaX-box prenylation motif. Thus, upon blue-light illumination, it was proposed that CRY2(PHR) would translocate to the membrane, localising RGS2(Δ1-53) in proximity to the endogenous GPCR-fused Gαq subunit and allow for the hydrolysis of GTP to GDP and subsequent termination of Gαq signalling. In comparison to other optogenetic systems for the inactivation of Gα proteins using RGS proteins, the PIGM-Iq system offers selectivity towards the Gαq signalling pathway. This was achieved through careful inclusion and removal of key domains within the RGS2 protein to maximise Gαq inhibition whilst limiting interactions with other Gα proteins.

It is worth noting that expression of the CRY2/CIBN system alone caused a slight decrease in calcium efflux when exposed to light compared to control cells. This may be due to high levels of CIBN expression on the membrane which may interfere with Gαq signalling. It would be interesting in future experiments to see if this effect is still present even in the absence of light. This effect may also be more pronounced due to the use of HEK cells and their level of overexpression. This effect may be reduced in neurons. We have consistently observed lower expression levels of CRY2/CIBN systems in neurons compared to HEK cells. Despite this, however, experiments looking at PIGM-Iq (-light) appear to have relatively comparable calcium profiles to those of control cells. Differences between experiments may also therefore be due to experimental variation and time-dependent cell health.

Overall, the results support the proposed model of PIGM-Iq activity, which involved the relocation of the constitutively active RGS2 enzymatic domain from the cytosol, where it has minimal function, to the membrane to achieve the suppression of Gαq signalling in a light-dependent manner. The inhibition of Gαq signalling by PIGM-Iq was also found to be reversible and reactivable.

It is interesting to note that the higher light intensity did not lead to greater translocation or functional inhibition and the level of expression did not correlate largely to the amount of inhibition. It is also worth noting that despite previous reports that wild type RGS2 is capable of blocking Gαi and adenylate cyclase activity, we did not detect measurable inhibition of these pathways with PIGM-Iq. Whereas the lack of activity on AC can be contributed to the removal of the N-terminus segment, the lack of activity on Gαi is not as simple to interpret. This lack of observed inhibition is likely to be a combination of protein structure, orientation at the

membrane after light recruitment and a balance between protein concentration and affinity. There is also a possibility that the assay used did not possess the sensitivity to detect this inhibition, or that inhibition occurred beyond the timeframe of the experiment.

In this study, it was observed that PIGM-Iq displays a level of background activity. The most likely reasoning is due to the use of the TRITC filter set, which does possess the ability to transmit excitatory wavelengths down to ~530 nm. It is known that the absorption profile of cryptochromes occurs maximally within the UVA/blue light range, with a peak absorbance at 450 nm; however, absorption does exist at wavelengths above 500 nm, although at a reduced level compared to 450nm (Ahmad, Grancher et al. 2002, Banerjee, Schleicher et al. 2007). Activation of CRY2(PHR) by high intensity 514nm light, as well as prolonged, high intensity 561 nm light, has been confirmed; however, this was not observed at lower intensities (Kennedy, Hughes et al. 2010, Tucker, Vrana et al. 2014). Taking this into consideration, it may be possible that the imaging of O-GECO1 fluorescence may cause a low level of PIGM-Iq stimulation. This stimulation is not enough to cause full Gαq inhibition, but it may result in a level of modulation that leads to an alteration of calcium spikes, even in the absence of blue light. Future experiments should consider the use of an excitation filter that does not permit the activation of CRY2(PHR), paired with the use of R-GECO1, which possess an excitation and emission peak at 561 nm and 589 nm, respectively (Wu, Liu et al. 2013).

Overall, it can be concluded that PIGM-Iq reduces Gαq-linked calcium efflux upon exposure to blue light when expressed in mammalian HEK cells. It can also be concluded that this inhibitory effect is specific to Gαq, and that PIGM-Iq does not appear to inhibit either Gαs or Gαi-linked signalling in mammalian cell culture.

Chapter 3 │ Validation of PIGM-Iq in behaving *C. elegans*

3.1 Introduction

As PIGM-Iq was able to supress Gαq signalling robustly in mammalian cell lines, it was subsequently tested in the nematode - *Caenorhabditis elegans.* A valuable feature of *C. elegans* in regard to this project is the prior characterisation of Gαq mutants in the literature. If functional in these animals, PIGM-Iq-expressing worms should share a similar behaviour phenotype after light illumination. In addition, as these mutant strains possesses Gαq proteins with constitutive altered activity, PIGM-Iq could present a valuable tool in the *C. elegans* field, allowing for temporally controlled Gαq signalling disruption with cell type specificity, limiting developmental or long-term effects.

3.1.1 GPCRs and G proteins in C. elegans

The *C. elegans* genome encodes more than 1000 GPCRs, signalling through 21 Gα subunits (Matúš and Prömel 2018). These subunits have high sequence homology to their mammalian counterparts and couple to conserved intracellular signalling cascades. As a result, *C. elegans* have been utilised for decades as a powerful system to investigate the mechanisms underlying GPCR and G protein function, as well as their involvement in various biological processes.

3.1.2 EGL-30 – *the Gαq of* C. elegans

In 1996, the homolog of mammalian Gαq in *C. elegans* was identified in a seminal paper by Brundage et al. (Brundage, Avery et al. 1996). In this paper, a previously uncharacterised *C. elegans* strain - *egl-30* - was found to have a mutation in a gene possessing 83% sequence homology to that of the mammalian Gαq G protein (Fig. A1). It was found that *C. elegans* Gαq could effectively activate endogenous PLCβ in mammalian cells, as well as functionally couple to mammalian Gαq-linked GPCRs (Brundage, Avery et al. 1996). The functional activity of *C. elegans* Gαq was also found to possess comparable efficacy in mammalian cells to mouse Gαq family G proteins. It was therefore deemed likely that the *C. elegans* Gαq pathway underwent similar molecular interactions to that of the mammalian Gαq pathway.

C. elegans egl-30 mutants that have little to no Gαq function were either sub-viable, arrested at various stages of development, or were flaccid and paralysed (Brundage, Avery et al. 1996). In *egl-30* mutant strains that possessed reduced function, but not total loss-of-

function (*egl-30(ad803)* and *egl-30(ad806)*), animals retained eggs in the uterus, displayed uncoordinated, slow movement and reduced pharyngeal pumping (Brundage, Avery et al. 1996). When over-expressing Gαq, the animals had empty gonads, early egg laying and hyperactive movement, phenotypes opposite to that of the animals containing defective Gαq proteins (Brundage, Avery et al. 1996).

In a study by Lackner et al., DAG production resulting from the interaction between *egl-30*/Gαq and PLCβ in the neuromuscular junction resulted in the release of neurotransmitter at the synapse (Fig. 3.1) (Lackner, Nurrish et al. 1999). It was described that Gαq activity was involved in acetylcholine release at the neuromuscular junction, in concert with Gαi, resulting in muscle contraction and relaxation involved in locomotion and pharyngeal pumping, as well

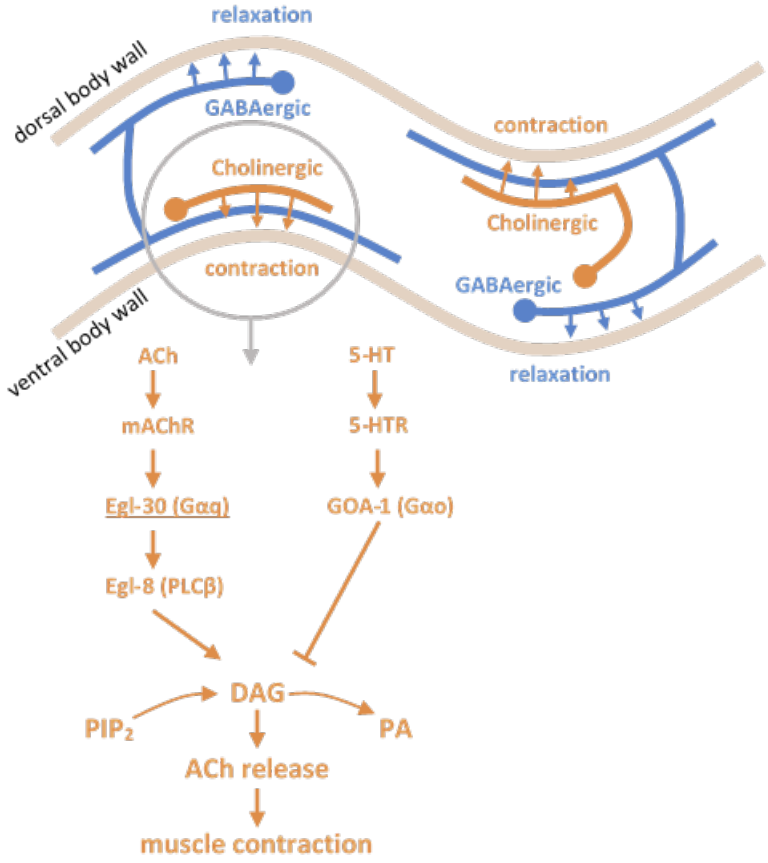

Figure 3.1 | *Movement in* C. elegans *is mediated by the simultaneous contraction and relaxation of opposite body wall segments*. Contraction of the ventral body wall muscle occurs through the actions of acetylcholine (ACh) through the Gαq-linked muscarinic acetylcholine receptor (mAChR). This eventuates in the production of DAG and the release of ACh into the neuromuscular junction, resulting in contraction. This is opposed by the actions of the Gαo-linked serotonin (5-HT) GPCR, which inhibits the production of DAG in cholinergic neurons. Simultaneous relaxation of the dorsal wall is produced through the actions of ACh-stimulated GABA release from GABAergic motor neurons. This pattern of contraction and relaxation along the length of the worm results in the production of a sinusoidal wave and the generation of forward locomotion. Figure based on Lackner, Nurrish et al. 1999, Han, Bellemer et al. 2015, and Altun, Z.F. and Hall, D.H. 2011 (WormAtlas.org).

as vulval contraction for egg laying (Hajdu-Cronin, Chen et al. 1999, Lackner, Nurrish et al. 1999, Altun 2011, Han, Bellemer et al. 2015, Thapliyal and Babu 2018).

Due to the well-documented reliance of *C. elegans* locomotion on Gαq activity, we proposed that activtion of PIGM-Iq in the motoneurons would result in a reduction in the production of DAG at the neuromuscular juction, therefore decreasing the release of acetylcholine at the synapse. As a result, the animals should display altered coordination, resulting in reduced locomotion when illuminated with blue light, but should have little to no locomotion defects when not illuminated.

3.2 Methods

3.2.1 C. elegans *husbandry*

Wild type (N2) *C. elegans* (gift from Dr Zhitao Hu, Queensland Brian Institute) were maintained on 60 mm plates containing standard nematode growth medium (NGM) (3g NaCl, 17g agar, 2.5g tryptone, 1ml 1M CaCl2, 1ml 5mg/ml cholesterol in ethanol, 1ml 1M MgSO4 and 25ml 1M KPO4 made up to 1 litre with H2O) seeded with *E. coli* (OP50). Worms were cultured at 20ºC and transferred to a fresh seeded plate every 2-3 days.

3.2.2 Generation of transgenic C. elegans

Sequence alignment between *Homo sapiens* GNAQ (NCBI Reference Sequence: NM_002072.5) and *C. elegans* EGL-30 (NCBI accession number AAB04059.1) was generated using Clustal Omega (EMBL-EBI) (Sievers, Wilm et al. 2011, Madeira, Park et al. 2019).
Transgene was created using starndard cloning techniques. Breifly, RGS2(Δ1-53)-CRY2(PHR)-T2A-CIBN-eGFP-CaaX or RGS2(Δ1-53)-CRY2(PHR)^{D387A}-T2A-CIBN-eGFP-CaaX were transferred to JB6-Psnb1 vectors using the oligonucelotide primers: KpnI-T7-5F: 5’-attggtacccactatagggagaccc-3’ and CaaX-TAA-MluI-3RC: 5’-aagacaaagtgtgtaattatgtaaacgcgtatt-3’. The KpnI restriction enzyme site located within the sequence of CRY2 was removed using the overlapping PCR technique using the following oligonucleotide primers: CRY2-KpnI remove-5F: 5’-tagagttgggcaccaattacgcaaag-3’ and CRY2-KpnI remove-3RC: 5’-ctttgcgtaattggtgcccaactcta-3’. The two inserts were ligated into the JB6-Psnb1 vector to create JB6-Psnb1-RGS2(Δ1-53)-CRY2(PHR)-T2A-CIBN-eGFP-CaaX and JB6-Psnb1-RGS2(Δ1-53)-CRY2(PHR)^{D387A}-T2A-CIBN-eGFP-CaaX. Both

trasnegenes were under the control of the Synaptobrevin-1 promotor (Psnb-1) for pan-neuronal expression.

The plasmids were introduced into the N2 animals via microinjection. Worms were injected on an agarose pad composed of 2% agarose. These were constructed by dropping 200µl of heated agarose onto a 50 x 24 mm glass coverslip. Immediately, another coverslip was placed on top and the agarose was allowed to dry for 60 seconds. The top coverslip was then removed, and the pad left to dry overnight at room temperature.

Glass micropipettes were prepared using 1.5 mm glass capillaries (Harvard apparatus, 1.5 OD x 0.86 ID x 100 L mm, Cat# W3 30-0057) pulled to the appropriate size using a micropipette puller (Sutter Instrument model P-1000). Pulled pipettes were loaded with injection solution composed of the following components in M9 solution:

Table 3.1 | injection solution components for the production of transgenic C. elegans

Component	**Amount**
Plasmid DNA: JB6-Psnb1::RGS2(Δ1-53)::CRY2(PHR)::T2A::CIBN::eGFP::CaaX Or JB6-psnb1::RGS2(Δ1-53)::CRY2(PHR)^{D387A}::T2A::CIBN::eGFP::CaaX	50ng/ul
Co-injection marker: pCFJ90-Pmyo-2::mCherry::unc-54utr	5ng/ul
DNA ladder	45ng/ul

Worms to be injected were positioned so that gonads were visible, immobilised on an 2% agarose pad and covered with halocarbon oil (Sigma-Aldrich, Cat# H8773). Injections were performed on a Leica DM IRB inverted microscope equipped with a pico-liter microinjector (Warner Instruments model PLI-10) and micromanipulator. Worms were injected with the transgene in the gonad, and once completed, were revived in PBS until movement was seen. Following this, injected worms were moved to a new seeded NGM plate and propagated for 2 days. Expression of the co-injection marker was then detected using a fluorescence stereomicroscope. Worms found to be expressing the marker were transferred to separate seeded NGM plates. This was continued until a stable line was created.

Worms were imaged on fresh 2% agarose pads using a fixed stage upright fluorescent microscope (Olympus BX51WI) equipped with a Scientific CMOS camera ((Hamamatsu, ORCA- Flash4.0) and a water immersion objective (40×/NA0.8 (Olympus)) and white light LED (X-Cite 110LED, Excelitas Technologies). Light intensity through this source was maintained at 20% of maximum intensity, and worms were imaged at 2x2 binning with a 50ms exposure time. GFP (excitation at 470 nm) was imaged using a GFP filter set (472/30, FF495-Di03, FF01-520/35). Image acquisition was performed using Micro-Manager© 1.4.22.

3.2.3 C. elegans *locomotion*

Locomotion assays were performed on 60 mm NGM plates pre-incubated at 20ºC. Plates were seeded with 30ul of fresh OP50 *E. coli* overnight culutre, and left to dry. Once dry, plates were immediately covered and used within 1hr. Staged adult hemaphrodites were transferred to a pre-seeded NGM plate and allowed to habituate for 3 minutes. Once habituated, locomotion was recorded for 1 minute (QIClick™ Digital CCD Camera, QImaging). The plate was transferred to a transilluminator (Major Science BlueView MBE-300) and illuminated for 30 seconds (470 nm, 0.30 mW/mm^2). Locomotion was then recorded 1 minute post-illumination for a total of 1 minute. Proceeding this, worms were incubated in the dark for 20 minutes at 20ºC, after which another set of pre- and post-illumination locomtion meaurements were performed as described above. Body bends per minute were calculated by counting the number of flexions that occurred anterior to the pharynx as the worm moved forward. Movement was not counted during spontaneous reversals, and the flexion occuring directly after this movement was ignored.

Statistical analyses were performed, and graphs were produced with Prism 8.3 software (GraphPad Software, San Diego, California USA, www.graphpad.com).

3.3 Results

The *C. elegans* EGL-30 Gαq posseses 83% sequence homolgy to mammalian Gαq (Figure A1) (Lackner, Nurrish et al. 1999), and is capable of activating mammalian PLCβ. This suggests the structure-function relationship of Gαq is conserved with EGL-30 and mammalian RGS2 would likely to have the same inhibitory effects on EGL-30 as mammalian Gαq. The ability of intact wild-type RGS2 to interact effectively with worm Gaq was first

tested. Transgenic animals expressing full-length mammalian RGS2 were either not viable or sub-viable. Sub-viable animals often did not reach maturity, arresting at vaious stages of development (data not shown). Transgenic animals that did survive to adulthood were paralysed and did not produce transgenic offspring. The phenotype of these animals was consistent with that reported in the literature for mutant lines possessing severely defective Gαq (Brundage, Avery et al. 1996, Lackner, Nurrish et al. 1999). Thus, it was concluded that mammalian RGS2 possessed the ability to negativly regulate *C. elegans* Gαq.

Transgenic lines of PIGM-Iq and PIGM-Iq^{D387A} were generated. PIGM-Iq and PIGM-Iq^{D387A} expression was confirmed in all major ganglia and process bundles of the nervous system by visualising the eGFP fluorescence associated with CIBN-eGFP-CaaX (Fig. 3.2). Worms expressing PIGM-Iq did appear to grow at a slower rate compared to wild type N2 animals, or those expressing PIGM-Iq^{D387A} (data not shown). For both transgenic lines, animals expressing high levels of the tool either failed to hatch or arrested soon after (data not shown). Together these suggest CRY2(PHR)/CIBN may still have low level background binding (as PIGM-Iq worms grow slower than the PIGM-Iq^{D387A} line) and that the RGS domain, when overexpressed, may still have weak background GAP activity even in the absence of light illumination and recruitment to the membrane (as high expressors of both PIGM-Iq and PIGM-Iq^{D387A} both have limited viability).

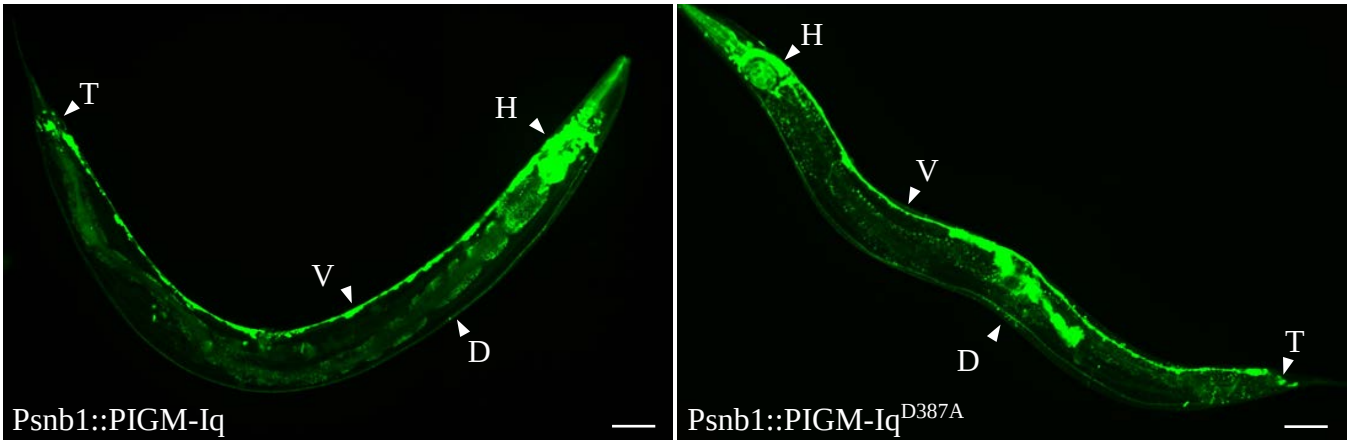

Fig 3.2 | *Pan-neuronal expression of eGFP-tagged PIGM-Iq and PIGMIq^{D387A} in* C. elegans showing major ganglia (head (HG) and tail ganglia (TG)) and process bundles (dorsal (DC) and ventral cord (VC)). The fluorescence observed is from the green fluorescence of eGFP. Scale bar, 50 µm.

3.2.1 Locomotion rate is decreased upon light exposure in worms expressing PIGM-I

To validate the ability of PIGM-Iq to inhibit Gαq in *C. elegans* under the control of light illumination, locomotion rate was assessed by analysisng body bends per minute. To ensure that blue light did not affect the locomotion rate of animals, body bends of wild type N2 animals upon light exposure was analysed. No significant decrease in locomotion rate was observed in these animals when exposed to blue light at either time points; however, an overal decrease in movement was seen over time (Fig 3.3, a). This same trend was also present in transgenic

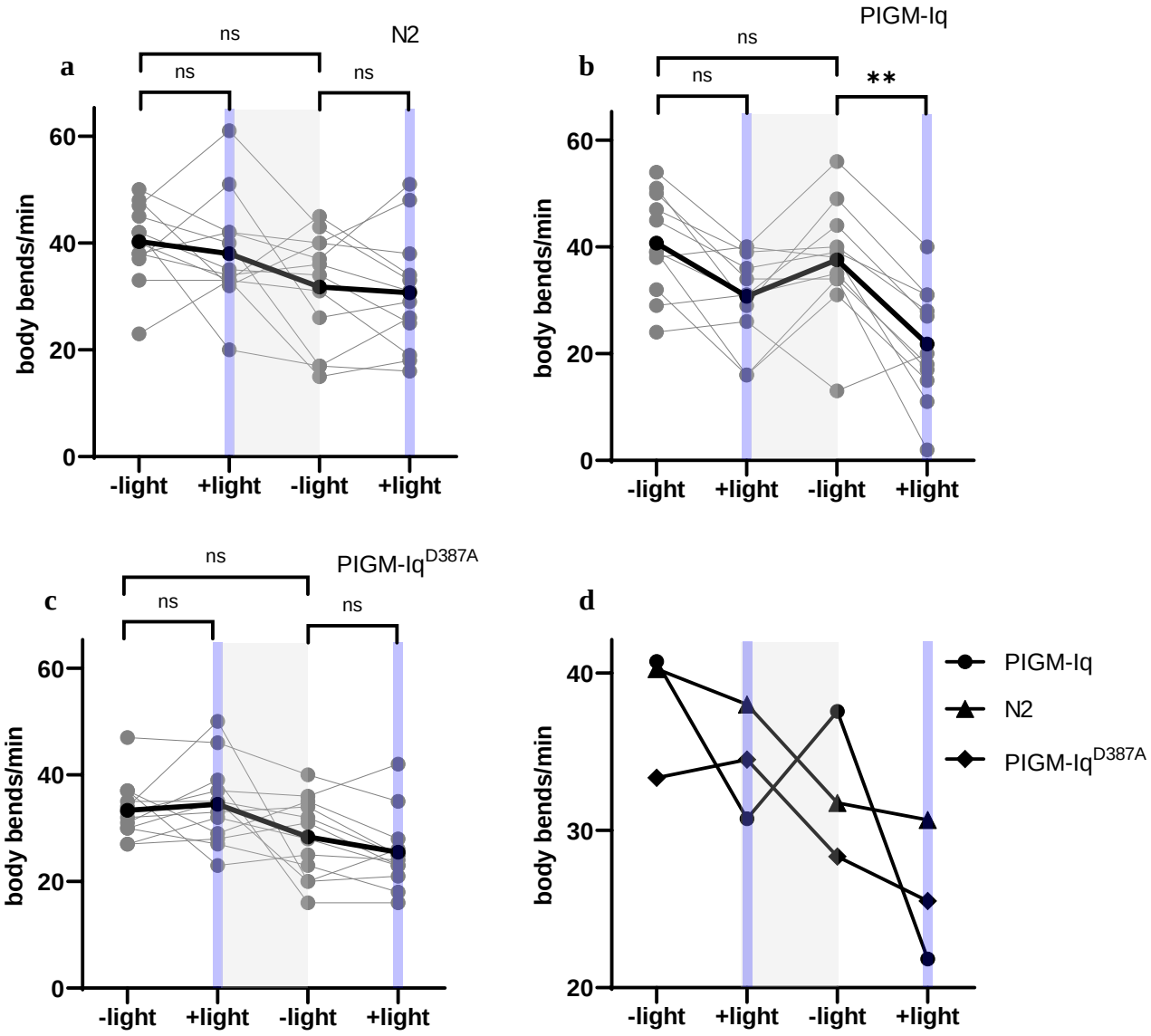

Figure 3.3 | PIGM-Iq reduces locomotion in C. elegans *when exposed to blue light.* Body bends per minute of **a,** WT *C. elegans* (n = 9) and transgenic animals expressing either the **b,** PIGM-Iq (n = 11) or **c,** PIGM-Iq^{D387A} (n = 12) pan-neuronally, and **d,** a comparison of the average locomotion rate of each line. Each point represents the number of body bends performed in a minute by freely moving animals on NGM, black lines indicate the average locomotion rate of each line, blue bars represent blue light illumination (30 seconds, 470 nm, 0.30 mW/mm^2, and grey bars represent a 20-minute period of rest in the dark. One-way ANOVA with Tukey's multiple comparisons test, ns P >0.05, **P < 0.005, N = 11-12 worms/line from ≥ 3 experiments.

worms expressing PIGM-Iq^{D387A} (Fig. 3.3, c), with no significant difference in locomotion observed upon light exposure. PIGM-Iq^{D387A} did show a background reduction in locomotion rate in comparison to both wild type and PIGM-Iq-expressing animals (Fig 3.3, d).

Worms expressing PIGM-Iq did not show a baseline locomotion deficit (Fig 3.3, d). However, when exposed to blue light, a decrease in locomotion rate was observed (Fig 3.3, b), but was not found to differ significantly from pre-exposure locomotion. This defect could be rescued by 20 minutes rest in the dark, with locomotion returning to a rate similar to that seen before light exposure. When exposed to light a second time, worms showed a significant decrease in body bend rate compared to pre-exposure that was larger than that observed upon initial exposure.

3.4 Discussion

To validate the effectiveness of PIGM-Iq *in vivo, C. elegans* locomotion was chosen due to its dependence on Gαq signalling for muscle contraction (Brundage, Avery et al. 1996, Lackner, Nurrish et al. 1999). It was therefore hypothesised that, upon blue light illumination of transgenic animals expressing PIGM-Iq pan-neuronally, a reversible decrease in locomtion rate would be observed.

Transgenic animals confirmed to express PIGM-Iq pan-neuronally demonstrated a baseline level of movement comparable to that of WT animals. This suggests that PIGM-Iq possess limited affinity for Egl-30 Gαq in the dark. This reduced background effect compared to that seen in HEK293A cells may be due to slight differences in protein conformation between *C. elegans* and mammalian Gαq, reducing the affinity between RGS2(Δ1-53) and *egl-30* Gαq. However, when PIGM-Iq or its light insensitive variants are highly expressed, the individual animals have reproductive difficulty as reported with *egl-30* mutants. This suggests that the RGS domain of RGS2, when overexpressed cytosolically at high concentration, can still have Gαq inhibitory effects without membrane recruitment. However, in the experiments presented in this study, we cannot rule out other possible effects of overexpression on reproduction such as protein misfolding or accumulation-related disruption of cellular function not related to RGS function. Secondly, animals expressing PIGM-Iq did appear to grow at a slower rate, with plates reaching maximum capacity later than WT animals or those expressing the light insensitive PIGM-Iq. This may be due to a level of background binding between CRY2(PHR) and CIBN when expressed at high levels. This possible effect of overexpression could be reduced by future experiments employing the CRY2(535) variant with reduced

background activity (Taslimi, Vrana et al. 2014) or to use altered genetic sequence of PIGM-Iq that has reduced *C. elegans* codon usage. Furthermore, future experiments could employ transgenic lines using a different, more relevant, promotor, which could reduce off-target effects.

Upon blue light exposure of the PIGM-Iq worms, a decrease in locomotion was observed. This suggests that light activation of PIGM-Iq may cause the inhibition of Egl-30 Gαq at the neuromuscular junction, therefore decreasing the ability for muscle contraction and therefore movement. When allowed to recover for 20 minutes in the dark, these animals appeared to lose their movement deficit, with average locomotion returning to a pre-illumination rate. This suggests that PIGM-Iq can revert to an inactive conformation in this timeframe, releasing the inhibition of Gαq and allowing for effective muscle contraction. However, this movement could once again be reduced upon further light illumination.

Interestingly, a larger movement deficit was observed upon the delivery of the second epoch of blue light. Following initial illumination and reversion in the dark, locomotion appeared similar to that of pre-illumination levels. Thus, this excludes the possibility that the tool is undergoing incomplete reversion during the 20-minute time period. A more likely explanation for the more prominent locomotory decrease is the possibility that the tool is located more favourably following initial activation. This may allow for more efficient translocation of the tool and thus a more pronounced inhibitory phenotype.

Locomotion rate did not decrease to a rate of that reported in the literature. This is likely due to the transient nature of the tool. Results reported in the literature are derived from animals possessing mutations in the *egl-30* gene. As a result, the animals experience defective Gαq function throughout development. This likely influences the development of the nervous system and motor circuit, resulting in a severe movement phenotype. In future experiments, it may be valuable to investigate whether activation of PIGM-Iq during various timepoints throughout development exacerbates the observed deficit.

As expected, no inhibition of locomotion rate was seen in animals expressing PIGM-Iq^{D387A} when exposed to light. However, a light-independent decrease in baseline locomotion was observed in these animals. A possible explanation for this is varied expression between lines, possibly resulting in higher expression of PIGM-Iq^{D387A} and a more pronounced background effect. A time-dependent decrease in locomotion was also observed in N2 animals. Thiss may be due to fatigue over time. This phenomenon, although more prominent during swimming in comparison to crawling, has been described in the literature (Laranjeiro, Harinath et al. 2017, Schuch, Govindarajan et al. 2020). Further experiments using other behavioural

readouts known to be dependent on EGL-30 function, such as chemotaxis response to the attractant 2-heptanone, could be used to validate the results presented in the current study (Zhang, Zhao et al. 2016).

Chapter 4 │ Validation of PIGM-Iq in behaving *D. melanogaster*

4.1 Introduction

To further assess the effect of PIGM-Iq *in vivo* and modulate Gαq-linked behaviours in live animals, PIGM-Iq was introduced into the fruit fly, *Drosophila melanogaster*. *D. melanogaster* have more complex learning and memory processes such as those involved in associative learning during male courtship conditioning. Like the *C. elegans* model, biological signalling in fruit flies have mostly been studied using genetic knockouts and mutants, which have developmental effects and lack temporal control. Unlike opsin-based optogenetic tools in the fly, which require retinoid dietary supplements, PIGM-Iq is purely genetically encoded. This provides additional convenience and reduces undesired consequences associated with additional manipulations.

4.1.1 Associative learning in D. melanogaster

Associative memories linked to olfaction are formed in the insect brain structure of the mushroom body (MB) (Aso, Hattori et al. 2014). The MB, a structure functionally analogous to the mammalian hippocampus, processes sensory information and influences behaviour in response to stimuli that have been encountered previously (Krashes, Keene et al. 2007). Disruption to the MB has been reported to cause severe defects in associative learning in insects (Heisenberg, Borst et al. 1985, de Belle and Heisenberg 1994). Through various experimental procedures, it has been confirmed that the MB is the main area for associative odour learning in *D. melanogaster* (Connolly, Roberts et al. 1996, Dubnau, Grady et al. 2001, Schwaerzel, Heisenberg et al. 2002).

The MB is made up of bilaterally symmetrical units within the brain of the fly, each consisting of bundles of intrinsic neurons known as Kenyon cells (KCs) (Aso, Hattori et al. 2014). KCs receive excitable input from projection neurons of the antennal lobe that terminate in the calyx, the major input site of the MB (Aso, Hattori et al. 2014). From the calyx, KCs extend axonal projections into the lobes, the primary output region of the MB (Aso, Hattori et al. 2014). KCs can be functionally divided into seven classes, consisting of three αβ-type KCs and two γ-type KCs. The axonal arbours of the αβ cells bifurcate at the heel of the MB, forming the horizontal β/β' lobes and the vertical α/α' lobes, whilst the γ cells extend an axonal projection forming a single, horizontal lobe (Aso, Hattori et al. 2014).

4.1.2 Octopamine in associative learning

Octopamine, the invertebrate functional counterpart of noradrenaline, has been linked to appetitive memory formation in the fruit fly, as well as in other insects including the honeybee and locust (Farooqui, Robinson et al. 2003, Schwaerzel, Monastirioti et al. 2003, Unoki, Matsumoto et al. 2005, Kim, Lee et al. 2013). It was found that flies containing defective tyramine β-hydroxylase, an enzyme needed to convert tyramine to octopamine, were unable to form appetitive associative memories (Kim, Lee et al. 2013). Furthermore, exogenous octopamine supplementation was demonstrated to rescue this deficit through the alpha1-like octopamine mushroom body - or OAMB - receptor.

4.1.3 The OAMB receptor

The OAMB receptor is highly expressed in the MB of the insect brain, as well as the female oviducts and male spermathecae (Lee, Seong et al. 2003). The two isoforms of the receptor, the OAMB-AS and OAMB-K3, have both been observed to couple to increases in $[Ca^{2+}]_i$, with the latter also linked to the production of cAMP (Han, Millar et al. 1998, Lee, Rohila et al. 2009). The OAMB receptor has been found to possess a moderate level of sequence similarity within the transmembrane domains of human Gαq-linked α1 adrenergic receptors (52–55%), and human Gαi-linked α2 and primarily Gαs-linked β adrenergic receptors (45–50%) (Han, Millar et al. 1998). As a result, literature has suggested that OAMB receptors in the oviduct couple to Gαq (Lee, Rohila et al. 2009). However, the identity of the G protein involved in signal transduction upon OAMB receptor activation in the MB it is yet to be confirmed. The ambiguity of the G protein linked to the OAMB receptor in the MB provides an opportunity to utilise PIGM-Iq system to determine the coupling of Gαq with OAMB in different signalling situations.

4.1.4 The OAMB receptor and courtship conditioning

D. melanogaster males possess the intrinsic ability to perform a stereotypical sequence of behaviours known as a courtship ritual (Han and Kim 2010, Bontonou and Wicker-Thomas 2014). When presented with a female, the male will orient his body axis toward her (orienting). The male then proceeds to chase the female (following), often touching her abdomen with his forelegs (tapping). This allows for the perception of cuticular hydrocarbons on the female

abdominal cuticle. The male will then unilaterally extend his wings, vibrating them in turn to produce what is known as the courtship song (singing). In unfertilised females, this causes a reduction in locomotion. This signals to the male the willingness of the female to accept the courtship attempt, which is followed by licking for further pheromonal perception. The male will then attempt copulation. These behaviours are repeated until the female allows for copulation, which proceeds for 15-20 minutes. For an extensive review on courtship behaviour, see (Han and Kim 2010, Bontonou and Wicker-Thomas 2014).

Despite the apparent embedded nature of this behaviour, male courtship is subject to plasticity; a phenomenon known as courtship conditioning (Griffith and Ejima 2009, Montague and Baker 2016, Mezzera, Brotas et al. 2020). When a male is paired with a fertilised female, male courtship behaviour causes the female to extrude her ovipositor, blocking copulation attempts. Females may also actively avoid the male or even demonstrate aggressive behaviours. In response, the male begins to associate female-associated pheromones with aversive courtship-inhibiting cues, such as rejection. As a result, when males are subsequently paired with receptive adult females, they demonstrate a reduction in courtship behaviour due to an anticipatory response associated with previous rejection. This response has been likened to associative learning, with female pheromones acting as the conditioned stimulus (CS) and female rejection behaviour the unconditioned stimulus (US). Courtship conditioning is covered more extensively in the following papers (Tompkins, Siegel et al. 1983, Mehren, Ejima et al. 2004, Mezzera, Brotas et al. 2020).

Octopaminergic neurons and the MB OA receptor, OAMB, are important for courtship conditioning

Zhou et al. (2012) showed that OA and the OAMB receptor was important for associative learning during courtship conditioning in *D. melanogaster* males (Zhou, Huang et al. 2012). Male flies lacking functional tyramine β hydroxylase (TβH), an enzyme required in the conversion of tyramine to octopamine, were found to have significantly impaired courtship conditioning responses. This deficit was rescued through the expression of a TβH transgene in octopaminergic (OAergic) neurons, thus confirming the necessity of OA in the male courtship conditioning response.

To further understand the involvement of OA in conditioning, *shibire (Shi^{ts})*, a temperature sensitive variant of dynamin able to inhibit synaptic transmission, was expressed in OAergic neurons (Zhou, Huang et al. 2012). It was found that silencing of the synaptic

outputs of these neurons in males whilst being presented with an unreceptive female also resulted in ineffective courtship conditioning, suggesting that the synaptic release of these neurons is important in the associative phase of courtship learning.

Considering these findings, it was hypothesised that OAergic neurons may be involved in the processing of aversive stimuli. To test this, temperature sensitive TRPA1 (temperature-sensitive ion channel) was expressed in OAergic neurons, resulting in the activation of these neurons at moderately increased temperatures (Zhou, Huang et al. 2012). It was found that the activation of OAergic neurons during pairing of a naïve male with a receptive female resulted in the creation of an artificial courtship conditioning response, thus further supporting the notion that OA may be involved in mediating aversive cues during courtship.

As OAMB is enriched in the MB, an area strongly associated with learning and memory, it was proposed that OAMB-expressing neurons of the MB may also be involved in this process. As anticipated, inhibition of these neurons through the expression of *Shi*^{ts} caused a reduction in courtship conditioning (Zhou, Huang et al. 2012). This reduction was also seen in OAMB null males and was rescued by the expression of OAMB transgene both pan-neuronally and in the MB. However, activating these same neurons with TRPA1 as described previously did not cause artificial conditioning. This is consistent with the notion that similar sets of MB neurons are required for both appetitive and aversive learning, and that the extrinsic neurons are the determinant of the association valency. In this case, it appears that OAergic neurons convey aversive cues, allowing the MB to associate these cues with other stimuli.

OAergic neurons and OAMB are responsible for conveying the aversive pheromonal stimuli, cVA

It has been previously demonstrated that *cis*-Vaccenyl Acetate (cVA), a pheromone transferred from the male to the female during copulation, is a key aversive pheromone involved in courtship conditioning. Zhou et al. (2012) demonstrated using *in vivo* calcium imaging that OAMB-expressing neurons of the MB responded in a dose-dependent manner to cVA (Zhou, Huang et al. 2012). It was also found that males that had previously undergone courtship conditioning showed a larger increase in calcium in these neurons when presented with cVA in comparison to naïve males. Considering this, it was suggested that OAergic neurons may relay information regarding cVA to OAMB-expressing neurons of the MB, and that this association is enhanced by courtship conditioning training. This was further confirmed through the demonstration that single OAergic neurons directly innervate the MB.

Overall, the courtship conditioning response appears to be a well-suited paradigm by which to validate the contributions of Gαq to the OAMB singling pathway using PIGM-Iq. The well-defined time-period in which this association occurs, paired with the selectivity is well suited to optogenetic manipulation and should allow for the direct manipulation of OAMB without a large amount of cross-inhibition to other Gαq-coupled GPCRs. *D. melanogaster* Gαq possesses 77% similarity to mammalian Gαq and is therefore hypothesised to interact with PIGM-Iq in a similar manner (Fig. A2). Activation of PIGM-Iq and the subsequent reduction of OAMB signal transduction in males undergoing courtship training should result in a decrease in the courtship conditioning response.

4.2 Methods

4.2.1 Fly husbandry

Flies were maintained at 25ºC (70% humidity) on standard fly food (100g live yeast, 75g glucose, 8g agar, 55g corn meal, 10g wheat flour, 5ml 8.5% phosphoric acid, 5ml 85% propionic acid, to 1L with H2O) on a 12-hour light/dark cycle in 30ml vials.

4.2.2 Generation of transgenic D. melanogaster

Sequence alignment between *Homo sapiens* GNAQ (NCBI Reference Sequence: NM_002072.5) and *D. melanogaster* Dmel/GNAQ (NCBI accession number NP_725196.1) was generated using Clustal Omega (EMBL-EBI) (Sievers, Wilm et al. 2011, Madeira, Park et al. 2019).

Constructs to be injected for the generation of transgenic *D. melanogaster* are listed in table 4.1 and were generated as described previously. Briefly, RGS2(Δ1-53)-CRY2(PHR)-T2A-CIBN-eGFP-CaaX and RGS2(Δ1-53)-CRY2(PHR)^{D387A}-T2A-CIBN-eGFP-CaaX were cloned between the XhoI and XbaI sites in the pJFRC18-8xLexAop2 vector in place of mCD8::GFP.

Table 4.1 | Components for the production of transgenic *D. melanogaster*

	Name of construct
Template constructs	
1	pJFRC18-8XLexAop2-mCD8::GFP
Constructs encoding PIGM-Iq	
2	pJFRC18-8XLexAop2-RGS2(Δ1-53)::CRY2(PHR)::T2A::CIBN::eGFP::CaaX
3	pJFRC18-8XLexAop2-RGS2(Δ1-53)::CRY2(PHR)(D387A)::T2A::CIBN::eGFP::CaaX

This vector was chosen to limit transgene expression, as vectors containing higher copies of the lexAop site may amplify background activity of the transgene. The T2A sequence has been shown to be functional when expressed in *D. melanogaster* (Lee, Zirin et al. 2018). All constructs were eluted in molecular biology grade water (Sigma-Aldrich) to limit embryonic toxicity during the injection process.

Injections were performed as described previously by Nicolas Gompel and Eva Ayla Schröder (Schröder 2015). Briefly, preceding injection, $y^{1}w^{67c23}$;P(CaryP)attP40 flies (Bloomington Stock Centre) were harvested and grown at 25ºC in 200ml bottles. 4-5-day old flies were then moved to an egg-laying chamber 18hrs prior to the time of injection. On the morning of injection, yeast paste was added to the egg lay plate. Flies were then incubated at room temperature (~22ºC). A suitable number of flies (~100) for injection preparation were determined to lay approximately 100 eggs on apple-juice agar plate every 25-30 minutes.

The purified plasmid of interest was then loaded into a micropipette (for methods for preparing micropipettes, see *C. elegans* injection section, chapter 3). Injection of embryos was performed within the first 45 minutes after egg laying to ensure blastoderm cellularisation had not yet occurred. Once aligned on a coverslip, embryos were covered with organic olive oil and injected in the posterior end of the embryo (needle penetration did not exceed one-third of the posterior length of the body).

Following injection, embryos were placed in standard food and grown at 25ºC until pupae emerged. Each pupa was then collected and placed in an individual tube and allowed to develop until hatching. Following hatching, flies were crossed to w[1118] (Bloomington Stock Centre) and transgenic progeny collected (identified by the presence of eye colour) resulting in the creation of two transgenic lines: $y^{1}w^{67c23}$;P(8XLexAop2::RGS2(Δ-53)::CRY2(PHR)::T2A::CIBN::eGFP::CaaX)attP40 and $y^{1}w^{67c23}$;P(8XLexAop2::RGS2(Δ-53)::CRY2(PHR)^{D387A}::T2A::CIBN::eGFP::CaaX)attP40. Flies were not backcrossed to the control Canton-S line as these flies were not available at the time of the experiment. Once complete, the progeny were then crossed to specific LexA driver lines in vials partially protected from light (vial was covered partially with paper, leaving a 2-3cm gap at top of vial, to prevent excessive light entering and prevent possible tool activation) to produce transgenic flies that express the transgene either pan-neuronally (R57C10-LexA (Bloomington Stock Centre)) or within the Kenyon cells of the mushroom body (R13F02-LexA (Bloomington Stock Centre)) and CIBN-eGFP-CaaX expression confirmed by confocal microscopy (brain dissections, nc82 staining to visualise gross brain morphology and imaging performed by Dr

Caroline Delandre and Mr John McMullen). Confocal settings used to image brains were kept constant between samples of the same driver to allow for comparison of expression level between PIGM-Iq and PIGM-Iq^{D387A}.

4.2.3 Courtship conditioning assay

Courtship conditioning was performed as described previously (van Swinderen and Hall 1995, Zhou, Huang et al. 2012). Training and testing were performed at room temperature (21ºC ± 2ºC) with no humidity control. Test males and virgin flies for testing were isolated immediately following eclosion and aged separately for 5-7 days. Test males were housed in groups no larger than 4 per vial to limit male-male aggression. Test males were housed in vials partially protected from light to limit activation of the tool by the LEDs of the incubators during aging. For the generation of mated females, virgin females were housed with males for 5 days to ensure mating. Courtship repression training was then conducted with transgenic male flies within 1 hour of the initiation of the light-cycle to ensure maximal activity and consistency. Mated females were mildly anaesthetised using CO_2 and placed into a 0.5ml Eppendorf tube containing a moist tissue to maintain humidity. Once the mated female had fully recovered, test males were gently aspirated into the tube containing a mated female (trained) or alone (naïve). Flies were then either illuminated with pulsed blue light or left in ambient room lighting for 1 hour. Blue light illumination was delivered via a custom LED array (470 nm) for 10 seconds every 5 minutes for the duration of the training period using an LED Driver Control Panel V3.2.2 (Mightex). This pattern of stimulation was previously shown to cause continuous membrane association of PIGM-Iq without loss of binding efficacy in HEK293A cells (Chapter 2). Males assigned to the trainer group who did not attempt to court the mated female within 10 minutes from the initiation of training were excluded from further testing.

Following training, males were gently aspirated into the test chamber, consisting of a 24-well cell culture plate sealed with parafilm, and left to acclimatise for 10 minutes. A virgin female was then aspirated into the chamber containing the male. Addition of the female initiated the testing period, and the male was videoed for 10 minutes. These videos were then manually analysed for courtship behaviours by an individual blinded to the lighting condition and training group assigned to that male. Trials where little to no courtship attempts were initiated by the naïve male were removed on account of environmental and housing issues.
Learning index of male flies in each condition was then calculated using the following formula:

$$LI = (CI_{naïve} - CI_{trained})/CI_{naive}$$

Raw data was processed in Microsoft Excel (2010). Statistical analysis was performed, and graphs were produced using GraphPad Prism 8.3 (GraphPad Software, San Diego, California USA, www.graphpad.com). A Kruskal-Wallis test was performed to analyse the data followed by a Dunn's multiple comparison test to identify significance between different conditions of the same line. A Mann-Whitney test was used to compare the learning index of Canton-S flies.

4.3 Results

To establish an assay to measure Gαq-linked courtship conditioning, sexually naïve 4-6-day old males were paired with a pre-mated female for 1 hour for training. Naïve males were not paired with a female during training. Males exposed to light during training received pulsed blue light for 10 seconds every 5min (470 nm) for the duration of the training period (Fig. 4.1, a). Males were then transferred to a testing chamber with a virgin female of similar age. The male's courtship attempts were then scored according to a pre-defined set of behaviours described in the methods section.

When paired with a virgin female, Canton-S (WT) naïve males had an average courtship index of 0.61 (Fig. 4.1, b). However, males trained with a pre-mated female displayed a significantly reduced capacity to perform courtship behaviour when paired with a virgin female, as expected; with males demonstrating an intact courtship conditioning response ((+ light: CI = 0.28) (-light: CI = 0.25)). Furthermore, this courtship conditioning response did not significantly alter when males were exposed to blue light during training (P>0.9999). This is supported by the comparable learning index seen for both groups ((+ light: LI 0.55) (-light: LI 0.59)), demonstrating an intact ability to learn the association between female-associated cues and rejection despite differences in light exposure (Fig. 4.1, c).

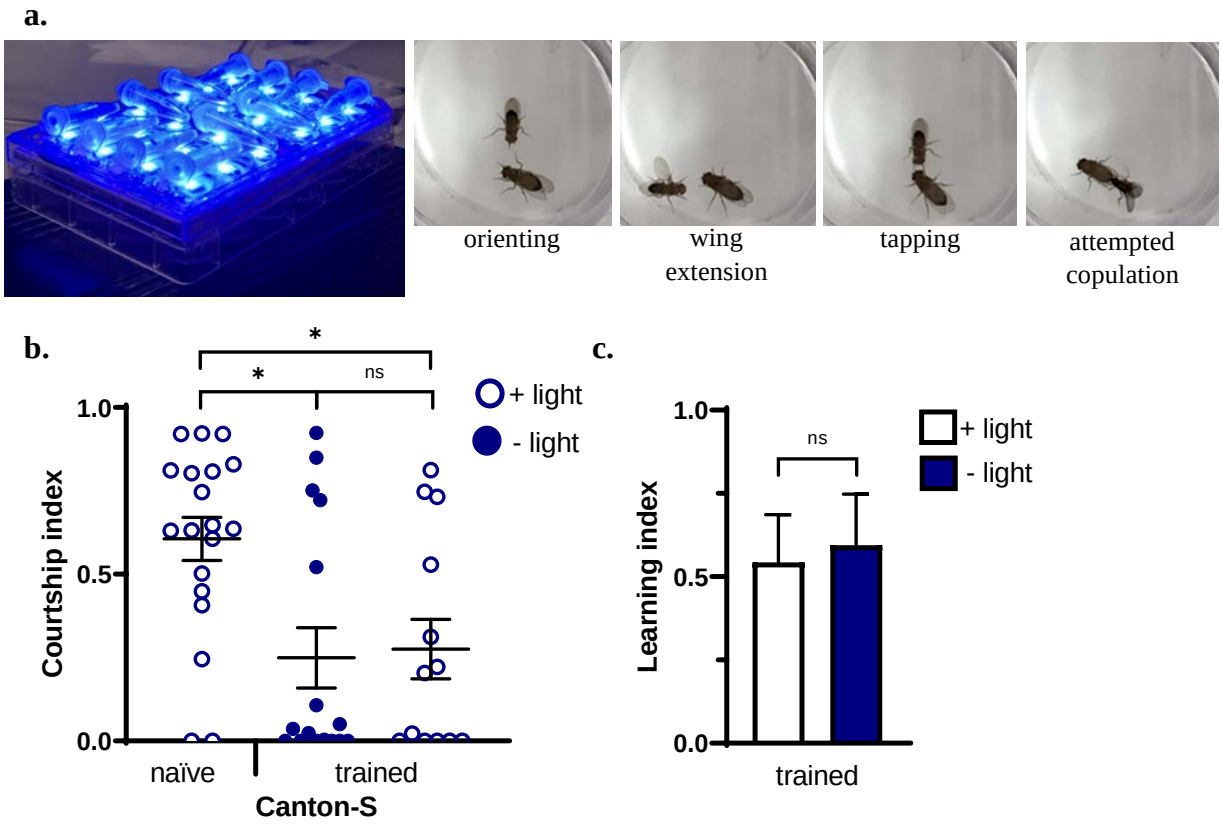

Figure 4.1 ⁄ Validation of the courtship conditioning assay in D. melanogaster. a, 5-7 day old, sexually naïve males were trained with pre-mated females for 1 hour and pulsed with blue light for 10 seconds every 5min (470 nm). Males were then transferred to testing chambers containing a virgin female and their courtship behaviour was scored over a 10-minute period. b, courtship index of male canton-S flies, Kruskal-Wallis test, ns P >0.05, *P < 0.05. c, Learning index of male canton-S flies, Mann-Whitney test, ns P >0.05. N = 13-19 flies/condition. Error bars indicate SEM.

4.3.1 PIGM-Iq prevents associative learning in D. melanogaster during courtship conditioning

To assess the ability of PIGM-Iq to inhibit Gαq-linked associative memory formation during courtship conditioning, male flies expressing pan-neuronally driven PIGM-Iq underwent training and testing as described above. As expected, naïve males not exposed to a pre-mated female trainer demonstrated a high level of courtship behaviour towards the virgin female tester (CI = 0.66) (Fig. 4.2, b). Trained males not exposed to light showed an intact courtship response to virgin females, with little to no courtship activity observed in these flies. This differed significantly to that of naïve males (CI = 0.22). However, male PIGM-Iq flies exposed to blue light during training were seen to have a mean CI comparable to that of naïve flies (CI = 0.53), demonstrating an inability of these males to undergo courtship conditioning. The courtship index of these males also differed significantly from those not exposed to light. This deficit in courtship conditioning was not seen in males expressing the light-insensitive variant of PIGM-Iq. Naïve males showed intact levels of courtship (CI = 0.70). The averaged CI of trained males was found to be significantly reduced compared to naïve males ((+ light: CI = 0.21) (-light: CI = 0.15).

The LI of males expressing PIGM-Iq exposed to light was significantly reduced compared to those not exposed to light ((+ light: LI = 0.21,) (-light: LI = 0.67) (Fig. 4.4, c). Males expressing the light-insensitive variant of PIGM-Iq, however, showed no significant difference between light and dark conditions ((+ light: LI = 0.70,) (-light: LI = 0.79) P >0.9999). There was also no significance difference observed between dark exposed flies expressing PIGM-Iq and flies expressing the light-insensitive PIGM-Iq exposed to either condition (P>0.9999).

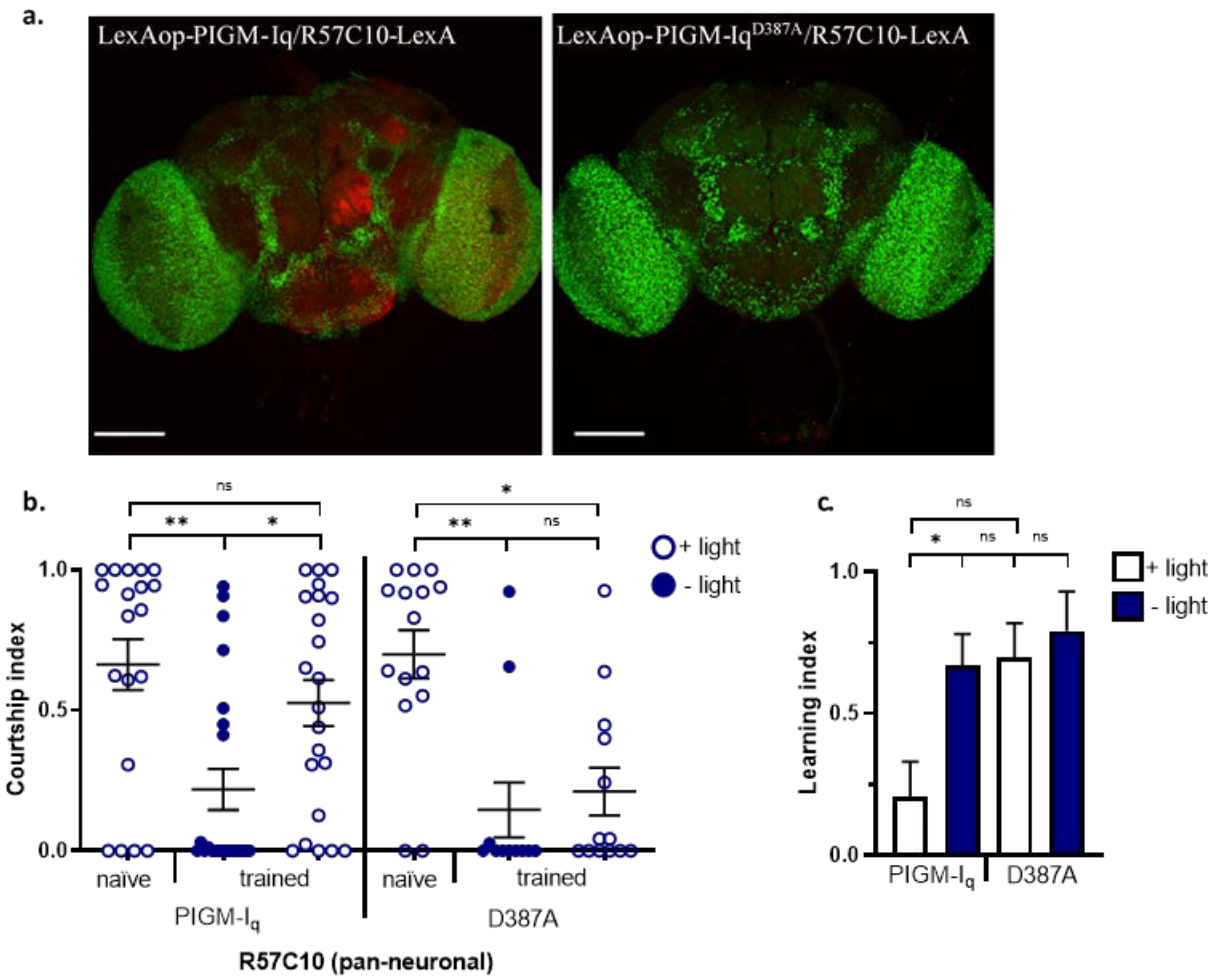

Figure 4.2 | *Pan-neuronal PIGM-Iq inhibits learning during courtship conditioning in* D. melanogaster. **a,** R57C10-LexA-driven PIGM-I_q and PIGM-Iq^{D387A} expression (green) in the adult fly brain (nc82 staining in red), Scale bar 100 μm **b,** courtship index of male PIGM-I_q and PIGM-Iq^{D387A} flies, Kruskal-Wallis test, ns P >0.05, *P < 0.05, **P <0.01. **c,** Learning index of male PIGM-I_q and PIGM-Iq^{D387A} flies, Kruskal-Wallis test, ns P >0.05, *P <0.05. N = 11-22 flies/condition. Error bars indicate SEM.

4.3.2 Associative learning during courtship conditioning may be dependent on Gαq activation in the mushroom body of male D. melanogaster.

PIGM-Iq suppression of the courtship conditioning response may be due to Gαq inhibition in neural processes associated with courtship or the direct acquisition of sensory information, and not associated with learning due to pan-neuronal expression. To test whether PIGM-Iq was causing inhibition of Gαq-linked associative learning, we tested male flies expressing PIGM-Iq in only the MB of the brain and the assay was performed in these flies.

As expected, blue-light activation of MB PIGM-Iq caused an increase in courtship attempts by trained males (CI = 0.60) (Fig. 4.3, b). The CI after the increase was comparable

to that seen in naïve males. However, the CI after the increase was not significantly different from the courtship index observed for trained males not exposed to light (CI = 0.29). A reduction in courtship compared to naive males (CI = 0.49) was seen in trained males expressing the light-insensitive variant of the tool which did not differ significantly between light on and off conditions ((+ light: CI = 0.017) (-light: CI = 0.22). The reduction seen between naïve males and trained males exposed to light was significantly different; however, the reduction between naïve males and those not exposed to light was not found to be significant. It was noted that the courtship index of light-insensitive variant expressing naïve flies was slightly reduced compared to the average naïve courtship index observed in other experiments.

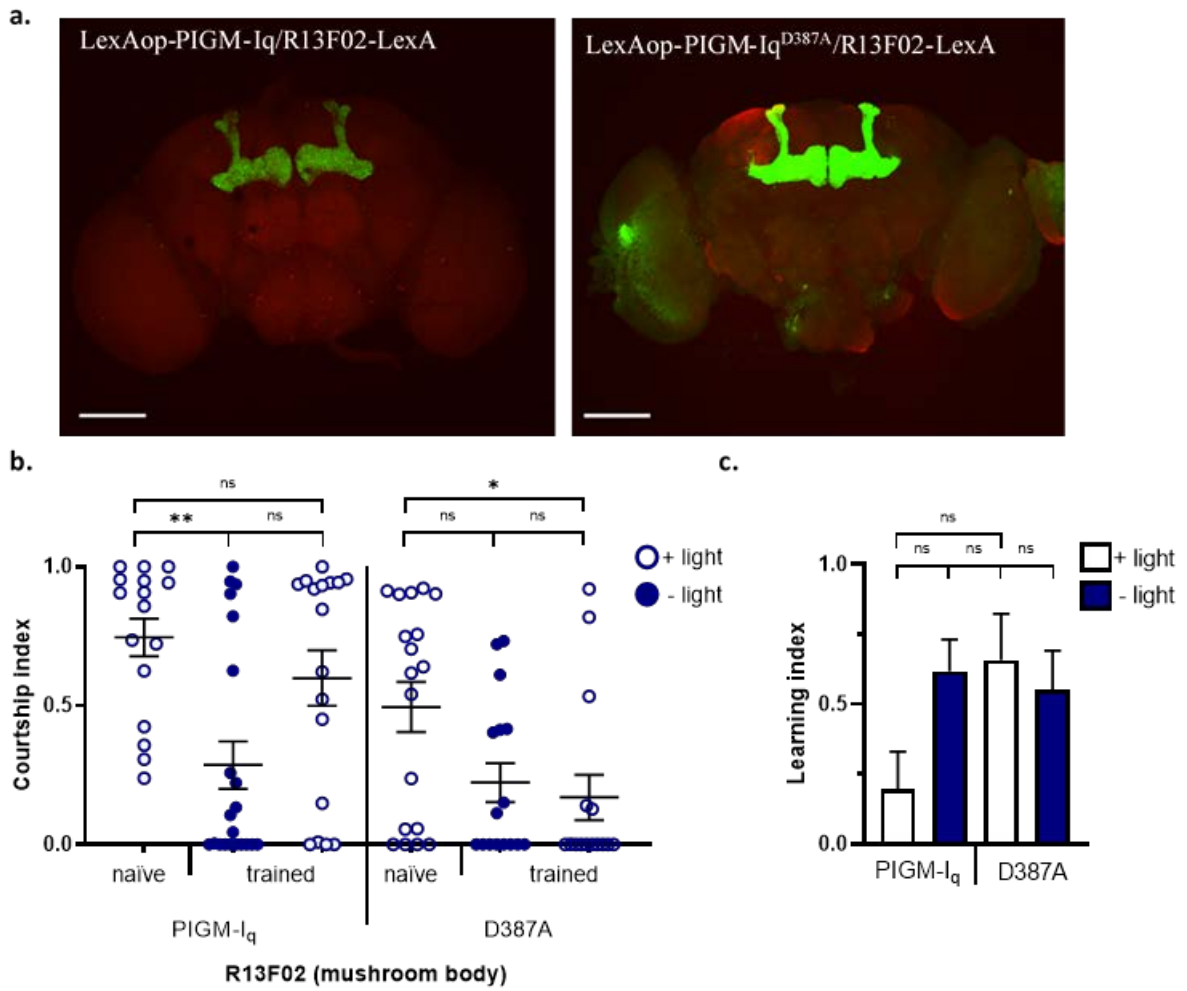

Figure 4.3 | *Mushroom body PIGM-Iq may inhibit learning during courtship conditioning in* D. melanogaster. **a,** R13F02-LexA-driven PIGM-I_q and PIGM-Iq^{D387A} expression (green) in the adult fly brain (nc82 staining in red), Scale bar 100 µm **b,** courtship index of male PIGM-I_q and PIGM-Iq^{D387A} flies, Kruskal-Wallis test, ns P >0.05, *P < 0.05, **P <0.01. **c,** Learning index of male PIGM-I_q and PIGM-Iq^{D387A} flies, Kruskal-Wallis test, ns P >0.05. N = 15-21 flies/condition. Error bars indicate SEM.

The learning index of MB PIGM-Iq expressing flies, although reduced, did not differ significantly between light on and off conditions ((+ light: LI = 0.0.20) (-light: LI = 0.62), (Fig.

4.5, c). Furthermore, the learning indices of all other conditions did not differ significantly from one another.

4.4 Discussion

As the setup used in the current study differed slightly to some of those described in previous studies, we validated the ability of male fruit flies to undergo courtship conditioning using the protocol described earlier. Using Canton-S flies, we found that male flies were able to learn to reduce courtship attempts to virgin females following training with an unreceptive mated female. This confirmed that the protocol used was sufficient to produce courtship repression. Furthermore, it allowed for the establishment that intermittent blue light pulses did not appear to affect the male's ability to undergo conditioning. In support of this, there was no observable effects of blue light exposure on the male. For instance, blue light exposure during an active courtship attempt did not appear to stop or alter the progression of the behaviour in any discernible manner which acts as a control for the effects of visual system blue light sensory input.

The results presented in this study generally supported the idea that Gαq activated by the OAMB receptor within the mushroom body mediates courtship learning. Like the results from previous chapters, there are indicators that suggest the high level of PIGM-Iq expression could have a level of background activity between different components of the tool as the courtship index of flies expressing PIGM-Iq not exposed to light is slightly increased compared to that of the light-insensitive variant-expressing flies. The effects of pan-neuronal expression of PIGM-Iq are stronger than that of MB-targeted expression, but this appears to be introduced by the higher and noisier background activity of PIGM-Iq when using the pan-neuronal driver line. Again, these results suggest high level of PIGM-Iq expression paired with non-specific expression can introduce a high level of background inhibitory activity and moderate to low level of expression appear to be sufficient to mediate the inhibitory effects.

Although the results suggest that Gαq activity in the mushroom body is important for the courtship conditioning response in male fruit flies, we cannot conclusively determine whether this is the case. This highlights one of the limitations of the PIGM-Iq approach - a lack of receptor specificity. To dissect the signalling pathways precisely, a combination of genetics, pharmacology, and other molecular biology techniques would be required. In future experiments, it may also be more relevant to drive the expression of PIGM-Iq in the subset of Kenyon cells known to express OAMB. This would limit a large proportion of the inhibitory

activity of the tool to the OAMB receptor, thus reducing the possible inactivation of other Gαq-linked receptors during the training period.

It would also be advantageous in future experiments to examine expression levels of PIGM-Iq prior to conducting behavioural experiments to examine whether high expression level contributes to an increase in background activity of the tool, as well as to select with a similar expression level. Furthermore, using a PIGM-Iq line backcrossed to Canton-S, rather than W1118, may also assist when comparing the results obtained using this fly line to those of the control Canton-S flies.

Chapter 5 | Summary, future directions, and conclusions

5.1 Summary

The current study presents the development and validation of an optogenetic inhibitor of Gαq signalling, PIGM-Iq. We have shown that PIGM-Iq effectively inhibits Gαq-linked calcium efflux in mammalian stable cells in a light dependent manner, with a low level of background activity. The selectivity of the tool in mammalian cells was also confirmed, with no observable interactions with either the Gαs or Gαi signalling pathways. The ability of PIGM-Iq to function in live animals was then demonstrated, with Gαq-linked behaviours inhibited in both *C. elegans* and *D. melanogaster*.

In summary, the design and validation of an RGS2-based optogenetic tool described in this study presents a reversible, light-induced inhibitor of endogenous Gαq-linked GPCR signalling that was previously absent from the molecular toolbox. This tool presents many advantages over current techniques used to manipulate GPCR signalling, including high spatiotemporal resolution, selectivity, and reversibility of inhibition, as well as the ability to be easily packaged for virus delivery. Its demonstrated ability to effectively function in both mammalian and invertebrate systems drastically increases the scope of its application for the investigation of G protein signalling and neuromodulation in a wide variety of fields. Future studies will focus on the methods to selectively target different Gαq-linked GPCRs, as well as the development of optogenetic inhibitors of the Gαi signalling pathways using a similar design.

Although the design of PIGM-Iq appears to be similar to that of opto-RGS2 (Hannanta-Anan and Chow 2018), the current study has the following considerable differences:

1. PIGM-Iq is selective for the Gαq signalling pathway. Literature suggests that full-length wildtype RGS2 has the ability inhibit adenylate cyclase activity (Sinnarajah, Dessauer et al. 2001, Salim, Sinnarajah et al. 2003, Roy, Baragli et al. 2006). The interaction between RGS2 and AC was mapped to the first 19 amino acids of the N-terminus (Salim, Sinnarajah et al. 2003). Thus, PIGM-Iq features an N-terminal truncation of the first 53 amino acids to remove both the AC interaction site and the membrane binding domain. It was then confirmed that PIGM-Iq did not possess any activity toward either the Gαs (including AC) or Gαi signalling pathways. Selectivity toward the Gαq signalling pathway was further confirmed by our collaborator – Ms Silvia Vicenzi – in an axon turning assay in cultured dorsal root ganglia neurons, where

PIGM-Iq robustly inhibited Gαq-linked attraction without impeding Gαi-linked repulsion. In contrast, opto-RGS2 was designed as a light-activated mimetic of wildtype RGS2 (Hannanta-Anan and Chow 2018); hence this tool likely possesses inhibitory activity toward both Gαq and AC.

2. Opto-RGS2 is designed so that the RGS-box domain is fused to the C-terminus of CRY2(PHR) (CRY2(PHR)-RGS2(77-211)) (Hannanta-Anan and Chow 2018). The opto-RGS2 system also employs the use of the native N-terminal targeting domain of RGS2 to localise CIBN at the membrane. It is likely that this results in a more favourable localisation of the RGS-box domain within appropriate membrane compartments upon light-induced recruitment. It is also possible that the N-terminal domain itself may possess the ability to bind the third intracellular loop of Gαq-linked GPCRs.
3. PIGM-Iq functions *in vivo*. This is the first known study to demonstrate the effects of a light recruited RGS domain as an optogenetic inhibitor of Gαq signalling in behaving model organisms. In the current study, PIGM-Iq was seen to function to a degree in two invertebrate models – *C. elegans* and *D. melanogaster*, however, further experiments are needed to confirm this. PIGM-Iq was also utilised by our collaborator - Ms Silvia Vicenzi - in the zebrafish, *Danio rerio*, where she showed that activation during larval development resulted in paralysis, an effect that was not observed in transgenic animals expressing PIGM-Iq^{D387A} (see PhD thesis of Ms Silvia Vicenzi for more information).

The main limitation of the tool was centred around background activity, likely attributed to overexpression of the tool. It was found that, across all three models tested, overexpression was counterproductive and lead to high levels of background inhibition. This may be improved by utilising optimised imaging conditions and the 'low background' CRY535/CIB1 pair in future studies (Taslimi, Zoltowski et al. 2016). The CRY2/CIB1 coding sequences used in the current study is codon-optimised for mammalian expression and the overall coding sequence of PIGM-Iq is predicted to express well in mammalian, *C. elegans* and drosophila models (the current codon adaptation indices of the current sequence is 0.81, 0.63 and 0.73 in rat, *C. elegans* and *drosophila* models respectively using the Genscript online rare codon usage analysis tool https://www.genscript.com/tools/rare-codon-analysis). By using alternative codon sequences such as the original CRY2/CIBN sequence from *Arabidopsis* used by Kennedy *et al*, the codon adaptation indices can be reduced to 0.72 in rat and 0.66 in *drosophila* (remain 0.65 in *C.elegans*). It may be still possible to reduce these values to ~0.5 or below in particular model system using customised codons to control expression levels.

Although PIGM-Iq was demonstrated to effectively inhibit Gαq signalling via suppression of calcium efflux, other aspects of Gαq signalling were not covered. Upon GPCR activation, the Gα subunit and Gβγ subunit are separated, interacting with effectors to initiate various signalling cascades. This study investigated the inhibition of the Gαq signalling pathway; however, the impact on the Gβγ signalling pathway was not investigated. It is hypothesised that inhibition of the Gα subunit by PIGM-Iq would lead to a re-association of the Gα subunit and Gβγ subunits, as was shown with opto-RGS4 (O'Neill and Gautam 2014).

This study does not confirm whether the signalling cascade initiated by DAG is affected. It is hypothesised that the inhibition of Gαq signalling by PIGM-Iq would disrupt its interaction with all effectors, and that suppression of calcium efflux indicates a suppression of PLC activation, thus the production of both IP_3 and DAG from PIP_2. However, this cannot be confirmed without experimentally validating the inhibition of Gαq-linked DAG-mediated signalling.

Furthermore, the long-term effects of RGS2 RGS domain overexpression were not assessed. It has been previously identified by Nguyen et al. that RGS2 inhibits the activity of the guanine nucleotide exchange factor (GEF), eIF2b, resulting in a reduction in *de novo* protein synthesis (Nguyen, Ming et al. 2009). The GTP-bound, active state of eIF2 is able to form a complex with initiator Met-tRNA, which then binds the 40S ribosomal subunit, resulting in the initiation of protein synthesis (Nguyen, Ming et al. 2009, Beilsten-Edmands, Gordiyenko et al. 2015). The ability of RGS2 to block eIF2B GEF function was found to be independent of RGS domain function (Nguyen, Ming et al. 2009). Although the possibility for PIGM-Iq to inhibit eIF2B exists, the optogenetic nature of the tool does allow for light and dark state comparisons rather than wild-type and genetic mutant comparisons seen in traditional techniques. Consequently, it may be possible to avoid the influence of this interaction and its outcomes on the interpretation of results regarding Gαq. Despite this, caution should be taken when drawing conclusion about Gαq function when using this tool.

5.2 Future directions

5.2.1 Development of endogenous receptor specific PIGM-Iq

Although the PIGM-Iq system displays selectivity toward the Gαq subunit, it cannot be used to distinguish between different Gαq-linked GPCRs. A method to selectively target specific GPCRs of interest and localise the RGS domain to these receptors would drastically increase

the applications of this tool. One method that could utilised is nanobodies to localise the CIBN component of PIGM-Iq (CIBN-eGFP-NB) to specific GPCRs of interest. Ideally these nanobodies would selectively target the activated state of the GPCR such as the published 5-HT_{2A} and mu-opioid receptor nanobodies (Stoeber, Jullié et al. 2018, English, Olsen et al. 2019). This would allow for the light-activated recruitment of an RGS domain to the activated receptor of interest, followed by the inhibition of the associated Gαq subunit. However, it would need to be ensured that neither the nanobody itself, nor the presence of CIBN, interrupted GPCR signalling, as some nanobodies are designed to lock receptors in certain conformations upon binding.

5.2.2 Development of optogenetic inhibitors of Gαi

To expand upon methods to optogenetically inhibit Gαq signalling, work has begun on a tool to selectively inhibit Gαi-linked signalling using a similar method as that described for PIGM-Iq. Although an optogenetic inhibitor for Gαi, opto-RGS4, already exists, literature suggests that RGS4 is non-selective and can act as a GAP for both Gαi and Gαq (Yan, Chi et al. 1997, Zeng, Xu et al. 1998). Therefore, an RGS protein with high selectivity toward Gαi is needed.

RGS10 is a selective and potent GAP for Gαi subunits (Hunt, Fields et al. 1996). RGS10 consists of an RGS-box domain and short, N- and C-terminal extensions, making it one of the smallest and structurally simple RGS proteins and is primarily localised to the nucleus and cytoplasm of the cell (Chatterjee and Fisher 2000, Burgon, Lee et al. 2001, Lee, McCoy et al. 2008, Almutairi, Lee et al. 2020). Nuclear localisation is believed to be induced through phosphorylation of serine at position 168 by cAMP-dependent kinase A (Burgon, Lee et al. 2001).

Preliminary results show that removal of the C-terminus of RGS10 and the addition of a nuclear export sequence increases the cytoplasmic localisation of the protein with no visible membrane accumulation (data not shown). Preliminary results of light recruitment of RGS10 to the membrane suggest it has no effects on Gαq-associated calcium increase and could effectively suppress Gαi signalling (data not shown). However, more detailed testing and characterisation of this ‘PIGM-Ii’ (Gαi) tool is necessary.

5.2.3 Development of optogenetic inhibitors for Gαs or adenylate cyclase

In addition to the current study, many attempts were made to develop an optogenetic inhibitor for Gαs/adenylate cyclase. SNX13, an RGS protein believed to be specific for Gαs (Zheng, Ma et al. 2001)was a possible candidate to be adapted to the 'PIGM-Is' (Gαs) system; however, problems were encountered upon recovering constructs from bacteria after transformation. Non-RGS-domain-based tools were also developed and tested which included peptides from the caveolin-1 protein (Toya, Schwencke et al. 1998), the RGS2 N-terminal peptide and a light-activated Gαi system. However, no measurable inhibition of Gαs signalling was observed in the preliminary experiments, possibly because most of the inhibitors tested rely on steric hinderance rather than enzymatic activity which would require a higher concentration of inhibitory protein at the membrane to mediate inhibition. To expand on this, an optogenetically activated cAMP-specific phosphodiesterase is currently being trialled. However, more detailed testing and validation are still in progress for these tools and are beyond the scope of this thesis due to time limitations.

5.3 Conclusions

In neuroscientific research, the disruption of signal processing pathways or circuitry tend to have greater physiological relevance than artificial activation. The disruption of cellular signalling in genetically defined cells during behavioural tasks can highlight the involvement of cellular events important for the performance of that behaviour. G protein signalling is a fundamental aspect of neural function, and its physiological role in neuromodulation has yet to be fully understood. Despite the large array of chemical and optogenetic-based tools already available to manipulate neuromodulation, tools that can achieve selective, light-activated inhibition of G protein signalling are still lacking. The current study demonstrates the production of a 'first generation' selective trimeric G protein signalling inhibitor with possible expansions of such tools to other trimeric G protein signalling pathways or specific GPCR. The current version of PIGM-Iq would still be useful in the investigation of how trimeric G protein signalling leads to behaviour and should be useful in neuroscientific research even with its current limitations. Future work investigating the expansion of this type of tool and possibility for receptor selectivity would have much greater value and impact in neuroscientific research.

5.1 Appendix

Table 5.1 Protein sequence of PIGM-Iq

RGS2(Δ1-53)-CRY2(PHR)-T2A-CIBN-eGFP-CaaX	MTPGKPKTGKKSKQQTFIKPSPEEALLWAEAFDELLASKYGLAAFRAFLK SEFCEENIEFWLACEDFKKTKSPQKLSSKARKIYTDFIEKEAPKEINIDF QTKTLIAQNIQEATSGCFTTAQKRVYSLMENNSYPRFLESEFYQDLCKKP QITTEPHATTGGGSGGGSMKMDKKTIVWFRRDLRIEDNPALAAAAHEGSV FPVFIWCPEEEGQFYPGRASRWWMKQSLAHLSQSLKALGSDLTLIKTHNT ISAILDCIRVTGATKVVFNHLYDPVSLVRDHTVKEKLVERGISVQSYNGD LLYEPWEIYCEKGKPFTSFNSYWKKCLDMSIESVMLPPPWRLMPITAAAE AIWACSIEELGLENEAEKPSNALLTRAWSPGWSNADKLLNEFIEKQLIDY AKNSKKVVGNSTSLLSPYLHFGEISVRHVFQCARMKQIIWARDKNSEGEE SADLFLRGIGLREYSRYICFNFPFTHEQSLLSHLRFFPWDADVDKFKAWR QGRTGYPLVDAGMRELWATGWMHNRIRVIVSSFAVKFLLLPWKWGMKYFW DTLLDADLECDILGWQYISGSIPDGHELDRLDNPALQGAKYDPEGEYIRQ WLPELARLPTEWIHHPWDAPLTVLKASGVELGTNYAKPIVDIDTARELLA KAISRTREAQIMIGAASGGGSGGGGAGASGGGSGGGEGRGSLLTCGDVEE NPGPRTGGSGGGSMNGAIGGDLLLNFPDMSVLERQRAHLKYLNPTFDSPL AGFFADSSMITGGEMDSYLSTAGLNLPMMYGETTVEGDSRLSISPETTLG TGNFKAAKFDTETKDCNEAAKKMTMNRDDLVEEGEEEKSKITEQNNGSTK SIKKMKHKAKKEENNFSNDSSKVTKELEKTDYIGGGGAGIDMVSKGEELF TGVVPILVELDGDVNGHKFSVSGEGEGDATYGKLTLKFICTTGKLPVPWP TLVTTLTYGVQCFSRYPDHMKQHDFFKSAMPEGYVQERTIFFKDDGNYKT RAEVKFEGDTLVNRIELKGIDFKEDGNILGHKLEYNYNSHNVYIMADKQK NGIKVNFKIRHNIEDGSVQLADHYQQNTPIGDGPVLLPDNHYLSTQSALS KDPNEKRDHMVLLEFVTAAGITLGMDELYKGKKKKKKSKTKCVIM*

```
GNAQ        MTLESIMACCLSEEAKEARRINDEIERQLRRDKRDARRELKLLLLGTGESGKSTFIKQMR        60
EGL-30      ------MACCLSEEAREQKRINQEIEKQLQRDKRNARRELKLLLLGTGESGKSTFIKQMR        54
                  *********:* :***:***:**:****:************************

GNAQ        IIHGSGYSDEDKRGFTKLVYQNIFTAMQAMIRAMDTLKIPYKYEHN--KAHAQLVREVDV        118
EGL-30      IIHGQGYSEEDKRAHIRLVYQNVFMAIQSMIRAMDTLDIKFGNESEELQEKAAVVREVDF        114
            ****.***:****.. :*****:* *:*:********.* :  * :  : :* :*****.

GNAQ        EKVSAFENPYVDAIKSLWNDPGIQECYDRRREYQLSDSTKYYLNDLDRVADPAYLPTQQD        178
EGL-30      ESVTSFEEPYVSYIKELWEDSGIQECYDRRREYQLTDSAKYYLSDLRRLAVPDYLPTEQD        174
            *.*::**:***. **.**:* ************:**:****.** *:* * ****:**

GNAQ        VLRVRVPTTGIIEYPFDLQSVIFRMVDVGGQRSERRKWIHCFENVTSIMFLVALSEYDQV        238
EGL-30      ILRVRVPTTGIIEYPFDLEQIIFRMVDVGGQRSERRKWIHCFENVTSIMFLVALSEYDQV        234
            :*****************:.:**************************************

GNAQ        LVESDNENRMEESKALFRTIITYPWFQNSSVILFLNKKDLLEEKIMYSHLVDYFPEYDGP        298
EGL-30      LVECDNENRMEESKALFRTIITYPWFTNSSVILFLNKKDLLEEKILYSHLADYFPEYDGP        294
            ***.********************  *****************:****.*********

GNAQ        QRDAQAAREFILKMFVDLNPDSDKIIYSHFTCATDTENIRFVFAAVKDTILQLNLKEYNL        358
EGL-30      PRDPIAAREFILKMFVDLNPDADKIIYSHFTCATDTENIRFVFAAVKDTILQHNLKEYNL        354
             **   ***************:****************************** *******

GNAQ        V   359
EGL-30      V   355
            *
```

Figure A1 | *Sequence alignment of* Homo sapiens *G protein subunit alpha q (GNAQ) and* C. elegans *G protein subunit alpha q (EGL-30).* Sequence alignment showing 83% similarity between the amino acids of QNAQ and EGL-30. (‘*’ indicated fully conserved residues, ‘:’ indicates residues with strongly similar properties, ‘.’ Indicates residues with weakly similar properties.) GNAQ (NCBI Reference Sequence NM_002072.5) EGL-30 (NCBI Reference Sequence AAB04059.1). Alignment performed using Clustal Omega (EMBL-EBI) ((Sievers, Wilm et al. 2011, Madeira, Park et al. 2019).

```
GNAQ          MTLESIMACCLSEEAKEARRINDEIERQLRRDKRDARRELKLLLLGTGESGKSTFIKQMR    60
Dmel/GNAQ     ------MECCLSEEAKEQKRINQEIEKQLRRDKRDARRELKLLLLGTGESGKSTFIKQMR    54
                    * ********* :***:***:*********************************

GNAQ          IIHGSGYSDEDKRGFTKLVYQNIFTAMQAMIRAMDTLKIPYKYEHNKAHAQLVREVDVEK    120
Dmel/GNAQ     IIHGSGYSDEDKRGYIKLVFQNIFMAMQSMIKAMDMLKISYGQGEHSELADLVMSIDYET    114
              **************: ***:**** ***:**:*** *** *   .:.  *:** .:* *.

GNAQ          VSAFENPYVDAIKSLWNDPGIQECYDRRREYQLSDSTKYYLNDLDRVADPAYLPTQQDVL    180
Dmel/GNAQ     VTTFEDPYLNAIKTLWDDAGIQECYDRRREYQLTDSAKYYLSDLARIEQADYLPTEQDIL    174
              *::**:**::***:**:* *************:**:****.** *: :  ****:**:*

GNAQ          RVRVPTTGIIEYPFDLQSVIFRMVDVGGQRSERRKWIHCFENVTSIMFLVALSEYDQVLV    240
Dmel/GNAQ     RARVPTTGILEYPFDLDGIVFRMVDVGGQRSERRKWIHCFENVTSIIFLVALSEYDQILF    234
              *.*******:******:.::*************************:**********:*.

GNAQ          ESDNENRMEESKALFRTIITYPWFQNSSVILFLNKKDLLEEKIMYSHLVDYFPEYDGPQR    300
Dmel/GNAQ     ESDNENRMEESKALFRTIITYPWFQNSSVILFLNKKDLLEEKIMYSHLVDYFPEYDGPKQ    294
              ************************************************************::

GNAQ          DAQAAREFILKMFVDLNPDSDKIIYSHFTCATDTENIRFVFAAVKDTILQLNLKEYNLV     359
Dmel/GNAQ     DHAAAKQFVLKKYLACNPDPERQCYSHFTTATDTENIKLVFCAVKDTIMQNALKEFNLG     353
              *  **::*:** ::  *** ::  ***** *******::**.******:*  ***:**
```

Figure A2 | *Sequence alignment of* Homo sapiens *G protein subunit alpha q (GNAQ) and* D. melanogaster *G protein subunit alpha q (Dmel/GNAQ).* Sequence alignment showing 77% similarity between the amino acids of QNAQ and Dmel/GNAQ. (‘*’ indicated fully conserved residues, ‘:’ indicates residues with strongly similar properties, ‘.’ Indicates residues with weakly similar properties.) GNAQ (NCBI Reference Sequence NM_002072.5), Dmel/GNAQ (NCBI Reference Sequence NP_725196.1). Alignment performed using Clustal Omega (EMBL-EBI) (Sievers, Wilm et al. 2011, Madeira, Park et al. 2019).

Software used:

All diagrams were made using Microsoft Word (version 2105)

All images and image stack files were processed using Imagej (Rasband, W.S., ImageJ, U. S. National Institutes of Health, Bethesda, Maryland, USA) https://imagej.nih.gov/ij/

Raw data was handled using Microsoft Excel (version 2105)

All graphs were made, and statistical analysis perfmored, using GraphPad Prism 8.3 (GraphPad Software, San Diego, California USA, www.graphpad.com).

LED Driver Control Panel V3.2.2 was used to control LED (Mightex)

Micro-Manager 1.4.22 was used for microscopy (Edelstein, Tsuchida et al. 2014)

Sequence alignments were performed using Clustal Omega (EMBL-EBI) (Sievers, Wilm et al. 2011, Madeira, Park et al. 2019).

Codon adaption indices were found using the Genscript online rare codon usage analysis tool (https://www.genscript.com/tools/rare-codon-analysis)

List of chemicals used (details not mentioned in text):

Agar bacteriological (Oxoid, Cat# LP0011)
Agencourt CleanSEQ (Beckman Coulter, Cat# A29151)
Ampicillin (Bio Basic, Cat# AB0028)
$CaCl_2 \cdot 2H_2O$ (Sigma-Aldrich, Cat# C3306-500G)
D-Glucose (Sigma-Aldrich, Cat# G5767-500G)
DNA Ladder (New England Biolabs, Cat# N3200S)
Ethanol (Sigma-Aldrich, Cat# E7023-500ML)
HBSS solution (10X) (Gibco, Cat# 14185052)
KCl (Sigma-Aldrich, Cat# P9541-500G)
$MgCl_2 \cdot 6H_2O$ (Sigma-Aldrich, Cat# 63068-250G)
NaCl (Sigma-Aldrich, Cat# S7653-5KG)
Tryptone (Oxoid, Cat# LP0042)
Yeast Extract (Oxoid, Cat# LP0021)

List of cloning reagents (details not mentioned in text):

AgeI-HF (New England Biolabs, Cat# R3552)
BamHI-HF (New England Biolabs, Cat# R3136)
KpnI-HF (New England Biolabs, Cat# R3142S)
MluI-HF (New England Biolabs, Cat# R3198S)
T4 ligase (Invitrogen, Cat# 15224-017)
XbaI (New England Biolabs, Cat# R0145)
Zymoclean Gel DNA Recovery Kit (Zymo Research, Cat# D4002)

References

Ahmad, M., N. Grancher, M. Heil, R. C. Black, B. Giovani, P. Galland and D. Lardemer (2002). "Action spectrum for cryptochrome-dependent hypocotyl growth inhibition in Arabidopsis." Plant Physiol **129**(2): 774-785.

Airan, R. D., K. R. Thompson, L. E. Fenno, H. Bernstein and K. Deisseroth (2009). "Temporally precise in vivo control of intracellular signalling." Nature **458**(7241): 1025-1029.

Almutairi, F., J. K. Lee and B. Rada (2020). "Regulator of G protein signaling 10: Structure, expression and functions in cellular physiology and diseases." Cell Signal **75**: 109765.

Altun, Z. F. a. H., D.H. (2011). "Nervous system, general description." WormAtlas.

Anderson, G. R., E. Posokhova and K. A. Martemyanov (2009). "The R7 RGS protein family: multi-subunit regulators of neuronal G protein signaling." Cell Biochem Biophys **54**(1-3): 33-46.

Armbruster, B. N., X. Li, M. H. Pausch, S. Herlitze and B. L. Roth (2007). "Evolving the lock to fit the key to create a family of G protein-coupled receptors potently activated by an inert ligand." Proceedings of the National Academy of Sciences **104**(12): 5163-5168.

Armbruster, B. N., X. Li, M. H. Pausch, S. Herlitze and B. L. Roth (2007). "Evolving the lock to fit the key to create a family of G protein-coupled receptors potently activated by an inert ligand." Proc Natl Acad Sci U S A **104**(12): 5163-5168.

Asli, A., I. Sadiya, M. Avital-Shacham and M. Kosloff (2018). ""Disruptor" residues in the regulator of G protein signaling (RGS) R12 subfamily attenuate the inactivation of Gα subunits." Sci Signal **11**(534).

Aso, Y., D. Hattori, Y. Yu, R. M. Johnston, N. A. Iyer, T. T. Ngo, H. Dionne, L. F. Abbott, R. Axel, H. Tanimoto and G. M. Rubin (2014). "The neuronal architecture of the mushroom body provides a logic for associative learning." Elife **3**: e04577.

Atwood, B. K., J. Lopez, J. Wager-Miller, K. Mackie and A. Straiker (2011). "Expression of G protein-coupled receptors and related proteins in HEK293, AtT20, BV2, and N18 cell lines as revealed by microarray analysis." BMC Genomics **12**: 14.

Azam, S., M. E. Haque, M. Jakaria, S.-H. Jo, I.-S. Kim and D.-K. Choi (2020). "G-Protein-Coupled Receptors in CNS: A Potential Therapeutic Target for Intervention in Neurodegenerative Disorders and Associated Cognitive Deficits." Cells **9**(2): 506.

Bærentzen, S., A. Casado-Sainz, D. Lange, V. Shalgunov, I. M. Tejada, M. Xiong, E. T. L'Estrade, F. G. Edgar, H. Lee, M. M. Herth and M. Palner (2019). "The Chemogenetic Receptor Ligand Clozapine N-Oxide Induces in vivo Neuroreceptor Occupancy and Reduces Striatal Glutamate Levels." Frontiers in Neuroscience **13**(187).

Bailes, H. J., L. Y. Zhuang and R. J. Lucas (2012). "Reproducible and sustained regulation of Galphas signalling using a metazoan opsin as an optogenetic tool." PLoS One **7**(1): e30774.

Bailes, H. J., L. Y. Zhuang and R. J. Lucas (2012). "Reproducible and sustained regulation of Gαs signalling using a metazoan opsin as an optogenetic tool." PLoS One **7**(1): e30774.

Ballister, E. R., C. Aonbangkhen, A. M. Mayo, M. A. Lampson and D. M. Chenoweth (2014). "Localized light-induced protein dimerization in living cells using a photocaged dimerizer." Nat Commun **5**: 5475.

Banerjee, R., E. Schleicher, S. Meier, R. M. Viana, R. Pokorny, M. Ahmad, R. Bittl and A. Batschauer (2007). "The signaling state of Arabidopsis cryptochrome 2 contains flavin semiquinone." J Biol Chem **282**(20): 14916-14922.

Beilsten-Edmands, V., Y. Gordiyenko, J. C. K. Kung, S. Mohammed, C. Schmidt and C. V. Robinson (2015). "eIF2 interactions with initiator tRNA and eIF2B are regulated by post-translational modifications and conformational dynamics." Cell Discovery **1**(1): 15020.

Bender, D., M. Holschbach and G. Stocklin (1994). "Synthesis of n.c.a. carbon-11 labelled clozapine and its major metabolite clozapine-N-oxide and comparison of their biodistribution in mice." Nucl Med Biol **21**(7): 921-925.

Bennett, M. V. and R. S. Zukin (2004). "Electrical coupling and neuronal synchronization in the Mammalian brain." Neuron **41**(4): 495-511.

Berlin, S., T. Keren-Raifman, R. Castel, M. Rubinstein, C. W. Dessauer, T. Ivanina and N. Dascal (2010). "G alpha(i) and G betagamma jointly regulate the conformations of a G betagamma effector, the neuronal G protein-activated K+ channel (GIRK)." J Biol Chem **285**(9): 6179-6185.

Berman, D. M., T. M. Wilkie and A. G. Gilman (1996). "GAIP and RGS4 are GTPase-activating proteins for the Gi subfamily of G protein alpha subunits." Cell **86**(3): 445-452.

Bernstein, L. S., S. Ramineni, C. Hague, W. Cladman, P. Chidiac, A. I. Levey and J. R. Hepler (2004). "RGS2 binds directly and selectively to the M1 muscarinic acetylcholine receptor third intracellular loop to modulate Gq/11alpha signaling." J Biol Chem **279**(20): 21248-21256.

Birgul, N., C. Weise, H. J. Kreienkamp and D. Richter (1999). "Reverse physiology in drosophila: identification of a novel allatostatin-like neuropeptide and its cognate receptor structurally related to the mammalian somatostatin/galanin/opioid receptor family." Embo j **18**(21): 5892-5900.

Bonaventura, J., M. A. Eldridge, F. Hu, J. L. Gomez, M. Sanchez-Soto, A. M. Abramyan, S. Lam, M. Boehm, C. Ruiz, M. Farrell, A. Moreno, I. M. G. Faress, N. Andersen, J. Y. Lin, R. Moaddel, P. Morris, L. Shi, D. R. Sibley, S. V. Mahler, S. Nabavi, M. G. Pomper, A. Bonci, A. G. Horti, B. J. Richmond and M. Michaelides (2018). "Chemogenetic ligands for translational neurotheranostics." bioRxiv: 487637.

Bontonou, G. and C. Wicker-Thomas (2014). "Sexual Communication in the Drosophila Genus." Insects **5**: 439-458.

Breitwieser, G. E. and G. Szabo (1988). "Mechanism of muscarinic receptor-induced K+ channel activation as revealed by hydrolysis-resistant GTP analogues." J Gen Physiol **91**(4): 469-493.

Brundage, L., L. Avery, A. Katz, U. J. Kim, J. E. Mendel, P. W. Sternberg and M. I. Simon (1996). "Mutations in a C. elegans Gqalpha gene disrupt movement, egg laying, and viability." Neuron **16**(5): 999-1009.

Burgon, P. G., W. L. Lee, A. B. Nixon, E. G. Peralta and P. J. Casey (2001). "Phosphorylation and nuclear translocation of a regulator of G protein signaling (RGS10)." J Biol Chem **276**(35): 32828-32834.

Burgon, P. G., W. L. Lee, A. B. Nixon, E. G. Peralta and P. J. Casey (2001). "Phosphorylation and Nuclear Translocation of a Regulator of G Protein Signaling (RGS10)*." Journal of Biological Chemistry **276**(35): 32828-32834.

Burnett, C. J. and M. J. Krashes (2016). "Resolving Behavioral Output via Chemogenetic Designer Receptors Exclusively Activated by Designer Drugs." The Journal of neuroscience : the official journal of the Society for Neuroscience **36**(36): 9268-9282.

Cardin, J. A., M. Carlen, K. Meletis, U. Knoblich, F. Zhang, K. Deisseroth, L. H. Tsai and C. I. Moore (2009). "Driving fast-spiking cells induces gamma rhythm and controls sensory responses." Nature **459**(7247): 663-667.

Chan, R. K. and C. A. Otte (1982). "Isolation and genetic analysis of Saccharomyces cerevisiae mutants supersensitive to G1 arrest by a factor and alpha factor pheromones." Mol Cell Biol **2**(1): 11-20.

Chan, R. K. and C. A. Otte (1982). "Physiological characterization of Saccharomyces cerevisiae mutants supersensitive to G1 arrest by a factor and alpha factor pheromones." Mol Cell Biol **2**(1): 21-29.

Chatterjee, T. K. and R. A. Fisher (2000). "Cytoplasmic, nuclear, and golgi localization of RGS proteins. Evidence for N-terminal and RGS domain sequences as intracellular targeting motifs." J Biol Chem **275**(31): 24013-24021.

Chatterjee, T. K. and R. A. Fisher (2000). "Cytoplasmic, Nuclear, and Golgi Localization of RGS Proteins: EVIDENCE FOR N-TERMINAL AND RGS DOMAIN SEQUENCES AS INTRACELLULAR TARGETING MOTIFS*." Journal of Biological Chemistry **275**(31): 24013-24021.

Chen, X., H. Choo, X. P. Huang, X. Yang, O. Stone, B. L. Roth and J. Jin (2015). "The first structure-activity relationship studies for designer receptors exclusively activated by designer drugs." ACS Chem Neurosci **6**(3): 476-484.

Chidiac, P., A. J. Sobiesiak, K. N. Lee, R. Gros and C. H. Nguyen (2014). "The eIF2B-interacting domain of RGS2 protects against GPCR agonist-induced hypertrophy in neonatal rat cardiomyocytes." Cellular Signalling **26**(6): 1226-1234.

Chow, B. Y., X. Han, A. S. Dobry, X. Qian, A. S. Chuong, M. Li, M. A. Henninger, G. M. Belfort, Y. Lin, P. E. Monahan and E. S. Boyden (2010). "High-performance genetically targetable optical neural silencing by light-driven proton pumps." Nature **463**(7277): 98-102.

Connolly, J. B., I. J. Roberts, J. D. Armstrong, K. Kaiser, M. Forte, T. Tully and C. J. O'Kane (1996). "Associative learning disrupted by impaired Gs signaling in Drosophila mushroom bodies." Science **274**(5295): 2104-2107.

Coward, P., H. G. Wada, M. S. Falk, S. D. Chan, F. Meng, H. Akil and B. R. Conklin (1998). "Controlling signaling with a specifically designed Gi-coupled receptor." Proc Natl Acad Sci U S A **95**(1): 352-357.

Crosson, S. and K. Moffat (2002). "Photoexcited structure of a plant photoreceptor domain reveals a light-driven molecular switch." Plant Cell **14**(5): 1067-1075.

de Belle, J. S. and M. Heisenberg (1994). "Associative odor learning in Drosophila abolished by chemical ablation of mushroom bodies." Science **263**(5147): 692-695.

De Marco, R. J., A. H. Groneberg, C. M. Yeh, L. A. Castillo Ramírez and S. Ryu (2013). "Optogenetic elevation of endogenous glucocorticoid level in larval zebrafish." Front Neural Circuits **7**: 82.

De Vries, L., E. Elenko, L. Hubler, T. L. Jones and M. G. Farquhar (1996). "GAIP is membrane-anchored by palmitoylation and interacts with the activated (GTP-bound) form of G alpha i subunits." Proc Natl Acad Sci U S A **93**(26): 15203-15208.

Deisseroth, K. (2015). "Optogenetics: 10 years of microbial opsins in neuroscience." Nat Neurosci **18**(9): 1213-1225.

Deng, W., E. M. Goldys, M. M. Farnham and P. M. Pilowsky (2014). "Optogenetics, the intersection between physics and neuroscience: light stimulation of neurons in physiological conditions." **307**(11): R1292-1302.

Dohlman, H. G., D. Apaniesk, Y. Chen, J. Song and D. Nusskern (1995). "Inhibition of G-protein signaling by dominant gain-of-function mutations in Sst2p, a pheromone desensitization factor in Saccharomyces cerevisiae." Mol Cell Biol **15**(7): 3635-3643.

Dong, X., S. Han, M. J. Zylka, M. I. Simon and D. J. Anderson (2001). "A diverse family of GPCRs expressed in specific subsets of nociceptive sensory neurons." Cell **106**(5): 619-632.

Druey, K. M., K. J. Blumer, V. H. Kang and J. H. Kehrl (1996). "Inhibition of G-protein-mediated MAP kinase activation by a new mammalian gene family." Nature **379**(6567): 742-746.

Duan, L., J. Hope, Q. Ong, H.-Y. Lou, N. Kim, C. McCarthy, V. Acero, M. Z. Lin and B. Cui (2017). "Understanding CRY2 interactions for optical control of intracellular signaling." Nature Communications **8**(1): 547.

Dubnau, J., L. Grady, T. Kitamoto and T. Tully (2001). "Disruption of neurotransmission in Drosophila mushroom body blocks retrieval but not acquisition of memory." Nature **411**(6836): 476-480.

Dulin, N. O., A. Sorokin, E. Reed, S. Elliott, J. H. Kehrl and M. J. Dunn (1999). "RGS3 inhibits G protein-mediated signaling via translocation to the membrane and binding to Galpha11." Molecular and cellular biology **19**(1): 714-723.

Edelstein, A. D., M. A. Tsuchida, N. Amodaj, H. Pinkard, R. D. Vale and N. Stuurman (2014). "Advanced methods of microscope control using μManager software." Journal of Biological Methods **1**(2): e10.

English, J. G., R. H. J. Olsen, K. Lansu, M. Patel, K. White, A. S. Cockrell, D. Singh, R. T. Strachan, D. Wacker and B. L. Roth (2019). "VEGAS as a Platform for Facile Directed Evolution in Mammalian Cells." Cell **178**(3): 748-761.e717.

Enomoto, K., M. Takano, S. Ariyoshi and T. Asakawa (1995). "Mechanism and properties of inhibition of purified rat brain adenylate cyclase by G protein beta gamma-subunits." Jpn J Pharmacol **69**(3): 239-250.

Ersek, M., M. M. Cherrier, S. S. Overman and G. A. Irving (2004). "The cognitive effects of opioids." Pain Manag Nurs **5**(2): 75-93.

Farooqui, T., K. Robinson, H. Vaessin and B. H. Smith (2003). "Modulation of early olfactory processing by an octopaminergic reinforcement pathway in the honeybee." J Neurosci **23**(12): 5370-5380.

Freddolino, P. L., K. H. Gardner and K. Schulten (2013). "Signaling mechanisms of LOV domains: new insights from molecular dynamics studies." Photochem Photobiol Sci **12**(7): 1158-1170.

Fung, B. K., J. B. Hurley and L. Stryer (1981). "Flow of information in the light-triggered cyclic nucleotide cascade of vision." Proc Natl Acad Sci U S A **78**(1): 152-156.

Gainetdinov, R. R., R. T. Premont, L. M. Bohn, R. J. Lefkowitz and M. G. Caron (2004). "Desensitization of G protein-coupled receptors and neuronal functions." Annu Rev Neurosci **27**: 107-144.

Galvan, E. J., T. Perez-Rosello, G. Gomez-Lira, E. Lara, R. Gutierrez and G. Barrionuevo (2015). "Synapse-specific compartmentalization of signaling cascades for LTP induction in CA3 interneurons." Neuroscience **290**: 332-345.

Gasser, C., S. Taiber, C. M. Yeh, C. H. Wittig, P. Hegemann, S. Ryu, F. Wunder and A. Möglich (2014). "Engineering of a red-light-activated human cAMP/cGMP-specific phosphodiesterase." Proc Natl Acad Sci U S A **111**(24): 8803-8808.

Glantz, S. T., E. J. Carpenter, M. Melkonian, K. H. Gardner, E. S. Boyden, G. K.-S. Wong and B. Y. Chow (2016). "Functional and topological diversity of LOV domain photoreceptors." Proceedings of the National Academy of Sciences **113**(11): E1442-E1451.

Gomez, J. L., J. Bonaventura, W. Lesniak, W. B. Mathews, P. Sysa-Shah, L. A. Rodriguez, R. J. Ellis, C. T. Richie, B. K. Harvey, R. F. Dannals, M. G. Pomper, A. Bonci and M. Michaelides (2017). "Chemogenetics revealed: DREADD occupancy and activation via converted clozapine." Science **357**(6350): 503-507.

Goutaudier, R., V. Coizet, C. Carcenac and S. Carnicella (2019). "DREADDs: The Power of the Lock, the Weakness of the Key. Favoring the Pursuit of Specific Conditions Rather than Specific Ligands." eneuro **6**(5): ENEURO.0171-0119.2019.

Govorunova, E. G., O. A. Sineshchekov, R. Janz, X. Liu and J. L. Spudich (2015). "NEUROSCIENCE. Natural light-gated anion channels: A family of microbial rhodopsins for advanced optogenetics." Science **349**(6248): 647-650.

Gresset, A., J. Sondek and T. K. Harden (2012). "The phospholipase C isozymes and their regulation." Sub-cellular biochemistry **58**: 61-94.

Griffith, L. C. and A. Ejima (2009). "Courtship learning in Drosophila melanogaster: diverse plasticity of a reproductive behavior." Learn Mem **16**(12): 743-750.

Gu, S., J. He, W. T. Ho, S. Ramineni, D. M. Thal, R. Natesh, J. J. Tesmer, J. R. Hepler and S. P. Heximer (2007). "Unique hydrophobic extension of the RGS2 amphipathic helix domain imparts increased plasma membrane binding and function relative to other RGS R4/B subfamily members." J Biol Chem **282**(45): 33064-33075.

Guntas, G., R. A. Hallett, S. P. Zimmerman, T. Williams, H. Yumerefendi, J. E. Bear and B. Kuhlman (2015). "Engineering an improved light-induced dimer (iLID) for controlling the localization and activity of signaling proteins." Proceedings of the National Academy of Sciences **112**(1): 112-117.

Guntas, G., R. A. Hallett, S. P. Zimmerman, T. Williams, H. Yumerefendi, J. E. Bear and B. Kuhlman (2015). "Engineering an improved light-induced dimer (iLID) for controlling the localization and activity of signaling proteins." Proc Natl Acad Sci U S A **112**(1): 112-117.

Gurevich, V. V. and E. V. Gurevich (2017). "Molecular Mechanisms of GPCR Signaling: A Structural Perspective." International journal of molecular sciences **18**(12): 2519.

Hagena, H., N. Hansen and D. Manahan-Vaughan (2016). "β-Adrenergic Control of Hippocampal Function: Subserving the Choreography of Synaptic Information Storage and Memory." Cereb Cortex **26**(4): 1349-1364.

Hague, C., L. S. Bernstein, S. Ramineni, Z. Chen, K. P. Minneman and J. R. Hepler (2005). "Selective inhibition of alpha1A-adrenergic receptor signaling by RGS2 association with the receptor third intracellular loop." J Biol Chem **280**(29): 27289-27295.

Hajdu-Cronin, Y. M., W. J. Chen, G. Patikoglou, M. R. Koelle and P. W. Sternberg (1999). "Antagonism between G(o)alpha and G(q)alpha in Caenorhabditis elegans: the RGS protein EAT-16 is necessary for G(o)alpha signaling and regulates G(q)alpha activity." Genes Dev **13**(14): 1780-1793.

Hallett, R. A., S. P. Zimmerman, H. Yumerefendi, J. E. Bear and B. Kuhlman (2016). "Correlating in Vitro and in Vivo Activities of Light-Inducible Dimers: A Cellular Optogenetics Guide." ACS Synth Biol **5**(1): 53-64.

Han, B., A. Bellemer and M. R. Koelle (2015). "An evolutionarily conserved switch in response to GABA affects development and behavior of the locomotor circuit of Caenorhabditis elegans." Genetics **199**(4): 1159-1172.

Han, K.-A. and Y.-C. Kim (2010). "Courtship Behavior: The Right Touch Stimulates the Proper Song." Current Biology **20**(1): R25-R28.

Han, K.-A., N. S. Millar and R. L. Davis (1998). "A Novel Octopamine Receptor with Preferential Expression inDrosophila Mushroom Bodies." The Journal of Neuroscience **18**(10): 3650.

Hannanta-Anan, P. and B. Y. Chow (2018). "Optogenetic Inhibition of Gα(q) Protein Signaling Reduces Calcium Oscillation Stochasticity." ACS synthetic biology **7**(6): 1488-1495.

Haraguchi, K. and M. Rodbell (1991). "Carbachol-activated muscarinic (M1 and M3) receptors transfected into Chinese hamster ovary cells inhibit trafficking of endosomes." Proc Natl Acad Sci U S A **88**(14): 5964-5968.

Hartmann, J., E. Dragicevic, H. Adelsberger, H. A. Henning, M. Sumser, J. Abramowitz, R. Blum, A. Dietrich, M. Freichel, V. Flockerzi, L. Birnbaumer and A. Konnerth (2008). "TRPC3 channels are required for synaptic transmission and motor coordination." Neuron **59**(3): 392-398.

Haubensak, W., P. S. Kunwar, H. Cai, S. Ciocchi, N. R. Wall, R. Ponnusamy, J. Biag, H. W. Dong, K. Deisseroth, E. M. Callaway, M. S. Fanselow, A. Luthi and D. J. Anderson (2010). "Genetic dissection of an amygdala microcircuit that gates conditioned fear." Nature **468**(7321): 270-276.

Heisenberg, M., A. Borst, S. Wagner and D. Byers (1985). "Drosophila mushroom body mutants are deficient in olfactory learning." J Neurogenet **2**(1): 1-30.

Heximer, Scott P. (2013). "A “New Twist” on RGS Protein Selectivity." Structure **21**(3): 319-320.

Heximer, S. P., H. Lim, J. L. Bernard and K. J. Blumer (2001). "Mechanisms governing subcellular localization and function of human RGS2." J Biol Chem **276**(17): 14195-14203.

Heximer, S. P., S. P. Srinivasa, L. S. Bernstein, J. L. Bernard, M. E. Linder, J. R. Hepler and K. J. Blumer (1999). "G protein selectivity is a determinant of RGS2 function." J Biol Chem **274**(48): 34253-34259.

Heximer, S. P., N. Watson, M. E. Linder, K. J. Blumer and J. R. Hepler (1997). "RGS2/G0S8 is a selective inhibitor of Gqalpha function." Proc Natl Acad Sci U S A **94**(26): 14389-14393.

Hirano, M., M. Takebe, T. Ishido, T. Ide and S. Matsunaga (2019). "The C-terminal region affects the activity of photoactivated adenylyl cyclase from Oscillatoria acuminata." Sci Rep **9**(1): 20262.

Huang, K.-P. (1989). "The mechanism of protein kinase C activation." Trends in Neurosciences **12**(11): 425-432.

Huang, Y. and A. Thathiah (2015). "Regulation of neuronal communication by G protein-coupled receptors." FEBS Lett **589**(14): 1607-1619.

Hunnicutt, B. J., B. R. Long, D. Kusefoglu, K. J. Gertz, H. Zhong and T. Mao (2014). "A comprehensive thalamocortical projection map at the mesoscopic level." Nat Neurosci **17**(9): 1276-1285.

Hunt, T. W., T. A. Fields, P. J. Casey and E. G. Peralta (1996). "RGS10 is a selective activator of G alpha i GTPase activity." Nature **383**(6596): 175-177.

Ilg, A.-K., T. Enkel, D. Bartsch and F. Bähner (2018). "Behavioral Effects of Acute Systemic Low-Dose Clozapine in Wild-Type Rats: Implications for the Use of DREADDs in Behavioral Neuroscience." Frontiers in Behavioral Neuroscience **12**(173).

Iseki, M., S. Matsunaga, A. Murakami, K. Ohno, K. Shiga, K. Yoshida, M. Sugai, T. Takahashi, T. Hori and M. Watanabe (2002). "A blue-light-activated adenylyl cyclase mediates photoavoidance in Euglena gracilis." Nature **415**(6875): 1047-1051.

Jaeger, W. C., S. P. Armstrong, S. J. Hill and K. D. Pfleger (2014). "Biophysical Detection of Diversity and Bias in GPCR Function." Front Endocrinol (Lausanne) **5**: 26.

Jansen, V., L. Alvarez, M. Balbach, T. Strünker, P. Hegemann, U. B. Kaupp and D. Wachten (2015). "Controlling fertilization and cAMP signaling in sperm by optogenetics." Elife **4**.

Jia, J. M., J. Zhao, Z. Hu, D. Lindberg and Z. Li (2013). "Age-dependent regulation of synaptic connections by dopamine D2 receptors." Nat Neurosci **16**(11): 1627-1636.

Kandel, E. R. (2012). "The molecular biology of memory: cAMP, PKA, CRE, CREB-1, CREB-2, and CPEB." Mol Brain **5**: 14.

Kehrl, J. H. (1998). "Heterotrimeric G Protein Signaling: Roles in Immune Function and Fine-Tuning by RGS Proteins." Immunity **8**(1): 1-10.

Kennedy, M. J., R. M. Hughes, L. A. Peteya, J. W. Schwartz, M. D. Ehlers and C. L. Tucker (2010). "Rapid blue-light-mediated induction of protein interactions in living cells." Nat Methods **7**(12): 973-975.

Kim, J. M., J. Hwa, P. Garriga, P. J. Reeves, U. L. RajBhandary and H. G. Khorana (2005). "Light-driven activation of beta 2-adrenergic receptor signaling by a chimeric rhodopsin containing the beta 2-adrenergic receptor cytoplasmic loops." Biochemistry **44**(7): 2284-2292.

Kim, Y. C., H. G. Lee, J. Lim and K. A. Han (2013). "Appetitive learning requires the alpha1-like octopamine receptor OAMB in the Drosophila mushroom body neurons." J Neurosci **33**(4): 1672-1677.

Kimple, A. J., D. E. Bosch, P. M. Giguère and D. P. Siderovski (2011). "Regulators of G-protein signaling and their Gα substrates: promises and challenges in their use as drug discovery targets." Pharmacological reviews **63**(3): 728-749.

Kobilka, B. K. (2007). "G protein coupled receptor structure and activation." Biochim Biophys Acta **1768**(4): 794-807.

Koelle, M. R. (1997). "A new family of G-protein regulators - the RGS proteins." Curr Opin Cell Biol **9**(2): 143-147.

Koelle, M. R. and H. R. Horvitz (1996). "EGL-10 regulates G protein signaling in the C. elegans nervous system and shares a conserved domain with many mammalian proteins." Cell **84**(1): 115-125.

Konnerth, A., J. Dreessen and G. J. Augustine (1992). "Brief dendritic calcium signals initiate long-lasting synaptic depression in cerebellar Purkinje cells." Proceedings of the National Academy of Sciences of the United States of America **89**(15): 7051-7055.

Koyanagi, M. and A. Terakita (2014). "Diversity of animal opsin-based pigments and their optogenetic potential." Biochim Biophys Acta **1837**(5): 710-716.

Krashes, M. J., A. C. Keene, B. Leung, J. D. Armstrong and S. Waddell (2007). "Sequential use of mushroom body neuron subsets during drosophila odor memory processing." Neuron **53**(1): 103-115.

Lackner, M. R., S. J. Nurrish and J. M. Kaplan (1999). "Facilitation of synaptic transmission by EGL-30 Gqalpha and EGL-8 PLCbeta: DAG binding to UNC-13 is required to stimulate acetylcholine release." Neuron **24**(2): 335-346.

Lane, J. R., A. Abdul-Ridha and M. Canals (2013). "Regulation of G protein-coupled receptors by allosteric ligands." ACS Chem Neurosci **4**(4): 527-534.

Laranjeiro, R., G. Harinath, D. Burke, B. P. Braeckman and M. Driscoll (2017). "Single swim sessions in C. elegans induce key features of mammalian exercise." BMC Biology **15**(1): 30.

Lechner, H. A., E. S. Lein and E. M. Callaway (2002). "A genetic method for selective and quickly reversible silencing of Mammalian neurons." J Neurosci **22**(13): 5287-5290.

Lee, H.-G., S. Rohila and K.-A. Han (2009). "The octopamine receptor OAMB mediates ovulation via Ca2+/calmodulin-dependent protein kinase II in the Drosophila oviduct epithelium." PloS one **4**(3): e4716-e4716.

Lee, H., D. W. Kim, R. Remedios, T. E. Anthony, A. Chang, L. Madisen, H. Zeng and D. J. Anderson (2014). "Scalable control of mounting and attack by Esr1+ neurons in the ventromedial hypothalamus." Nature **509**(7502): 627-632.

Lee, H. G., C. S. Seong, Y. C. Kim, R. L. Davis and K. A. Han (2003). "Octopamine receptor OAMB is required for ovulation in Drosophila melanogaster." Dev Biol **264**(1): 179-190.

Lee, J.-K., M. K. McCoy, A. S. Harms, K. A. Ruhn, S. J. Gold and M. G. Tansey (2008). "Regulator of G-Protein Signaling 10 Promotes Dopaminergic Neuron Survival via Regulation of the Microglial Inflammatory Response." The Journal of Neuroscience **28**(34): 8517-8528.

Lee, J. H., R. Durand, V. Gradinaru, F. Zhang, I. Goshen, D. S. Kim, L. E. Fenno, C. Ramakrishnan and K. Deisseroth (2010). "Global and local fMRI signals driven by neurons defined optogenetically by type and wiring." Nature **465**(7299): 788-792.

Lee, P.-T., J. Zirin, O. Kanca, W.-W. Lin, K. L. Schulze, D. Li-Kroeger, R. Tao, C. Devereaux, Y. Hu, V. Chung, Y. Fang, Y. He, H. Pan, M. Ge, Z. Zuo, B. E. Housden, S. E. Mohr, S. Yamamoto, R. W. Levis, A. C. Spradling, N. Perrimon and H. J. Bellen (2018). "A gene-specific T2A-GAL4 library for Drosophila." eLife **7**: e35574.

Leung, C. C. Y. and Y. H. Wong (2017). "Role of G Protein-Coupled Receptors in the Regulation of Structural Plasticity and Cognitive Function." Molecules (Basel, Switzerland) **22**(7): 1239.

Li, X., D. V. Gutierrez, M. G. Hanson, J. Han, M. D. Mark, H. Chiel, P. Hegemann, L. T. Landmesser and S. Herlitze (2005). "Fast noninvasive activation and inhibition of neural and network activity by vertebrate rhodopsin and green algae channelrhodopsin." Proc Natl Acad Sci U S A **102**(49): 17816-17821.

Liggett, S. B. (2002). "Update on current concepts of the molecular basis of beta2-adrenergic receptor signaling." J Allergy Clin Immunol **110**(6 Suppl): S223-227.

Lin, B., A. Koizumi, N. Tanaka, S. Panda and R. H. Masland (2008). "Restoration of visual function in retinal degeneration mice by ectopic expression of melanopsin." Proc Natl Acad Sci U S A **105**(41): 16009-16014.

Lin, J. Y. (2011). "A user's guide to channelrhodopsin variants: features, limitations and future developments." Exp Physiol **96**(1): 19-25.

Lin, J. Y., P. M. Knutsen, A. Muller, D. Kleinfeld and R. Y. Tsien (2013). "ReaChR: a red-shifted variant of channelrhodopsin enables deep transcranial optogenetic excitation." Nat Neurosci **16**(10): 1499-1508.

Linden, D. J. and J. A. Connor (1991). "Participation of postsynaptic PKC in cerebellar long-term depression in culture." Science **254**(5038): 1656-1659.

Linden, D. J., K. Murakami and A. Routtenberg (1986). "A newly discovered protein kinase C activator (oleic acid) enhances long-term potentiation in the intact hippocampus." Brain Res **379**(2): 358-363.

Linden, D. J., F. S. Sheu, K. Murakami and A. Routtenberg (1987). "Enhancement of long-term potentiation by cis-unsaturated fatty acid: relation to protein kinase C and phospholipase A2." J Neurosci **7**(11): 3783-3792.

Liu, H., Q. Wang, Y. Liu, X. Zhao, T. Imaizumi, D. E. Somers, E. M. Tobin and C. Lin (2013). "Arabidopsis CRY2 and ZTL mediate blue-light regulation of the transcription factor CIB1 by distinct mechanisms." Proc Natl Acad Sci U S A **110**(43): 17582-17587.

Liu, H., X. Yu, K. Li, J. Klejnot, H. Yang, D. Lisiero and C. Lin (2008). "Photoexcited CRY2 interacts with CIB1 to regulate transcription and floral initiation in Arabidopsis." Science **322**(5907): 1535-1539.

Liu, Q. and C. L. Tucker (2017). "Engineering genetically-encoded tools for optogenetic control of protein activity." Current Opinion in Chemical Biology **40**: 17-23.

Lorenz-Fonfria, V. A. and J. Heberle (2014). "Channelrhodopsin unchained: structure and mechanism of a light-gated cation channel." Biochim Biophys Acta **1837**(5): 626-642.

Ludwig, A., X. Zong, M. Jeglitsch, F. Hofmann and M. Biel (1998). "A family of hyperpolarization-activated mammalian cation channels." Nature **393**(6685): 587-591.

Lyon, A. M., S. Dutta, C. A. Boguth, G. Skiniotis and J. J. Tesmer (2013). "Full-length Galpha(q)-phospholipase C-beta3 structure reveals interfaces of the C-terminal coiled-coil domain." Nat Struct Mol Biol **20**(3): 355-362.

MacLaren, D. A., R. W. Browne, J. K. Shaw, S. Krishnan Radhakrishnan, P. Khare, R. A. España and S. D. Clark (2016). "Clozapine N-Oxide Administration Produces Behavioral Effects in Long-Evans Rats: Implications for Designing DREADD Experiments." eNeuro **3**(5).

Macmillan, D. and J. G. McCarron (2010). "The phospholipase C inhibitor U-73122 inhibits Ca(2+) release from the intracellular sarcoplasmic reticulum Ca(2+) store by inhibiting Ca(2+) pumps in smooth muscle." Br J Pharmacol **160**(6): 1295-1301.

Madeira, F., Y. M. Park, J. Lee, N. Buso, T. Gur, N. Madhusoodanan, P. Basutkar, A. R. N. Tivey, S. C. Potter, R. D. Finn and R. Lopez (2019). "The EMBL-EBI search and sequence analysis tools APIs in 2019." Nucleic acids research **47**(W1): W636-W641.

Maeda, S., Q. Qu, M. J. Robertson, G. Skiniotis and B. K. Kobilka (2019). "Structures of the M1 and M2 muscarinic acetylcholine receptor/G-protein complexes." Science **364**(6440): 552.

Malenka, R. C., D. V. Madison and R. A. Nicoll (1986). "Potentiation of synaptic transmission in the hippocampus by phorbol esters." Nature **321**(6066): 175-177.

Mamidi, N., S. Panda, R. Borah and D. Manna (2014). "Synthesis and protein kinase C (PKC)-C1 domain binding properties of diacyltetrol based anionic lipids." Mol Biosyst **10**(11): 3002-3013.

Martin, B., R. Lopez de Maturana, R. Brenneman, T. Walent, M. P. Mattson and S. Maudsley (2005). "Class II G protein-coupled receptors and their ligands in neuronal function and protection." Neuromolecular Med **7**(1-2): 3-36.

Masseck, O. A., J. M. Rubelowski, K. Spoida and S. Herlitze (2011). "Light- and drug-activated G-protein-coupled receptors to control intracellular signalling." Exp Physiol **96**(1): 51-56.

Matúš, D. and S. Prömel (2018). "G Proteins and GPCRs in C. elegans Development: A Story of Mutual Infidelity." Journal of developmental biology **6**(4): 28.

Maurel, B., A. Le Digarcher, C. Dantec and L. Journot (2011). "Genome-wide profiling of G protein-coupled receptors in cerebellar granule neurons using high-throughput, real-time PCR." BMC Genomics **12**: 241.

McCudden, C. R., M. D. Hains, R. J. Kimple, D. P. Siderovski and F. S. Willard (2005). "G-protein signaling: back to the future." Cellular and molecular life sciences : CMLS **62**(5): 551-577.

Meecham, K. G., S. J. Boyle, J. C. Hunter and J. Hughes (1989). "An in vitro profile of activity for the (+) and (-) enantiomers of spiradoline and PD117302." Eur J Pharmacol **173**(2-3): 151-157.

Mehren, J. E., A. Ejima and L. C. Griffith (2004). "Unconventional sex: fresh approaches to courtship learning." Current Opinion in Neurobiology **14**(6): 745-750.

Mezzera, C., M. Brotas, M. Gaspar, H. J. Pavlou, S. F. Goodwin and M. L. Vasconcelos (2020). "Ovipositor Extrusion Promotes the Transition from Courtship to Copulation and Signals Female Acceptance in Drosophila melanogaster." Current Biology **30**(19): 3736-3748.e3735.

Minobe, E., S. Maeda, J. Xu, L. Hao, A. Kameyama and M. Kameyama (2014). "A new phosphorylation site in cardiac L-type Ca2+ channels (Cav1.2) responsible for its cAMP-mediated modulation." Am J Physiol Cell Physiol **307**(11): C999-c1009.

Mittal, Y., Y. Pavlova, M. Garcia-Marcos and P. Ghosh (2011). "Src homology domain 2-containing protein-tyrosine phosphatase-1 (SHP-1) binds and dephosphorylates G(alpha)-interacting, vesicle-associated protein (GIV)/Girdin and attenuates the GIV-phosphatidylinositol 3-kinase (PI3K)-Akt signaling pathway." J Biol Chem **286**(37): 32404-32415.

Mochizuki, N., Y. Ohba, E. Kiyokawa, T. Kurata, T. Murakami, T. Ozaki, A. Kitabatake, K. Nagashima and M. Matsuda (1999). "Activation of the ERK/MAPK pathway by an isoform of rap1GAP associated with G alpha(i)." Nature **400**(6747): 891-894.

Montague, S. A. and B. S. Baker (2016). "Memory Elicited by Courtship Conditioning Requires Mushroom Body Neuronal Subsets Similar to Those Utilized in Appetitive Memory." PLoS One **11**(10): e0164516.

Morri, M., I. Sanchez-Romero, A.-M. Tichy, S. Kainrath, E. J. Gerrard, P. P. Hirschfeld, J. Schwarz and H. Janovjak (2018). "Optical functionalization of human Class A orphan G-protein-coupled receptors." Nature communications **9**(1): 1950-1950.

Murphy, D. D. and M. Segal (1997). "Morphological plasticity of dendritic spines in central neurons is mediated by activation of cAMP response element binding protein." Proc Natl Acad Sci U S A **94**(4): 1482-1487.

Nagel, G., D. Ollig, M. Fuhrmann, S. Kateriya, A. M. Musti, E. Bamberg and P. Hegemann (2002). "Channelrhodopsin-1: a light-gated proton channel in green algae." Science **296**(5577): 2395-2398.

Nagel, G., T. Szellas, W. Huhn, S. Kateriya, N. Adeishvili, P. Berthold, D. Ollig, P. Hegemann and E. Bamberg (2003). "Channelrhodopsin-2, a directly light-gated cation-selective membrane channel." Proc Natl Acad Sci U S A **100**(24): 13940-13945.

Namkung, Y. and D. R. Sibley (2004). "Protein Kinase C Mediates Phosphorylation, Desensitization, and Trafficking of the D2 Dopamine Receptor*." Journal of Biological Chemistry **279**(47): 49533-49541.

Nance, M. R., B. Kreutz, V. M. Tesmer, R. Sterne-Marr, T. Kozasa and J. J. Tesmer (2013). "Structural and functional analysis of the regulator of G protein signaling 2-galphaq complex." Structure **21**(3): 438-448.

Neher, E. and T. Sakaba (2008). "Multiple roles of calcium ions in the regulation of neurotransmitter release." Neuron **59**(6): 861-872.

Newton, A. C. (1995). "Protein kinase C: structure, function, and regulation." J Biol Chem **270**(48): 28495-28498.

Nguyen, C. H., H. Ming, P. Zhao, L. Hugendubler, R. Gros, S. R. Kimball and P. Chidiac (2009). "Translational control by RGS2." J Cell Biol **186**(5): 755-765.

Niswender, C. M. and P. J. Conn (2010). "Metabotropic glutamate receptors: physiology, pharmacology, and disease." Annual review of pharmacology and toxicology **50**: 295-322.

Ntefidou, M., M. Iseki, M. Watanabe, M. Lebert and D. P. Häder (2003). "Photoactivated adenylyl cyclase controls phototaxis in the flagellate Euglena gracilis." Plant Physiol **133**(4): 1517-1521.

Nunn, C., H. Mao, P. Chidiac and P. R. Albert (2006). "RGS17/RGSZ2 and the RZ/A family of regulators of G-protein signaling." Semin Cell Dev Biol **17**(3): 390-399.

O'Neill, P. R. and N. Gautam (2014). "Subcellular optogenetic inhibition of G proteins generates signaling gradients and cell migration." Mol Biol Cell **25**(15): 2305-2314.

Oh, E., T. Maejima, C. Liu, E. Deneris and S. Herlitze (2010). "Substitution of 5-HT1A receptor signaling by a light-activated G protein-coupled receptor." J Biol Chem **285**(40): 30825-30836.

Palczewski, K. (2006). "G protein-coupled receptor rhodopsin." Annu Rev Biochem **75**: 743-767.

Park, H., N. Y. Kim, S. Lee, N. Kim, J. Kim and W. D. Heo (2017). "Optogenetic protein clustering through fluorescent protein tagging and extension of CRY2." Nature Communications **8**(1): 30.

Park, H., N. Y. Kim, S. Lee, N. Kim, J. Kim and W. D. Heo (2017). "Optogenetic protein clustering through fluorescent protein tagging and extension of CRY2." Nat Commun **8**(1): 30.

Parolaro, D., D. Vigano, N. Realini and T. Rubino (2007). "Role of endocannabinoids in regulating drug dependence." Neuropsychiatric disease and treatment **3**(6): 711-721.

Pathak, G. P., D. Strickland, J. D. Vrana and C. L. Tucker (2014). "Benchmarking of optical dimerizer systems." ACS Synth Biol **3**(11): 832-838.

Pavlos, N. J. and P. A. Friedman (2017). "GPCR Signaling and Trafficking: The Long and Short of It." Trends Endocrinol Metab **28**(3): 213-226.

Peng, L. Q., P. Li, Q. L. Zhang, L. Hong, L. P. Liu, X. Cui and B. R. Cui (2016). "cAMP induction by ouabain promotes endothelin-1 secretion via MAPK/ERK signaling in beating rabbit atria." Korean J Physiol Pharmacol **20**(1): 9-14.

Pereda, A. E. (2014). "Electrical synapses and their functional interactions with chemical synapses." Nature reviews. Neuroscience **15**(4): 250-263.

Pfeffer, C. K., M. Xue, M. He, Z. J. Huang and M. Scanziani (2013). "Inhibition of inhibition in visual cortex: the logic of connections between molecularly distinct interneurons." Nat Neurosci **16**(8): 1068-1076.

Riddle, E. L., R. A. Schwartzman, M. Bond and P. A. Insel (2005). "Multi-tasking RGS proteins in the heart: the next therapeutic target?" Circ Res **96**(4): 401-411.

Robinson, T. E., G. Gorny, V. R. Savage and B. Kolb (2002). "Widespread but regionally specific effects of experimenter- versus self-administered morphine on dendritic spines in the nucleus accumbens, hippocampus, and neocortex of adult rats." Synapse **46**(4): 271-279.

Rosenbaum, D. M., S. G. Rasmussen and B. K. Kobilka (2009). "The structure and function of G-protein-coupled receptors." Nature **459**(7245): 356-363.

Rost, B. R., F. Schneider-Warme, D. Schmitz and P. Hegemann (2017). "Optogenetic Tools for Subcellular Applications in Neuroscience." Neuron **96**(3): 572-603.

Roth, B. L. (2016). "DREADDs for Neuroscientists." Neuron **89**(4): 683-694.

Roth, B. L. (2016). "DREADDs for Neuroscientists." Neuron **89**(4): 683-694.

Roy, A. A., A. Baragli, L. S. Bernstein, J. R. Hepler, T. E. Hébert and P. Chidiac (2006). "RGS2 interacts with Gs and adenylyl cyclase in living cells." Cell Signal **18**(3): 336-348.

Salim, S., S. Sinnarajah, J. H. Kehrl and C. W. Dessauer (2003). "Identification of RGS2 and type V adenylyl cyclase interaction sites." J Biol Chem **278**(18): 15842-15849.

Salomon, M., J. M. Christie, E. Knieb, U. Lempert and W. R. Briggs (2000). "Photochemical and mutational analysis of the FMN-binding domains of the plant blue light receptor, phototropin." Biochemistry **39**(31): 9401-9410.

Salomon, M., W. Eisenreich, H. Dürr, E. Schleicher, E. Knieb, V. Massey, W. Rüdiger, F. Müller, A. Bacher and G. Richter (2001). "An optomechanical transducer in the blue light receptor phototropin from Avena sativa." Proc Natl Acad Sci U S A **98**(22): 12357-12361.

Schiltenwolf, M., M. Akbar, A. Hug, U. Pfüller, S. Gantz, E. Neubauer, H. Flor and H. Wang (2014). "Evidence of specific cognitive deficits in patients with chronic low back pain under long-term substitution treatment of opioids." Pain Physician **17**(1): 9-20.

Schneider, F., C. Grimm and P. Hegemann (2015). "Biophysics of Channelrhodopsin." Annu Rev Biophys **44**: 167-186.

Schobert, B. and J. K. Lanyi (1982). "Halorhodopsin is a light-driven chloride pump." J Biol Chem **257**(17): 10306-10313.

Schröder, N. G. a. E. A. (2015) "Drosophila germline transformation."

Schuch, K. N., L. N. Govindarajan, Y. Guo, S. N. Baskoylu, S. Kim, B. Kimia, T. Serre and A. C. Hart (2020). "Discriminating between sleep and exercise-induced fatigue using computer vision and behavioral genetics." J Neurogenet: 1-13.

Schwaerzel, M., M. Heisenberg and T. Zars (2002). "Extinction antagonizes olfactory memory at the subcellular level." Neuron **35**(5): 951-960.

Schwaerzel, M., M. Monastirioti, H. Scholz, F. Friggi-Grelin, S. Birman and M. Heisenberg (2003). "Dopamine and octopamine differentiate between aversive and appetitive olfactory memories in Drosophila." J Neurosci **23**(33): 10495-10502.

Schwartz, E. J., T. Blackmer, T. Gerachshenko and S. Alford (2007). "Presynaptic G-protein-coupled receptors regulate synaptic cleft glutamate via transient vesicle fusion." J Neurosci **27**(22): 5857-5868.

Sehgal, P., P. Szalai, C. Olesen, H. A. Praetorius, P. Nissen, S. B. Christensen, N. Engedal and J. V. Møller (2017). "Inhibition of the sarco/endoplasmic reticulum (ER) Ca(2+)-ATPase by thapsigargin

analogs induces cell death via ER Ca(2+) depletion and the unfolded protein response." J Biol Chem **292**(48): 19656-19673.

Siderovski, D. P., A. Hessel, S. Chung, T. W. Mak and M. Tyers (1996). "A new family of regulators of G-protein-coupled receptors?" Curr Biol **6**(2): 211-212.

Siegle, J. H. and M. A. Wilson (2014). "Enhancement of encoding and retrieval functions through theta phase-specific manipulation of hippocampus." Elife **3**: e03061.

Sievers, F., A. Wilm, D. Dineen, T. J. Gibson, K. Karplus, W. Li, R. Lopez, H. McWilliam, M. Remmert, J. Söding, J. D. Thompson and D. G. Higgins (2011). "Fast, scalable generation of high-quality protein multiple sequence alignments using Clustal Omega." Molecular Systems Biology **7**(1): 539.

Sinnarajah, S., C. W. Dessauer, D. Srikumar, J. Chen, J. Yuen, S. Yilma, J. C. Dennis, E. E. Morrison, V. Vodyanoy and J. H. Kehrl (2001). "RGS2 regulates signal transduction in olfactory neurons by attenuating activation of adenylyl cyclase III." Nature **409**(6823): 1051-1055.

Smith, K. S., D. J. Bucci, B. W. Luikart and S. V. Mahler (2016). "DREADDS: Use and application in behavioral neuroscience." Behav Neurosci **130**(2): 137-155.

Sohal, V. S., F. Zhang, O. Yizhar and K. Deisseroth (2009). "Parvalbumin neurons and gamma rhythms enhance cortical circuit performance." Nature **459**(7247): 698-702.

Soundararajan, M., F. S. Willard, A. J. Kimple, A. P. Turnbull, L. J. Ball, G. A. Schoch, C. Gileadi, O. Y. Fedorov, E. F. Dowler, V. A. Higman, S. Q. Hutsell, M. Sundström, D. A. Doyle and D. P. Siderovski (2008). "Structural diversity in the RGS domain and its interaction with heterotrimeric G protein alpha-subunits." Proc Natl Acad Sci U S A **105**(17): 6457-6462.

Spangler, S. M. and M. R. Bruchas (2017). "Optogenetic approaches for dissecting neuromodulation and GPCR signaling in neural circuits." Curr Opin Pharmacol **32**: 56-70.

Spoida, K., D. Eickelbeck, R. Karapinar, T. Eckhardt, M. D. Mark, D. Jancke, B. V. Ehinger, P. König, D. Dalkara, S. Herlitze and O. A. Masseck (2016). "Melanopsin Variants as Intrinsic Optogenetic On and Off Switches for Transient versus Sustained Activation of G Protein Pathways." Curr Biol **26**(9): 1206-1212.

Sprang, S. R. (2016). "Invited review: Activation of G proteins by GTP and the mechanism of Gα-catalyzed GTP hydrolysis." Biopolymers **105**(8): 449-462.

Stagkourakis, S., K. O. Smiley, P. Williams, S. Kakadellis, K. Ziegler, J. Bakker, R. S. E. Brown, T. Harkany, D. R. Grattan and C. Broberger (2020). "A Neuro-hormonal Circuit for Paternal Behavior Controlled by a Hypothalamic Network Oscillation." Cell **182**(4): 960-975.e915.

Stierl, M., P. Stumpf, D. Udwari, R. Gueta, R. Hagedorn, A. Losi, W. Gärtner, L. Petereit, M. Efetova, M. Schwarzel, T. G. Oertner, G. Nagel and P. Hegemann (2011). "Light modulation of cellular cAMP by a small bacterial photoactivated adenylyl cyclase, bPAC, of the soil bacterium Beggiatoa." J Biol Chem **286**(2): 1181-1188.

Stoeber, M., D. Jullié, B. T. Lobingier, T. Laeremans, J. Steyaert, P. W. Schiller, A. Manglik and M. von Zastrow (2018). "A Genetically Encoded Biosensor Reveals Location Bias of Opioid Drug Action." Neuron **98**(5): 963-976.e965.

Strickland, D., Y. Lin, E. Wagner, C. M. Hope, J. Zayner, C. Antoniou, T. R. Sosnick, E. L. Weiss and M. Glotzer (2012). "TULIPs: tunable, light-controlled interacting protein tags for cell biology." Nat Methods **9**(4): 379-384.

Stryjek-Kaminska, D., A. Piiper and S. Zeuzem (1996). "Epidermal growth factor regulates adenylate cyclase activity via Gs and Gi1-2 proteins in pancreatic acinar membranes." Biochem J **316 (Pt 1)**: 87-91.

Sullivan, R. M., H. Talangbayan, H. Einat and H. Szechtman (1998). "Effects of quinpirole on central dopamine systems in sensitized and non-sensitized rats1A preliminary report of this work was presented at the Society for Neuroscience meeting in San Diego, CA, November, 1995 ([66]).1." Neuroscience **83**(3): 781-789.

Swartz, T. E., P. J. Wenzel, S. B. Corchnoy, W. R. Briggs and R. A. Bogomolni (2002). "Vibration spectroscopy reveals light-induced chromophore and protein structural changes in the LOV2 domain of the plant blue-light receptor phototropin 1." Biochemistry **41**(23): 7183-7189.

Syrovatkina, V., K. O. Alegre, R. Dey and X.-Y. Huang (2016). "Regulation, Signaling, and Physiological Functions of G-Proteins." Journal of molecular biology **428**(19): 3850-3868.

Takahashi, A., K. Nagayasu, N. Nishitani, S. Kaneko and T. Koide (2014). "Control of Intermale Aggression by Medial Prefrontal Cortex Activation in the Mouse." PLOS ONE **9**(4): e94657.

Taslimi, A., J. D. Vrana, D. Chen, S. Borinskaya, B. J. Mayer, M. J. Kennedy and C. L. Tucker (2014). "An optimized optogenetic clustering tool for probing protein interaction and function." Nature Communications **5**(1): 4925.

Taslimi, A., B. Zoltowski, J. G. Miranda, G. P. Pathak, R. M. Hughes and C. L. Tucker (2016). "Optimized second-generation CRY2-CIB dimerizers and photoactivatable Cre recombinase." Nat Chem Biol **12**(6): 425-430.

Thanos, P. K., L. Robison, E. J. Nestler, R. Kim, M. Michaelides, M. K. Lobo and N. D. Volkow (2013). "Mapping brain metabolic connectivity in awake rats with muPET and optogenetic stimulation." J Neurosci **33**(15): 6343-6349.

Thapliyal, S. and K. Babu (2018). C. elegans Locomotion: Finding Balance in Imbalance. Biochemical and Biophysical Roles of Cell Surface Molecules. K. Chattopadhyay and S. C. Basu. Singapore, Springer Singapore**:** 185-196.

Thompson, K. J., E. Khajehali, S. J. Bradley, J. S. Navarrete, X. P. Huang, S. Slocum, J. Jin, J. Liu, Y. Xiong, R. H. J. Olsen, J. F. Diberto, K. M. Boyt, M. M. Pina, D. Pati, C. Molloy, C. Bundgaard, P. M. Sexton, T. L. Kash, M. J. Krashes, A. Christopoulos, B. L. Roth and A. B. Tobin (2018). "DREADD Agonist 21 Is an Effective Agonist for Muscarinic-Based DREADDs in Vitro and in Vivo." ACS Pharmacol Transl Sci **1**(1): 61-72.

Tompkins, L., R. W. Siegel, D. A. Gailey and J. C. Hall (1983). "Conditioned courtship inDrosophila and its mediation by association of chemical cues." Behavior Genetics **13**(6): 565-578.

Tovote, P., M. S. Esposito, P. Botta, F. Chaudun, J. P. Fadok, M. Markovic, S. B. E. Wolff, C. Ramakrishnan, L. Fenno, K. Deisseroth, C. Herry, S. Arber and A. Lüthi (2016). "Midbrain circuits for defensive behaviour." Nature **534**(7606): 206-212.

Toya, Y., C. Schwencke, J. Couet, M. P. Lisanti and Y. Ishikawa (1998). "Inhibition of adenylyl cyclase by caveolin peptides." Endocrinology **139**(4): 2025-2031.

Tschammer, N., M. Dorfler, H. Hubner and P. Gmeiner (2010). "Engineering a GPCR-ligand pair that simulates the activation of D(2L) by Dopamine." ACS Chem Neurosci **1**(1): 25-35.

Tsunematsu, T., K. F. Tanaka, A. Yamanaka and A. Koizumi (2013). "Ectopic expression of melanopsin in orexin/hypocretin neurons enables control of wakefulness of mice in vivo by blue light." Neurosci Res **75**(1): 23-28.

Tucker, C. L., J. D. Vrana and M. J. Kennedy (2014). "Tools for controlling protein interactions using light." Current protocols in cell biology **64**: 17.16.11-17.16.20.

Tuteja, N. (2009). "Signaling through G protein coupled receptors." Plant Signal Behav **4**(10): 942-947.

Tye, K. M., R. Prakash, S. Y. Kim, L. E. Fenno, L. Grosenick, H. Zarabi, K. R. Thompson, V. Gradinaru, C. Ramakrishnan and K. Deisseroth (2011). "Amygdala circuitry mediating reversible and bidirectional control of anxiety." Nature **471**(7338): 358-362.

Unoki, S., Y. Matsumoto and M. Mizunami (2005). "Participation of octopaminergic reward system and dopaminergic punishment system in insect olfactory learning revealed by pharmacological study." Eur J Neurosci **22**(6): 1409-1416.

Urban, D. J. and B. L. Roth (2015). "DREADDs (designer receptors exclusively activated by designer drugs): chemogenetic tools with therapeutic utility." Annu Rev Pharmacol Toxicol **55**: 399-417.

van Swinderen, B. and J. C. Hall (1995). "Analysis of conditioned courtship in dusky-Andante rhythm mutants of Drosophila." Learn Mem **2**(2): 49-61.

Vardy, E., J. E. Robinson, C. Li, R. H. J. Olsen, J. F. DiBerto, P. M. Giguere, F. M. Sassano, X. P. Huang, H. Zhu, D. J. Urban, K. L. White, J. E. Rittiner, N. A. Crowley, K. E. Pleil, C. M. Mazzone, P. D. Mosier, J. Song, T. L. Kash, C. J. Malanga, M. J. Krashes and B. L. Roth (2015). "A New DREADD Facilitates the Multiplexed Chemogenetic Interrogation of Behavior." Neuron **86**(4): 936-946.

Vučković, S., D. Srebro, K. S. Vujović, Č. Vučetić and M. Prostran (2018). "Cannabinoids and Pain: New Insights From Old Molecules." Frontiers in pharmacology **9**: 1259-1259.

Vuong, T. M. and M. Chabre (1991). "Deactivation kinetics of the transduction cascade of vision." Proc Natl Acad Sci U S A **88**(21): 9813-9817.

Walf, A. A. and C. A. Frye (2007). "The use of the elevated plus maze as an assay of anxiety-related behavior in rodents." Nat Protoc **2**(2): 322-328.

Wang, L., I. Z. Chen and D. Lin (2015). "Collateral pathways from the ventromedial hypothalamus mediate defensive behaviors." Neuron **85**(6): 1344-1358.

Wang, X., W. Zeng, A. A. Soyombo, W. Tang, E. M. Ross, A. P. Barnes, S. L. Milgram, J. M. Penninger, P. B. Allen, P. Greengard and S. Muallem (2005). "Spinophilin regulates Ca2+ signalling by binding the N-terminal domain of RGS2 and the third intracellular loop of G-protein-coupled receptors." Nat Cell Biol **7**(4): 405-411.

Watson, N., M. E. Linder, K. M. Druey, J. H. Kehrl and K. J. Blumer (1996). "RGS family members: GTPase-activating proteins for heterotrimeric G-protein alpha-subunits." Nature **383**(6596): 172-175.

Witten, I. B., S. C. Lin, M. Brodsky, R. Prakash, I. Diester, P. Anikeeva, V. Gradinaru, C. Ramakrishnan and K. Deisseroth (2010). "Cholinergic interneurons control local circuit activity and cocaine conditioning." Science **330**(6011): 1677-1681.

Wu, J., L. Liu, T. Matsuda, Y. Zhao, A. Rebane, M. Drobizhev, Y. F. Chang, S. Araki, Y. Arai, K. March, T. E. Hughes, K. Sagou, T. Miyata, T. Nagai, W. H. Li and R. E. Campbell (2013). "Improved orange and red Ca(2)+/- indicators and photophysical considerations for optogenetic applications." ACS Chem Neurosci **4**(6): 963-972.

Wu, Z., A. E. Autry, J. F. Bergan, M. Watabe-Uchida and C. G. Dulac (2014). "Galanin neurons in the medial preoptic area govern parental behaviour." Nature **509**(7500): 325-330.

Xie, Z., E. C. Chan and K. M. Druey (2016). "R4 Regulator of G Protein Signaling (RGS) Proteins in Inflammation and Immunity." Aaps j **18**(2): 294-304.

Yan, Y., P. P. Chi and H. R. Bourne (1997). "RGS4 inhibits Gq-mediated activation of mitogen-activated protein kinase and phosphoinositide synthesis." J Biol Chem **272**(18): 11924-11927.

Yatani, A., R. Mattera, J. Codina, R. Graf, K. Okabe, E. Padrell, R. Iyengar, A. M. Brown and L. Birnbaumer (1988). "The G protein-gated atrial K+ channel is stimulated by three distinct Gi alpha-subunits." Nature **336**(6200): 680-682.

Yin, J., K. M. Chen, M. J. Clark, M. Hijazi, P. Kumari, X. C. Bai, R. K. Sunahara, P. Barth and D. M. Rosenbaum (2020). "Structure of a D2 dopamine receptor-G-protein complex in a lipid membrane." Nature **584**(7819): 125-129.

Ying, S.-W., M. Futter, K. Rosenblum, M. J. Webber, S. P. Hunt, T. V. P. Bliss and C. R. Bramham (2002). "Brain-derived neurotrophic factor induces long-term potentiation in intact adult hippocampus: requirement for ERK activation coupled to CREB and upregulation of Arc synthesis." The Journal of neuroscience : the official journal of the Society for Neuroscience **22**(5): 1532-1540.

Yizhar, O., L. E. Fenno, M. Prigge, F. Schneider, T. J. Davidson, D. J. O'Shea, V. S. Sohal, I. Goshen, J. Finkelstein, J. T. Paz, K. Stehfest, R. Fudim, C. Ramakrishnan, J. R. Huguenard, P. Hegemann and K. Deisseroth (2011). "Neocortical excitation/inhibition balance in information processing and social dysfunction." Nature **477**(7363): 171-178.

Zamponi, G. W. and K. P. Currie (2013). "Regulation of Ca(V)2 calcium channels by G protein coupled receptors." Biochim Biophys Acta **1828**(7): 1629-1643.

Zemelman, B. V., G. A. Lee, M. Ng and G. Miesenbock (2002). "Selective photostimulation of genetically chARGed neurons." Neuron **33**(1): 15-22.

Zeng, W., X. Xu, S. Popov, S. Mukhopadhyay, P. Chidiac, J. Swistok, W. Danho, K. A. Yagaloff, S. L. Fisher, E. M. Ross, S. Muallem and T. M. Wilkie (1998). "The N-terminal Domain of RGS4 Confers Receptor-selective Inhibition of G Protein Signaling*." Journal of Biological Chemistry **273**(52): 34687-34690.

Zhang, B. X., X. Ma, Z. Shu, C. K. Yeh, R. H. Swerdlow and M. S. Katz (2006). "Differential regulation of intracellular calcium oscillations by mitochondria and gap junctions." Cell Biochem Biophys **44**(2): 187-203.

Zhang, C., N. Zhao, Y. Chen, D. Zhang, J. Yan, W. Zou, K. Zhang and X. Huang (2016). "The Signaling Pathway of Caenorhabditis elegans Mediates Chemotaxis Response to the Attractant 2-Heptanone in a Trojan Horse-like Pathogenesis." J Biol Chem **291**(45): 23618-23627.

Zheng, B., Y. C. Ma, R. S. Ostrom, C. Lavoie, G. N. Gill, P. A. Insel, X. Y. Huang and M. G. Farquhar (2001). "RGS-PX1, a GAP for GalphaS and sorting nexin in vesicular trafficking." Science **294**(5548): 1939-1942.

Zhou, C., H. Huang, S. M. Kim, H. Lin, X. Meng, K. A. Han, A. S. Chiang, J. W. Wang, R. Jiao and Y. Rao (2012). "Molecular genetic analysis of sexual rejection: roles of octopamine and its receptor OAMB in Drosophila courtship conditioning." J Neurosci **32**(41): 14281-14287.